Higgs Boson Phenomenology in the Type II Two Higgs Doublet Model (2HDM)

Fuakye Eric Gyabeng

A Thesis

in

The Department

of

Physics

Presented in Partial Fulfillment of the Requirements

for the Degree of

Master of Science (Physics) at

Concordia University

Montréal, Québec, Canada

19th March 2020

Concordia University

School of Graduate Studies

This is to certify that the thesis prepared

By: **Fuakye Eric Gyabeng**

Entitled: **Higgs Boson Phenomenology in the Type II Two Higgs Doublet Model (2HDM)**

and submitted in partial fulfillment of the requirements for the degree of

Master of Science (Physics)

complies with the regulations of this University and meets the accepted standards with respect to originality and quality.

Signed by the Final Examining Committee:

_____ Chair
Prof. Saurabh Maiti

_____ Examiner
Prof. Sushil K. Misra

_____ Examiner
Prof. Ingo Salzmann

_____ Supervisor
Prof. Mariana Frank

Approved by _____
Alexandre Champagne, Chair
Department of Physics

_____ 2020

_____
André Roy, Dean
Faculty of Arts & Science

Abstract

Higgs Boson Phenomenology in the Type II Two Higgs Doublet Model (2HDM)

Fuakye Eric Gyabeng

We present a strategy to study the parameter space of the Type – II CP conserving Two Higgs Doublet Model with a softly broken Z_2 symmetry by parametrizing the Higgs scalar potential in the physical basis. In this basis, the input parameters are the masses of the 4 scalar physical states, $m_{H^\pm}, m_A, m_H, m_h$, the ratio of the Higgs vacuum expectation values, $\tan\beta$, two mixing angles, α and β, and the softly breaking parameter scale of the Z_2 symmetry, M. Using the physical basis, we present numerical scans of the available 2HDM parameter region where we modify the Lilith program to study constraints from signal strength measurements of the 125GeV Higgs boson on the $\cos(\beta-\alpha)$ and $\tan\beta$ plane in the Type - II 2HDM. We also impose certain theoretical constraints on the masses of H, A, and $H^\pm$ to eliminate all exotic decays, and to allow space for SM particle decays. From these results, we define three benchmark scenarios, namely the decoupling limit, near the decoupling limit, and the crescent limit. The crescent limit allows us to probe non-SM Higgs phenomenology that is of interest for future LHC Higgs searches. Our results suggest that in the crescent limit, when kinematically accessible $H \to hh$, $A \to Zh$ and $H^\pm \to W^\pm h$ should become high priorities in searching for additional Higgs bosons.

Keywords— 2HDM, Higgs Physics, Z_2 Symmetry, Crescent limit, Lilith

Dedicated to my Grandfather, Jeremiah Gyabeng

Acknowledgments

First and above all, I would like to thank God for providing me this opportunity and granting me the capability to proceed successfully in my academic life. Indeed, this is the right time for me to express my sincere gratitude to the people whose influence made this work possible. A very exceptional thanks goes to my supervisor Prof. Mariana Frank for her intense supervision and guidance throughout this research. Thank you very much for all the support, compassion, encouragement, and the marvelous research environment that you created for me during my 2-year stay in the High Energy Physics Group at Concordia University.

I would like to thank Dr. Manuel Toharia whose relevant suggestions and contributions resemble more than that of a supervisor. His suggestions really paved many ways for my understanding of phenomenology.

Also, I would like to thank Prof. Champagne, our department Chair for the awesome research environment he created in the Department of Physics at Concordia University. Thank you, Prof. Bianucci and Prof. Zazubovits, for your spectacular advice. Thank you, Prof. Olivier Mattelaer, for your time and for answering my questions about MadGraph. To my committee, Prof. Misra and Prof. Ingo, I am grateful for your suggestions. Above all, I would like to thank my parents, siblings, friends, and colleagues for all their support and love.

Contribution of the Author

The original research work contained in this thesis is presented in Chapters 4 , 5 , and 6 and has been conducted in collaboration with Prof. Mariana Frank and Dr. Manuel Toharia.

In Chapters 4 , 5 , and 6 , some of the analytical and all computational calculations which led to the final results of the research were conducted by the author in partial fulfillment of the requirements for the Master of Science degree in the Department of Physics at Concordia University, Montreal, Quebec.

Contents

List of Figures

List of Tables

List of Acronyms

SM	Standard Model
ATLAS	A Toroidal LHC Apparatus
CMS	Compact Muon Solenoid
LHC	Large Hadron Collider
BSM	Beyond the Standard Model
CP	Charge Parity
2HDM	Two Higgs Doublet Model
2HDMC	Two Higgs Doublet Model Calculator
MSSM	Minimal Supersymmetric Standard Model
QED	Quantum Electrodynamics
QCD	Quantum Chromodynamics
HHG	Higgs Hunter's Guide
FCNC	Flavour Changing Neutral Current
LO	Leading Order
NLO	Next-to-Leading Order
EW	Electroweak
EWSB	Electroweak Symmetry Breaking
VEV	Vacuum Expectation Value
WEDM	Warped Extra Dimension Model

NNLO	Next-to-Next-to-Leading Order

Chapter 1

Introduction

1.1 Background information

Atoms are extremely important structures that make up all of the materials on earth. Atoms are present in the human bodies and they bond together to form molecular structures which make up matter. Matter is anything that has mass and occupies space. There are four states of matter, solid, liquid, gas, and plasma. Also, atoms are made up of protons, neutrons and electrons. These subatomic particles consist of fundamental particles of matter which are the basic building blocks of the universe. The study of these fundamental particles of the universe is referred to as particle physics, which has become a broader area of research interest to many since several decades ago. The study of particle physics therefore seeks to address the fundamental or elementary building blocks of matter and how they interact. The good news is that there is a very powerful framework which helps us to understand these elementary particles that build up the matter constituents around us and how they interact. This is the famous Standard Model(SM) of elementary particle physics as shown in Fig. 1.1 below. According to the SM, elementary particles can be grouped into two forms namely fermions and bosons. Fermions are spin $\frac{1}{2}$ particles which obey the Pauli's exclusion principle and can be categorized into quarks and leptons. Bosons on the other hand are spin 1 particles which mediate the interactions between the fundamental particles in the SM. Forces associated with a symmetry of Lagrangian are mediated by these spin 1

bosons ($\gamma, W^{\pm}, Z, g$). The four main fundamental interactions in nature are electromagnetic, weak, strong and gravity. Gravity is however not encoded in the SM and hence shall not be discussed in this thesis. An attempt to fit gravity into the SM has proven to be a very tough challenge because, on the scale of experiments in particle physics, gravity is by far the weakest among all the other fundamental interactions, although it is dominant on the scale of the universe[1, 2]. The comparative strength for gravitational interaction is of the order of 10^{-39} as compared to the weak force whose relative strength is about 10^{-7}[3]. The electromagnetic interaction unifies both the electric and magnetic fields [4], the weak force is responsible for the radioactive decay of certain nuclei [5] and the strong force is responsible for the formation of hadrons(such as protons and nucleons) [6], all four forces shown in Fig. 1.2 below. The electromagnetic and weak interactions are understood in recent times as manifestations of the same force called the electroweak interaction.

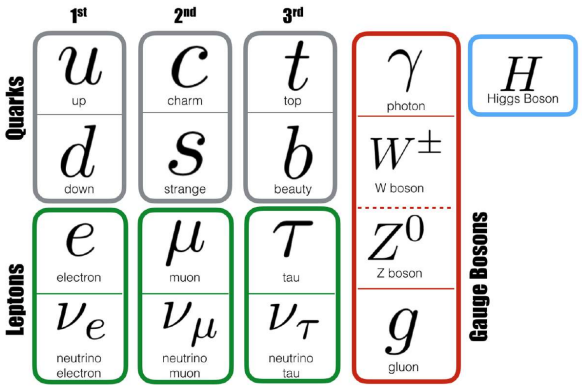

Figure 1.1: The standard model of elementary particles

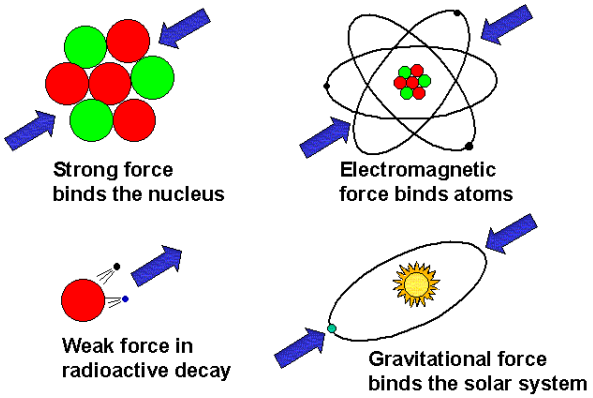

Figure 1.2: Fundamental forces of nature

Each type of interaction corresponds to the gauge symmetry group, and the theory exhibits an exact invariance under the combination of these symmetries[7]. Hence, the SM depends on certain gauge invariance principles for which the fundamental forces mediated by spin one gauge bosons occur. One of the strangest thing about the SM is that this gauge symmetry which gives a perfect description about particle interaction abysmally fails to describe the masses of the particles. This is actually the reason why we need to break the symmetry entirely for the particles to gain their masses. Hence, this leads to the concept of

Electroweak Symmetry Breaking (EWSB) which explains how the gauge bosons and fermions gain their masses. A simplest and easiest way to account for the concept of electroweak symmetry breaking is to enlarge the particle content of the SM by simply adding a complex scalar doublet, under $SU(2)_L$ where the vacuum expectation value of the scalar field appears non zero. This concepts of symmetry breaking is implemented by the Higgs mechanism. According to [8] , which focuses on broken symmetries and the masses of the gauge bosons, it was made explicitly clear that in the Higgs mechanism, a scalar Higgs field develops a non zero vacuum expectation value through it potential. During this mechanism, the particles acquire their masses proportionally to the vacuum expectation value and their Yukawa couplings to the Higgs field. Moreover, during spontaneous breaking of the electroweak symmetry, the 3 Goldstone bosons which appear are absorbed into both the $W^{\pm}$ and Z^0 boson such that these bosons become massive. After EWSB, a spin zero scalar boson called the Higgs boson remains. On July 4th 2012, both the ATLAS [9] and CMS [10] collaborations at the Large Hadron Collider (LHC) confirmed a spin 0 scalar boson with mass about 125 - 126 GeV. Analyses have confirmed that this observed boson is in remarkable agreement with that predicted by the SM. Hence, the discovery of such a boson was a milestone to our understanding of nature, a confirmation in particle physics to our understanding of EWSB and a vital ingredient for future studies on new physics beyond the SM.

1.2 Motivation for studying BSM Physics

Despite being the most successful theory of particle physics to date, the Standard Model is inherently an incomplete theory [11]. The SM does not adequately explain several fundamental physical phenomena in nature. This calls for extending the particle content of the SM and several studies have been carried out in the past [12–14]. From a theoretical perspective, there are several motivations to enlarge the scalar sector of the SM electroweak sector. Understanding the existence of dark matter in the universe is one of the motivations for studying BSM physics. Our present understanding of the universe tells us the universe is made of up of about 4% ordinary matter, 20% dark matter and 76% dark energy [15]. Dark matter is composed of particles that do not absorb, reflect, or emit light, so they cannot

be detected by observing electromagnetic radiation whereas dark energy is the hypothesized source of energy that is accelerating the expansion rate of the universe[16, 17]. Understanding dark matter is important to understanding the size, shape and future of the universe. Concepts of dark matter also help in explaining the formation and evolution of galaxies and clusters[18, 19]. Few works on dark matter physics can be found in [20] and [21]. Also, the baryon asymmetry of the universe, electroweak baryogenesis [22–24] and the strong CP problem [25, 26] serve as other reasons to extend the scalar sector of the SM. With these motivations to study BSM physics, in this thesis, we focus on the two Higgs doublet model (2HDM), one of the most simplistic extensions of the SM [12, 13] where we just add a second scalar Higgs doublet to the already existing one in the SM. Adding a second doublet leads to a richer phenomenology as there are now 8 degrees of freedom. Just like in the SM, 3 Goldstone bosons are absorbed by the $W^{\pm}$ and Z^0 bosons via spontaneous symmetry breaking leaving 4 physical scalar states. We discuss in detail the concepts of electroweak symmetry breaking with respect to the 2HDM in Chapter 3 of this thesis. The remaining 4 physical scalar states are the CP even states (h, H), CP odd (A) and the charged Higgs bosons $(H^{\pm})$. The discovered Higgs boson at the LHC is measured to be CP even, so by convention, we could either map h or H with the observed Higgs. The lighter CP even Higgs boson h may have couplings exactly like the SM-Higgs boson. This occurs in the so called decoupling limit. In another such limit, the heavier CP even boson H is SM-like, leaving h to be the lighter than the discovered Higgs. We have discussed these limits in Chapters 4, 5 and 6 of this thesis. 2HDMs can be categorized into four different classes based on which type of fermions couple to a specific doublet. These classes are usually grouped as Type I, Type II, X and Y. In this thesis, we focus on the Type II 2HDMs (MSSM-like) where up type quarks couple to one of the doublets and down type quarks and charged leptons couple to the second doublet. This second doublet appears in the most popular scenario of BSM, supersymmetry. MSSM which means minimal supersymmetric standard model is an extension to the SM that realizes supersymmetry[27, 28]. MSSM only considers the minimum number of new particle states and new interactions consistent with phenomenology. Supersymmetry is a basic principle that proposes the relationship between bosons and fermions such that

every SM particle has a superpartner yet undiscovered [29].

1.3 Brief Research Methodology

This section outlines brief research techniques we employed in probing the phenomenological aspects of the type II CP conserving 2HDM. To successfully achieve the purpose of this work, we scrutinize the physical mass eigenstates of the model. For the numerical analysis, we modified the two Higgs doublet model calculator (2HDMC) [30] to suit our research interest. We also performed a check on the model with the help of Mathematica [31]. One important parameter in the 2HDM is $\tan\beta$ which is defined as the ratio of the vacuum expectation values of the doublets. We then impose constraints from signal measurements of the observed 125.09 GeV Higgs boson at the LHC using the Lilith [32] Python embedded programming tool. Also, we choose three benchmark scenarios for our analysis. These benchmark scenarios can be found in section 3.3.2 . Lilith is a Python library that can also be used in C[33] and C++[34] /ROOT[35] programs and it includes the latest experimental measurements from both the ATLAS and CMS collaborations at the LHC. Also, easily to understand codes in Bash Shell Scripts[36], Python[37] and Perl[38] Programming were all written by myself from scratch to obtain possible decay rates and production cross sections which is very needful in our analysis. With these research tools and techniques in hand, we present both analytical and phenomenological discussions in Chapters 4 , 5 and 6 of this thesis.

1.4 Organization of this thesis

We organize the thesis into 7 chapters. The following are what each chapter contains: Chapter 1 focuses on a brief background overview of fundamental particles and their interactions in the SM. We also present the motivation for studying BSM physics and a brief research method in this chapter. In Chapter 2 , we review the SM Higgs sector, where we discuss the particle content of the SM, concepts of electroweak symmetry breaking and the Higgs mechanism. We also show the interaction of the SM Higgs boson with gauge bosons and fermions

and give mass expressions for both gauge bosons and the fermions. Finally, we discuss the production and decay rates of the SM Higgs. Chapter 3 highlights the CP conserving 2HDMs where we describe the Higgs potential in the different bases and to avoid many mathematical complexities, we only show how to find the Goldstone bosons, masses of the gauge bosons and fermions by minimizing the full scalar potential of the 2HDM. We also present in this chapter the Higgs interactions with gauge bosons and fermions as well as theoretical constraints in the 2HDM. We also discuss experimental constraints from LHC measurements of the 125.09GeV Higgs boson. In Chapter 4 , we present results and discussions for searches of the heavy Higgs within the type II 2HDM. In Chapter 5 , we present analytical expressions for the partial decay widths and phenomenological analysis for searches of the pseudoscalar Higgs, A within the type II 2HDM. Chapter 6 also presents analytical expressions for the partial decay widths and phenomenological analysis for searches of the charged Higgs, $H^{\pm}$ within the type II 2HDM. Finally, in Chapter 7 , we conclude the thesis by summarizing the main contributions examined in the previous chapters and providing recommendations that might be useful for future research studies.

Chapter 2

The Standard Model Higgs Sector

This chapter highlights the fundamental principles of the Standard Model Higgs sector. We first present the particle content of the SM, concepts of spontaneous symmetry breaking, and the Higgs mechanism, which describes the origin of particle masses. We also discuss the branching ratios and production cross section of the SM Higgs.

2.1 Particle content of the SM

The Standard Model (SM) is a relativistic quantum field theory based on $SU(3)_C \otimes SU(2)_L \otimes U(1)_Y$ gauge symmetry. The $SU(2)_L \otimes U(1)_Y$ forms the electroweak theory where L is a sub-index which refers to the fact that the weak $SU(2)$ group acts only on the left-handed projections of fermion states and Y is the hypercharge. The $SU(3)_C$ component gives a correct description to strong interactions in the SM. Up to date, the SM has proven to be in perfect agreement with experimental data. We have summarized the particle content of the SM in Table 2.1 below. From Table 2.1 , we show the spin one bosons (γ, W^+, W^-, Z, g). The scalar Higgs boson is the only spin 0 particle. The fermions are the spin half particles which come in 2 types, quarks and leptons. These are grouped into three generations. We have the up-type quarks and the down type quarks on the left which have charges of $+2/3$ and $-1/3$ respectively. The leptons are also grouped into 3 generations with electrons, muons, tauons, and their respective neutrinos. The neutrinos are neutral, whereas the electrons, muons and

tauons are negatively charged particles with charge -1.

Table 2.1: Particle content of the Standard Model

This table was taken from [39].

Bosons	**Scalars**
γ, W^+, W^-, Z^0, $g_{1\ldots8}$	ϕ (Higgs)
Fermions	
Quarks (each with 3 colour charges)	Leptons
$2/3:$ $\begin{pmatrix} u \\ d \end{pmatrix}$, $\begin{pmatrix} c \\ s \end{pmatrix}$, $\begin{pmatrix} t \\ b \end{pmatrix}$	neutral: $\begin{pmatrix} \nu_e \\ e^- \end{pmatrix}$, $\begin{pmatrix} \nu_\mu \\ \mu^- \end{pmatrix}$, $\begin{pmatrix} \nu_\tau \\ \tau^- \end{pmatrix}$
$-1/3:$	$-1:$

2.2 Concepts of Symmetry breaking

In this section, we review the basic concepts of spontaneous symmetry breaking of gauge symmetries.

2.2.1 Spontaneous symmetry breaking

For a spontaneous symmetry breaking to occur, the given Lagrangian must be continuously invariant under the symmetry. However, the vacuum which is the lowest state does not possess the same symmetry as it Lagrangian [40]. The mass terms in the Lagrangian for the gauge bosons and fermions are not allowed as such a Lagrangian is not gauge invariant. The weak bosons are not massless, hence there is the need for a mechanism through which both bosons and fermions can get their mass terms [41–44].

- **Simple example of symmetry breaking**

Now, let's begin with a very simple model for a real scalar field ϕ, with a specific potential term. We assume this real scalar field ϕ to be the Higgs field. The Lagrangian can be fully expressed in terms of the kinetic and potential terms as;

$$\mathcal{L} = \frac{1}{2}\left(\partial_\mu \phi\right)^2 - V\left(\phi\right) \tag{2.1}$$

Where the potential $V(\phi)$ is;

$$V(\phi) = \frac{1}{2}\mu^2\phi^2 + \frac{1}{4}\lambda\phi^4 \tag{2.2}$$

The above Lagrangian is symmetric or invariant under $\phi \to -\phi$ and λ is positive to ensure an absolute minimum in the Lagrangian. There are two different possibilities for the sign of μ^2, which are positive and negative values of μ^2.

With $\mu^2 > 0$, everything seems superficial. Let's see this by first minimizing the potential in equation 2.2 above. Minimizing this potential means taking the derivative of the potential with respect to ϕ and setting it to zero.

$$\begin{aligned} \frac{\partial V(\phi)}{\partial \phi} &= \frac{2}{2}\mu^2\phi + \frac{4}{4}\lambda\phi^3 \\ 0 &= \mu^2\phi + \lambda\phi^3 \\ 0 &= \phi\left(\mu^2 + \lambda\phi^2\right) \end{aligned} \tag{2.3}$$

From the minimization potential in equation 2.3 above, we can see that with $\mu^2 > 0$, the vacuum of such states corresponds to zero, that is

$$\mu^2 > 0 \to v = \langle\phi\rangle = 0 \tag{2.4}$$

Here, $SU(2)_L \times U(1)_Y$ symmetric is unbroken at the minimum and the Lagrangian describes a free particle of mass μ that has an additional four-point interaction $-\frac{1}{4}\lambda\phi^4$.

For $\mu^2 < 0$, the vacuum of this state does not correspond to zero. Again from equation 2.3, we see that if $\mu^2 < 0$, then we get;

$$\mu^2 < 0 \to v = \langle\phi\rangle = \pm\sqrt{\frac{-\mu^2}{\lambda}} \quad \text{or} \quad \mu^2 = -\lambda v^2 \tag{2.5}$$

We are much interested in this case as compared to the previous case since the non zero vacuum value breaks the $SU(2)_L \times U(1)_Y$ symmetry. By checking the potential, we see that it makes little sense to interpret the particle spectrum using the field ϕ since perturbation

theory around $\phi = 0$ will not converge as the vacuum is located at equation 2.5 above. Therefore, to investigate the particle spectrum in the theory, we will have to look at small perturbations around the minimum. To do this, it is more natural and appropriate to introduce a new field η which is simply a shift of the field ϕ that is centered at the vacuum: $\eta = \phi - v$. The next step is to write the Lagrangian with respect to this new field. For simplicity, we follow the Lagrangian in Eq. 2.1 then write out the kinetic and potential terms separately, and later give an expression for the full Lagrangian. The kinetic term is expressed as;

$$\begin{aligned}
\text{kinetic term} &= \frac{1}{2}\left(\partial_\mu \phi\right)\left(\partial^\mu \phi\right) \\
&= \frac{1}{2}\left(\partial_\mu \left(\eta + v\right)\right)\left(\partial^\mu \left(\eta + v\right)\right) \\
&= \frac{1}{2}\left(\partial_\mu \eta + \partial_\mu v\right)\left(\partial^\mu \eta + \partial^\mu v\right) \\
&= \frac{1}{2}\left(\partial_\mu \eta\right)\left(\partial^\mu \eta\right) \quad \text{since} \quad \partial_\mu v = \partial^\mu v = 0
\end{aligned} \tag{2.6}$$

The potential term can be written as;

$$\begin{aligned}
V\left(\phi\right) =& \frac{1}{2}\mu^2\phi^2 + \frac{1}{4}\lambda\phi^4 \\
&= \frac{1}{2}\mu^2\left(\eta + v\right)^2 + \frac{1}{4}\lambda\left(\eta + v\right)^4 \\
&= \frac{1}{2}\mu^2\left(\eta^2 + 2\eta v + v^2\right) + \frac{1}{4}\lambda\left(\eta^4 + 4\eta^3 v + 6\eta^2 v^2 + 4\eta v^3 + v^4\right)
\end{aligned} \tag{2.7}$$

But from equation 2.5, $\mu^2 = -\lambda v^2$

$$\begin{aligned}
V\left(\phi\right) =& \frac{-\lambda v^2}{2}\left(\eta^2 + 2\eta v + v^2\right) + \frac{1}{4}\lambda\left(\eta^4 + 4\eta^3 v + 6\eta^2 v^2 + 4\eta v^3 + v^4\right) \\
&= -\frac{\lambda\eta^2 v^2}{2} - \lambda\eta v^3 - \frac{\lambda v^4}{2} + \frac{1}{4}\lambda\eta^4 + \lambda\eta^3 v + \frac{3}{2}\eta^2 v^2 + \lambda\eta v^3 + \frac{1}{4}\lambda v^4 \\
&= \lambda v^2\eta^2 + \lambda v\eta^3 + \frac{1}{4}\lambda\eta^4 - \frac{1}{4}\lambda v^4
\end{aligned} \tag{2.8}$$

Combining both the kinetic 2.6 and potential 2.8 terms above, we can write out the full Lagrangian as:

$$\mathcal{L} = \frac{1}{2}\left(\partial_\mu \eta\right)\left(\partial^\mu \eta\right) - \lambda v^2 \eta^2 - \lambda v \eta^3 - \frac{1}{4}\lambda \eta^4 + \frac{1}{4}\lambda v^4 \tag{2.9}$$

This Lagrangian describes a particle η with mass:

$$m_\eta = \sqrt{2\lambda v^2} \tag{2.10}$$

This massive real scalar field is what we usually refer to as the Higgs field.

- **Breaking a global symmetry**

Having discussed a simple example of symmetry breaking in the previous section, we hereby present the idea of a global symmetry breaking where in reality, the SM Higgs sector is described by a weak isospin doublet. This means that we are free to introduce an additional complex field which has two degrees of freedom. Let us now consider the additional complex scalar field with two degrees of freedom as;

$$\phi = \frac{1}{\sqrt{2}}\left(\phi_1 + i\phi_2\right) \tag{2.11}$$

The Lagrangian in terms of the potential can be expressed as;

$$\mathcal{L} = \left(\partial_\mu \phi\right)^* \left(\partial^\mu \phi\right) - V\left(\phi\right), \qquad \text{with } V\left(\phi\right) = \mu^2\left(\phi^* \phi\right) + \lambda\left(\phi^* \phi\right)^2 \tag{2.12}$$

The above Lagrangian is invariant under $U(1)$ global symmetry, that is, it is invariant under the transformation $\phi^{'} \rightarrow e^{i\alpha}\phi$. The full Lagrangian in terms of ϕ_1 and ϕ_2 can be expressed as ;

$$\mathcal{L}\left(\phi_1, \phi_2\right) = \frac{1}{2}\left(\partial_\mu \phi_1\right)^2 + \frac{1}{2}\left(\partial_\mu \phi_2\right)^2 - \frac{1}{2}\mu^2\left(\phi_1^2 + \phi_2^2\right) - \frac{1}{4}\lambda\left(\phi_1^2 + \phi_2^2\right)^2 \tag{2.13}$$

Again, there are two distinct possibilities to treat the behavior of the particle by studying the Lagrangian, for which $\mu^2 > 0$ and $\mu^2 < 0$.

- **Case 1:** For $\mu^2 > 0$

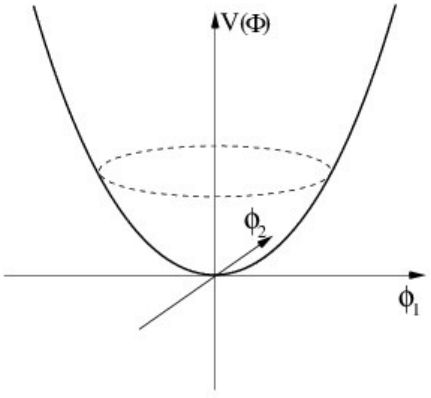

Figure 2.1: Potential $V(\phi)$ for $\mu^2 > 0$.

In this case, the vacuum occurs at $\phi_1 = \phi_2 = 0$ and is also symmetric in both ϕ_1 and ϕ_2. The Lagrangian describes two massive scalar particles each with mass μ in the given expression below;

$$\mathcal{L}(\phi_1, \phi_2) = \frac{1}{2}(\partial_\mu \phi_1)^2 - \frac{1}{2}\mu^2\phi_1^2 + \frac{1}{2}(\partial_\mu \phi_2)^2 - \frac{1}{2}\mu^2\phi_2^2 - \frac{1}{4}\lambda\left(\phi_1^2 + \phi_2^2\right)^2 \tag{2.14}$$

- **Case 2:** For $\mu^2 < 0$

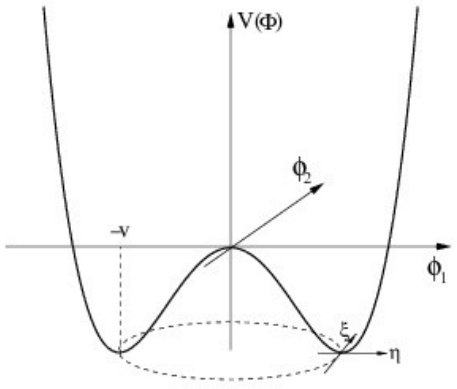

Figure 2.2: Potential $V(\phi)$ for $\mu^2 < 0$.

The sketch for the potentials in Figs. 2.1 and 2.2 were taken from [45].

In this case, there is not a single vacuum located at the point $\binom{0}{0}$. However, there exist an infinite number of vacua which satisfies the vev;

$$\sqrt{\phi_1^2 + \phi_2^2} = \frac{-\mu^2}{\lambda} = v \tag{2.15}$$

From the infinite number of vacua, we can choose ϕ_0 as $\phi_1 = v$ and $\phi_2 = 0$. Now, studying the Lagrangian under small fluctuations around the vacuum, it is natural to define the shifted fields η and ξ in terms of ϕ_1 and ϕ_2 as;

$$\eta = \phi_1 - v \quad \text{and} \quad \xi = \phi_2 \tag{2.16}$$

Hence, ϕ_0 can be expressed in terms of v and the shifted field ξ as;

$$\phi_0 = \frac{1}{\sqrt{2}} (\eta + v + i\xi) \tag{2.17}$$

We can now re-write the Lagrangian in terms of the shifted fields using;

$$\phi^2 = \phi^* \phi = \frac{1}{2} \left[(v + \eta)^2 + \xi^2 \right] \quad \text{and} \quad \mu^2 = -\lambda v^2 \tag{2.18}$$

From the Lagrangian in Eq. 2.13, we then write the kinetic and potential terms of the Lagrangian in terms of the shifted fields as;

$$\begin{aligned} \text{Kinetic term:} \quad \mathcal{L}(\eta, \xi) &= \frac{1}{2} \partial_\mu (\eta + v - i\xi) \partial^\mu (\eta + v + i\xi) \\ &= \frac{1}{2} (\partial_\mu \eta)^2 + (\partial_\mu \xi)^2, \quad \text{since} \quad \partial_\mu v = 0 \end{aligned} \tag{2.19}$$

$$\begin{aligned} \text{Potential:} \quad V(\eta, \xi) &= \mu^2 \phi^2 + \lambda \phi^4 \\ &= -\frac{1}{2} \lambda v^2 \left[(v + \eta)^2 + \xi^2 \right] + \frac{1}{4} \lambda \left[(v + \eta)^2 + \xi^2 \right]^2 \\ &= -\frac{1}{4} \lambda v^4 + \lambda v^2 \eta^2 + \lambda v \eta^3 + \frac{1}{4} \lambda \eta^4 + \frac{1}{4} \lambda \xi^4 + \lambda v \eta \xi^2 + \frac{1}{2} \lambda \eta^2 \xi^2 \end{aligned} \tag{2.20}$$

The full Lagrangian from Eqs. 2.19 and 2.20 can be written as;

$$\mathcal{L}(\eta, \xi) = \frac{1}{2}(\partial_\mu \eta)^2 - \left(\lambda v^2\right)\eta^2 + \frac{1}{2}(\partial_\mu \xi)^2 + 0 \cdot \xi^2 + \text{higher order terms} \tag{2.21}$$

This Lagrangian describes a massive scalar particle of mass η and a massless particle of mass ξ both identified as;

$$m_\eta = \sqrt{2\lambda v^2} = \sqrt{-2\mu^2} > 0 \quad \text{and} \quad m_\xi = 0 \tag{2.22}$$

To summarize what happens after continuously breaking a global symmetry, we see that an attempt to introduce some fluctuations around the vacuum expectation value yields one massive and a massless boson. While we assume that the massive particle corresponds to the SM Higgs boson, the massless boson is the so-called Nambu-Goldstone boson or the Goldstone boson [46, 47]. According to the Goldstone theorem [48, 49], if a continuous global symmetry is broken spontaneously, for each broken group generator, there must appear in the theory a massless particle called Nambu-Goldstone boson. Also, during the spontaneous symmetry breaking of the $SU(2)_L \otimes U(1)_Y$, 3 generators are broken [7, 50]. These three Goldstone bosons correspond to the longitudinal polarization components of the weak bosons, $W^\pm$ and Z. These Goldstone bosons are absorbed to give mass to the weak bosons [51].

2.3 The SM Higgs mechanism

The masses of all the elementary particles are generated by the spontaneous symmetry breaking of the EW symmetry, caused by the Higgs mechanism. This mechanism is implemented in the SM by introducing a complex $SU(2)_L$ scalar doublet Φ with hypercharge $Y_\Phi = \frac{1}{2}$. This complex doublet is described by a weak isospin doublet given by;

$$\Phi = \begin{pmatrix} \phi^+ \\ \phi^0 \end{pmatrix} = \frac{1}{\sqrt{2}} \begin{pmatrix} \phi_1^+ + i\phi_2^+ \\ \phi_3 + i\phi_4 \end{pmatrix} \tag{2.23}$$

Also, the Higgs mechanism assumes that there exist the Higgs field at every point of the space and the SM Lagrangian can be expressed as;

$$\mathcal{L}_{\Phi} = (\mathcal{D}_{\mu}\Phi)^{\dagger}(\mathcal{D}^{\mu}\Phi) - V(\Phi) + \mathcal{L}_{\text{Yukawa}}, \tag{2.24}$$

Where the first part of the equation defines the kinetic and gauge-interaction terms via the covariant derivative, the second term is the potential term as a function of Φ and the third term describes the Yukawa couplings of the scalar field to fermions. The potential $V(\Phi)$ can be written as;

$$V(\Phi) = -\mu^2\Phi^{\dagger}\Phi + \lambda(\Phi^{\dagger}\Phi)^2. \tag{2.25}$$

And the covariant derivative $\mathcal{D}_{\mu}$ is defined as;

$$\mathcal{D}_{\mu} = \partial_{\mu} - i\frac{g'}{2}B_{\mu} - i\frac{g}{2}W_{\mu}^{a}\sigma^{a}. \tag{2.26}$$

where B_{μ} is the gauge field for $U(1)_Y$ and W_{μ}, gauge field for $SU(2)_L$, $\frac{\sigma^a}{2}$, for $a = 1, 2, 3$ are the $SU(2)$ Lie Algebra operators proportional to the Pauli matrix σ^a. For a particular vacuum expectation value(vev) with a scalar field Φ, the SM symmetry can be spontaneously broken into a residual $U(1)_{em}$ symmetry. In a $U(1)_{em}$ gauge, the SM Higgs doublet is:

$$\Phi = \frac{1}{\sqrt{2}}\begin{pmatrix} 0 \\ v+h \end{pmatrix} \quad \text{with} \quad v = \sqrt{\frac{-\mu^2}{\lambda}} \tag{2.27}$$

This choice of the vev breaks the $SU(2)_L \times U(1)_Y$, but leaves $U(1)_{em}$ invariant. We indicate how the gauge group $SU(3)_C \otimes SU(2)_L \otimes U(1)_Y$ gets broken. The $SU(2)_L$ generators take the form;

$$\begin{aligned}
\sigma^1\Phi &= \begin{pmatrix} 0 & 1 \\ 1 & 0 \end{pmatrix}\begin{pmatrix} 0 \\ \frac{1}{\sqrt{2}}(v+h) \end{pmatrix} = \begin{pmatrix} \frac{1}{\sqrt{2}}(v+h) \\ 0 \end{pmatrix} \\
\sigma^2\Phi &= \begin{pmatrix} 0 & -i \\ i & 0 \end{pmatrix}\begin{pmatrix} 0 \\ \frac{1}{\sqrt{2}}(v+h) \end{pmatrix} = -i\begin{pmatrix} \frac{1}{\sqrt{2}}(v+h) \\ 0 \end{pmatrix} \\
\sigma^3\Phi &= \begin{pmatrix} 1 & 0 \\ 0 & -1 \end{pmatrix}\begin{pmatrix} 0 \\ \frac{1}{\sqrt{2}}(v+h) \end{pmatrix} = -i\begin{pmatrix} 0 \\ \frac{1}{\sqrt{2}}(v+h) \end{pmatrix}
\end{aligned} \tag{2.28}$$

And the $U(1)_Y$ generator takes the form;

$$Y_\Phi = +1 \tag{2.29}$$

As seen above, the $SU(2)_L \otimes U(1)_Y$ group has been broken. This is because all the generators are not invariant and the product is not equal to zero as well.

2.3.1 Interactions with Bosons

To obtain the masses of the gauge bosons, we need to study only the scalar part of the Lagrangian in Eq. 2.24. The potential $V(\phi)$ term gives rise to the mass terms of the Higgs boson and the Higgs self-interactions. For simplicity, we follow the step by step procedure outlined in [51–54]. Examining only the kinetic term of Eq. 2.24 ;

$$\mathcal{L}_{kin} = (\mathcal{D}_\mu \Phi)^\dagger (\mathcal{D}^\mu \Phi) \tag{2.30}$$

Applying the field Φ in Eq. 2.27 to the covariant derivative in Eq. 2.26

$$\mathcal{D}_\mu \Phi = \frac{1}{\sqrt{2}} \begin{pmatrix} -\frac{i}{2} g (W_\mu^1 - i W_\mu^2)(v+h) \\ \partial_\mu h + \frac{i}{2}(g W_\mu^3 - g' B_\mu)(v+h) \end{pmatrix}. \tag{2.31}$$

Dotting $\mathcal{D}_\mu \Phi$ into its Hermitian conjugate gives,

$$\begin{aligned} (\mathcal{D}_\mu \Phi)^\dagger (\mathcal{D}^\mu \Phi) = & \frac{1}{2}(\partial_\mu h)(\partial^\mu h) + \frac{1}{8} g^2 (v+h)^2 (W_\mu^1 - i W_\mu^2)(W^{1\mu} + i W^{2\mu}) \\ & + \frac{1}{8}(v+h)^2 \left(-g' B_\mu + g W_\mu^3\right)^2 \end{aligned} \tag{2.32}$$

From the first line of the above equation, the $\frac{1}{2}(\partial_\mu h)(\partial^\mu h)$ term explains a properly normalized kinetic term for the real scalar field h, the Higgs boson. For the second term on the same line, we note that the combinations $W^1 \pm i W^2$ corresponds to the charged W bosons

$$W_\mu^+ = \frac{W_\mu^1 - i W_\mu^2}{\sqrt{2}}, \qquad W_\mu^- = \frac{W_\mu^1 + i W_\mu^2}{\sqrt{2}}. \tag{2.33}$$

These combinations correspond to W^+ and W^- expressed in terms of the Pauli matrix as;

$$\begin{aligned} W^1_\mu\sigma^1 + W^2_\mu\sigma^2 &= \frac{1}{2}(W^1_\mu - iW^2_\mu)(\sigma^1 + i\sigma^2) + \frac{1}{2}(W^1_\mu + iW^2_\mu)(\sigma^1 - i\sigma^2) \\ &= \sqrt{2}\frac{W^1_\mu - iW^2_\mu}{\sqrt{2}}\sigma^+ + \sqrt{2}\frac{W^1_\mu + iW^2_\mu}{\sqrt{2}}\sigma^- \end{aligned} \tag{2.34}$$

Where

$$(\sigma^1 + i\sigma^2) = 2\sigma^+ = 2\begin{pmatrix} 0 & 1 \\ 0 & 0 \end{pmatrix} \tag{2.35}$$

And

$$(\sigma^1 - i\sigma^2) = 2\sigma^- = 2\begin{pmatrix} 0 & 0 \\ 1 & 0 \end{pmatrix} \tag{2.36}$$

- **Mass terms for the $W^\pm$ bosons**

From the above combinations, the second term on the first line of Eq. 2.32 can be expressed as;

$$\begin{aligned} \mathcal{L}_{21} &= \frac{1}{8}g^2(v+h)^2(W^1_\mu - iW^2_\mu)(W^{1\mu} + iW^{2\mu}) \\ &= \frac{1}{4}g^2(v+h)^2 W^+_\mu W^{-\mu} \\ &= \frac{g^2v^2}{4}W^+_\mu W^{-\mu} + \frac{g^2v}{2}hW^+_\mu W^{-\mu} + \frac{g^2}{4}hhW^+_\mu W^{-\mu}. \end{aligned} \tag{2.37}$$

The first term in Eq. 2.37 above is the mass term for the W boson;

$$\begin{aligned} M^2_W &= \frac{g^2v^2}{4} \\ M_W &= \frac{1}{2}vg \end{aligned} \tag{2.38}$$

The second and third lines in Eq. 2.37 correspond to the interactions of one or two Higgs bosons with W^+W^- which from Feynman rules takes the form;

$$\begin{aligned} hW^+_\mu W^-_\nu : &\qquad i\frac{g^2v}{2}g_{\mu\nu} = igM_W g_{\mu\nu} = 2i\frac{M^2_W}{v}g_{\mu\nu}, \\ hhW^+_\mu W^-_\nu : &\qquad i\frac{g^2}{4} \times 2!\, g_{\mu\nu} = 2i\frac{M^2_W}{v^2}g_{\mu\nu}, \end{aligned} \tag{2.39}$$

- **Mass terms for the Z bosons**

To be able to write out the mass terms for the Z bosons, we consider the third part of the Lagrangian in Eq. 2.32

$$\mathcal{L}_3 = \frac{1}{8}(v+h)^2\left(-g'B_\mu + gW_\mu^3\right)^2 \tag{2.40}$$

First, we consider the linear combinations of W_μ^3 and B_μ such that it does appear as a properly normalized real field in the terms below;

$$\begin{aligned}\left(gW_\mu^3 - g'B_\mu\right) &= \sqrt{g^2+g'^2}\left(\frac{g}{\sqrt{g^2+g'^2}}W_\mu^3 - \frac{g'}{\sqrt{g^2+g'^2}}B_\mu\right)\\ &\equiv \sqrt{g^2+g'^2}\left(c_W W_\mu^3 - s_W B_\mu\right)\\ &\equiv \sqrt{g^2+g'^2}\,Z_\mu,\end{aligned} \tag{2.41}$$

Where $s_W = \sin\theta_W$, $c_W = \cos\theta_W$ and θ_W is known as the weak mixing angle or the so-called Weinberg angle. From the third part of the Lagrangian in Eq. 2.32 ;

$$\begin{aligned}\mathcal{L}_3 &= \frac{1}{8}(v+h)^2\left(-g'B_\mu + gW_\mu^3\right)^2\\ &= \frac{1}{8}(g^2+g'^2)(v+h)^2 Z_\mu Z^\mu\\ &= \frac{(g^2+g'^2)v^2}{8}Z_\mu Z^\mu + \frac{(g^2+g'^2)v}{4}hZ_\mu Z^\mu + \frac{(g^2+g'^2)}{8}hhZ_\mu Z^\mu.\end{aligned} \tag{2.42}$$

The mass term of the Z boson arises from the first term of Eq. 2.42 above

$$\begin{aligned}M_Z^2 &= \frac{(g^2+g'^2)v^2}{4}\\ M_Z &= \frac{1}{2}v\sqrt{g^2+g'^2}\end{aligned} \tag{2.43}$$

Whereas the second and third terms in Eq. 2.42 give interactions of one or two Higgs bosons with ZZ which follows from Feynman rules as;

$$\begin{aligned} hZ_\mu Z_\nu : &\qquad i\frac{(g^2+g'^2)v}{4} \times 2!\, g_{\mu\nu} = i\sqrt{g^2+g'^2} M_Z g_{\mu\nu} = 2i\frac{M_Z^2}{v} g_{\mu\nu}, \\ hhZ_\mu Z_\nu : &\qquad i\frac{(g^2+g'^2)}{8} \times 2! \times 2!\, g_{\mu\nu} = 2i\frac{M_Z^2}{v^2} g_{\mu\nu}, \end{aligned} \tag{2.44}$$

- **Mass relation for the W and Z boson**

Although there is no absolute prediction for the masses of the W and the Z boson, there is however a clear prediction on the ratio between the two masses. Concepts from QED reveal that the photon couples to charge which allows us to relate e, g and g' as;

$$e = g\,(s_W) = g'\,(c_W) \tag{2.45}$$

From Eq. 2.45, we get;

$$\frac{g'}{g} = \tan(\theta_W) \tag{2.46}$$

And therefore;

$$\frac{M_W}{M_Z} = \frac{\frac{1}{2}vg}{\frac{1}{2}v\sqrt{g^2+g'^2}} = c_W \tag{2.47}$$

This predicted ratio is often expressed as the so-called Veltman parameter, ρ:

$$\rho = \frac{M_W^2}{M_Z^2 c_W^2} = 1 \tag{2.48}$$

The current measurements of the M_W, M_Z, and θ_W confirm this relation. Finally, the photon γ emerges as massless as;

$$\begin{aligned} \frac{1}{2}M_\gamma^2 &= 0 \\ M_\gamma &= 0 \end{aligned} \tag{2.49}$$

And the mass of the Higgs boson is also given as;

$$m_h = \sqrt{2\lambda v^2} \tag{2.50}$$

Although the vacuum expectation value, v is known to be $v \approx 246\text{GeV}$, since λ is a free parameter, the mass of the Higgs boson is not predicted in the SM.

2.3.2 Yukawa interactions and fermion mass generation

In this subsection, we look at the couplings of the Higgs doublet Φ to fermions. For simplicity, we present the masses for leptons and quarks, neglecting that of neutrinos.

- **Lepton masses**

A preliminary discussion on the SM fermionic sector in [51] reveals that from QED, the mass terms can be written as;

$$\begin{aligned} -m\bar{\psi}\psi &= -m\bar{\psi}P_L^2\psi - m\bar{\psi}P_R^2\psi \\ &= -m\bar{\psi}_R\psi_L - m\bar{\psi}_L\psi_R. \end{aligned} \tag{2.51}$$

Because the left-handed and right-handed fermions of the SM carry different $\text{SU}(2)_L \times \text{U}(1)_Y$ gauge charges, such mass terms are not gauge invariant and thus cannot be inserted by hand into the Lagrangian [39, 51]. Hence, we can conclude that the SM gauge symmetry forbids explicit mass terms for the fermionic degrees of freedom in the Lagrangian. The fermion mass terms must, therefore, be generated via gauge invariant renormalizable Yukawa couplings to the scalar field Φ. For a single generation, the most general gauge-invariant renormalizable Lagrangian terms involving the Higgs doublet and leptons is given as:

$$\mathcal{L}_{\text{Yukawa}} = -Y_e\bar{e}_R\Phi^\dagger L_L - Y_e^*\bar{L}_L\Phi e_R, \tag{2.52}$$

Where Y_e is the Yukawa coupling between the field Φ and the fermionic fields of the SM, L_L represents the left handed $SU(2)_L$ doublets of quarks and leptons while e_R are the corresponding right handed fermions. And the second term in Eq. 2.52 is the Hermitian conjugate of the first. In unitarity gauge, the field Φ takes the form;

$$\Phi = \begin{pmatrix} 0 \\ (v+h)/\sqrt{2} \end{pmatrix}, \tag{2.53}$$

and one can write $\Phi^\dagger L_L$ as;

$$\Phi^\dagger L_L = \left(0, \frac{v+h}{\sqrt{2}}\right) \begin{pmatrix} \nu_e \\ e \end{pmatrix}_L = \frac{v+h}{\sqrt{2}} e_L, \tag{2.54}$$

The Yukawa Lagrangian can be expressed finally as:

$$\begin{aligned} \mathcal{L}_{\text{Yukawa}} &= -Y_e \frac{1}{\sqrt{2}} \left[(v+h)\bar{e}_R e_L + (v+h)\bar{e}_L e_R\right] \\ &= -\frac{Y_e}{\sqrt{2}}(v+h)\bar{e}e \\ &= -\left(\frac{Y_e v}{\sqrt{2}}\right)\bar{e}e - \frac{Y_e}{\sqrt{2}} h\bar{e}e. \end{aligned} \tag{2.55}$$

The first term in the last line of Eq. 2.55 describes the mass term for the electron which takes the form:

$$m_e = \frac{Y_e v}{\sqrt{2}}. \tag{2.56}$$

Since the electron is a fermion with half-integer spin which obeys Pauli's exclusion principle, the general expression of the mass term for fermions can be written as;

$$m_f = \frac{Y_f v}{\sqrt{2}}. \tag{2.57}$$

Therefore, during spontaneous symmetry breaking Φ acquires a non-zero vacuum expectation value where each fermionic degree of freedom coupled to Φ gets a mass term with the mass parameter in Eq. 2.57 above. The Yukawa coupling of the fermions f to the SM Higgs boson y_f defined in terms of Feynman rule is proportional to Y_f;

$$y_f = \frac{Y_f}{\sqrt{2}} \tag{2.58}$$

And the coupling of the Higgs to fermions according to the Feynman rule in figure 2.3 below can be written as;

$$h\bar{f}f: \quad \frac{-iY_f}{\sqrt{2}} = \frac{-im_f}{v} \tag{2.59}$$

The Feynman rule for the $h\bar{e}e$ vertex can be found in [51]

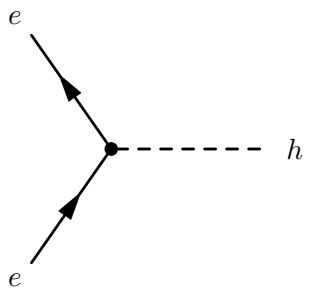

Figure 2.3: Feynman rule for the $h\bar{e}e$ vertex.

- **Quark masses**

Following Eq. 2.52, to describe a single generation of quarks, we write the most general gauge-invariant renormalizable Lagrangian terms involving the Higgs doublet and down type quarks as:

$$\mathcal{L}_{\text{Yukawa}} = -\left[y_d \bar{d}_R \Phi^\dagger Q_L + y_d^* \bar{Q}_L \Phi d_R\right], \tag{2.60}$$

Multiplying out the $\text{SU}(2)_L$ doublets in unitarity gauge,

$$\Phi^\dagger Q_L = \left(0, \frac{v+h}{\sqrt{2}}\right) \begin{pmatrix} u_L \\ d_L \end{pmatrix} = \frac{v+h}{\sqrt{2}} d_L, \tag{2.61}$$

and the Yukawa Lagrangian takes the form:

$$\mathcal{L}_{\text{Yukawa}} = -\left(\frac{y_d v}{\sqrt{2}}\right) \bar{d}d - \frac{y_d}{\sqrt{2}} h \bar{d}d. \tag{2.62}$$

The first term in Eq. 2.62 above is the mass term for the down quark,

$$m_d = \frac{y_d v}{\sqrt{2}} \tag{2.63}$$

And the second term describes the $h\bar{d}d$ coupling.

For up-type quarks, the gauge-invariant Lagrangian term is given as

$$\mathcal{L}_{\text{Yukawa}} = -\left[y_u \bar{u}_R \tilde{\Phi}^\dagger Q_L + y_u^* \bar{Q}_L \tilde{\Phi} u_R\right], \tag{2.64}$$

And the product of the $\mathrm{SU}(2)_L$ doublets in unitarity gauge is

$$\tilde{\Phi}^\dagger Q_L = \left(\frac{v+h}{\sqrt{2}}, 0\right)\begin{pmatrix} u_L \\ d_L \end{pmatrix} = \frac{v+h}{\sqrt{2}} u_L, \tag{2.65}$$

$$\mathcal{L}_{\text{Yukawa}} = -\left(\frac{y_u v}{\sqrt{2}}\right)\bar{u}u - \frac{y_u}{\sqrt{2}} h\bar{u}u. \tag{2.66}$$

The mass term for the up-quark takes the form

$$m_u = \frac{y_u v}{\sqrt{2}} \tag{2.67}$$

And the coupling is $h\bar{u}u$. However, since in the SM, there are three generations of quarks, we can rewrite our left- and right-handed quark fields with a generation index k,

$$Q_{Lk}, \quad u_{Rk}, \quad d_{Rk}, \qquad k = 1, 2, 3. \tag{2.68}$$

The most general form of the quark Yukawa Lagrangian is

$$\mathcal{L}^q_{\text{Yukawa}} = -\sum_{i=1}^{3}\sum_{k=1}^{3}\left[y^u_{ik}\bar{u}_{Ri}\tilde{\Phi}^\dagger Q_{Lk} + y^d_{ik}\bar{d}_{Ri}\Phi^\dagger Q_{Lk}\right] + \text{h.c.}, \tag{2.69}$$

where h.c. is the Hermitian conjugate and the dimensionless couplings y^u_{ik} and y^d_{ik} are (i,k) entries of 3×3 complex matrices.

Replacing Φ with its vacuum value $(0, v/\sqrt{2})^T$, we obtain the quark mass terms:

$$\mathcal{L}^q_{\text{Yukawa}} = -\left(\bar{u}_1, \bar{u}_2, \bar{u}_3\right)_R \mathcal{M}^u \begin{pmatrix} u_1 \\ u_2 \\ u_3 \end{pmatrix}_L - \left(\bar{d}_1, \bar{d}_2, \bar{d}_3\right)_R \mathcal{M}^d \begin{pmatrix} d_1 \\ d_2 \\ d_3 \end{pmatrix}_L + \text{h.c.}, \tag{2.70}$$

where

$$\mathcal{M}^u_{ik} = \frac{v}{\sqrt{2}} y^u_{ik}, \qquad \mathcal{M}^d_{ik} = \frac{v}{\sqrt{2}} y^d_{ik} \tag{2.71}$$

are the quark mass matrices in generation space, each containing 9 complex entries. Finally, the coupling of the Higgs to quarks according to the Feynman rules is

$$h\bar{q}q: \quad \frac{-iy_q}{\sqrt{2}} = \frac{-im_q}{v}, \tag{2.72}$$

where y_q is the appropriate eigenvalue of the Yukawa matrix y^u_{ik} or y^d_{ik}.

2.3.3 Higgs self-couplings

The Higgs self couplings can be obtained from the Higgs potential given as;

$$\mathcal{L}_V = -V(\Phi) = \mu^2\Phi^\dagger\Phi - \lambda(\Phi^\dagger\Phi)^2, \tag{2.73}$$

From unitary gauge, dotting the conjugate of the field Φ to itself gives;

$$\Phi^\dagger\Phi = \frac{1}{2}(h+v)^2, \tag{2.74}$$

Minimizing the potential gives $\mu^2 = \lambda v^2$ and Eq. 2.73 becomes

$$\mathcal{L}_V = -\lambda v^2 h^2 - \lambda v h^3 - \frac{\lambda}{4}h^4 + \text{const.} \tag{2.75}$$

From Eq. 2.75, the first term is the mass term for the Higgs, the second term and third term indicate an interaction vertex involving three Higgs hhh and four Higgs $hhhh$ boson respectively. These vertices according to Feynman rules follow the expressions;

$$hhh: \quad -i\lambda v \times 3! = -6i\lambda v = -3i\frac{m_h^2}{v}, \tag{2.76}$$

$$hhhh: \quad -i\frac{\lambda}{4} \times 4! = -6i\lambda = -3i\frac{m_h^2}{v^2}, \tag{2.77}$$

2.4 The SM Higgs Searches

2.4.1 Decay of the SM Higgs

We review the possible decay modes of the SM Higgs boson. First, we present schematic expressions for the partial decay widths of SM Higgs boson. No detailed calculations nor QCD radiative corrections are shown here. A detail review of QCD radiative corrections in the SM Higgs decay can be found in [45, 55]. We rely on conceptual understanding of the decay of the SM Higgs presented in [56] to write down explicit expressions for the partial widths of the SM Higgs.

2.4.2 Fermionic Decays

The partial decay rate of the Higgs boson decaying into a pair of fermions is expressed as;

$$\Gamma\left(h \to f\bar{f}\right) = \sqrt{2} G_F \frac{m_h m_f^2}{8\pi} N_c^f \left(1 - \frac{4m_f^2}{m_h^2}\right)^{3/2} \tag{2.78}$$

Where G_F is the Fermi coupling constant, m_f is the mass of fermion, m_h is the SM Higgs mass, N_c^f is the number of color factors for which quarks = 3 and leptons = 1. From Eq. 2.78 , the fermionic decays grows linearly with m_h and is proportional to the mass of the fermion m_f. It is proportional to the square of the Yukawa coupling (m_f/v) and also has the kinematic factor $\left[1 - 4m_f^2/m_h^2\right]^{3/2} \equiv \beta^3$, which is $\simeq 1$ when the decay is actually above the threshold (i.e., when $m_h \gg 2m_f$)

2.4.3 Bosonic Decays

The decay rates of the Higgs decaying into a pair of gauge bosons V $(V = W, Z)$ is given by:

$$\Gamma\left(h \to VV\right) = \sqrt{2} G_F \frac{m_h^3}{32\pi} \delta_V \left[1 - \frac{4m_V^2}{m_h^2} + \frac{12m_V^2}{m_h^4}\right] \left(\sqrt{1 - \frac{4m_V^2}{m_h^2}}\right), \text{ valid if } m_h > 2m_V \tag{2.79}$$

Where $\delta_W = 2$ and $\delta_Z = 1$. This expression grows with increasing SM Higgs mass term, m_h^3.

2.4.4 Three body decay modes

If $m_h < 2m_V$, the bosonic decay can only proceed through a virtual V (denoted as V^*). This is the case of the SM Higgs boson. For three-body decay modes, the partial decay widths are;

$$\Gamma(h \to W^+W^{-*} \to W^+ f\bar{f}') = \frac{G_F^2 m_W^4 m_h}{96\pi^3} F\left(\frac{m_W^2}{m_h^2}\right), \tag{2.80}$$

$$\Gamma(h \to ZZ^* \to Zf\bar{f}) = \frac{G_F^2 m_Z^4 m_h}{48\pi^3} F\left(\frac{m_Z^2}{m_h^2}\right)(I_f^2 + 2\sin^4\theta_W Q_f^2 - 2I_f \sin^2\theta_W Q_f), \tag{2.81}$$

Where I_f is the third component of the isospin and Q_f is the electromagnetic charge of the final state fermion f. The function $F(x)$ takes the form;

$$\begin{aligned} F(x) = &-|1-x|\left(\frac{47}{2}x - \frac{13}{2} + \frac{1}{x}\right) + 3(1-6x+4x^2)|\log\sqrt{x}| \\ &+ \frac{3(1-8x+20x^2)}{\sqrt{4x-1}}\cos^{-1}\left(\frac{3x-1}{2x^{3/2}}\right). \end{aligned} \tag{2.82}$$

2.4.5 Loop-induced decay modes

The loop induced decay modes for the SM Higgs are $h \to \gamma\gamma$, $h \to gg$, and $h \to Z\gamma$. We summarize the partial decay widths for each of these decay modes below.

- **Decay of SM Higgs into photons** $h \to \gamma\gamma$

The $h \to \gamma\gamma$ loop is dominated by the W boson loop where the W loop contribution receives a destructive interference from the top quark loop thereby reducing its partial width by roughly 30%. There is a small amount of bottom quark and tau lepton contribution in the loop. The partial decay width of the Higgs into a pair photons can be computed as;

$$\Gamma(h \to \gamma\gamma) = \frac{\sqrt{2}G_F \alpha_{\rm em}^2 m_h^3}{64\pi^3}|\sum_f Q_f^2 N_c^f I_f(m_h) + I_W(m_h)|^2 \tag{2.83}$$

Where the loop functions $I_f(m_h)$ and $I_W(m_h)$ are defined as;

$$I_f(m_h) = -\frac{4m_f^2}{m_h^2}\left[1 - \frac{m_h^2}{2}\left(1 - \frac{4m_f^2}{m_h^2}\right) C_0(0,0,m_h^2,m_f,m_f,m_f)\right] \tag{2.84}$$

$$I_W(m_h) = 1 + \frac{6m_W^2}{m_h^2} - 6m_W^2\left(1 - \frac{2m_W^2}{m_h^2}\right) C_0(0,0,m_h^2,m_f,m_f,m_f) \tag{2.85}$$

- **Decay of SM Higgs into gluons** $h \to gg$

This decay is dominated by the top quark loop where the bottom quark loop also contributes at the few-percent level and the partial decay width can be calculated as;

$$\Gamma(h \to gg) = \frac{\sqrt{2}G_F\alpha_s^2 m_h^3}{128\pi^3}|\sum_{f=q} I_f|^2 \tag{2.86}$$

- **Decay of SM Higgs into** $Z\gamma$

This decay channel is actually enhanced or dominated by the W boson loop where the top-quark loop contribution is very small. The partial width for Higgs to $Z\gamma$ is;

$$\Gamma(h \to Z\gamma) = \frac{\sqrt{2}G_F\alpha_{\rm em}^2 m_h^3}{128\pi^3}\left(1 - \frac{m_Z^2}{m_h^2}\right)^3 |\sum_f Q_f J_f(m_h) + J_W(m_h)|^2, \tag{2.87}$$

where the loop functions $J_f(m_h)$ and $J_W(m_h)$ are;

$$J_f(m_h) = -\frac{2N_c^f}{\sin\theta_W\cos\theta_W}(I_f(m_h) - 2Q_f\sin^2\theta_W)[J_1(m_f) - J_2(m_f)] \tag{2.88}$$

$$\begin{aligned} J_W(m_h) &= -\cot\theta_W \\ &\times \left\{4\left(3 - \tan^2\theta_W\right) J_2(m_W) + \left[\left(1 + \frac{m_h^2}{2m_W^2}\right)\tan^2\theta_W - \left(5 + \frac{m_h^2}{2m_W^2}\right)\right] J_1(m_W)\right\} \end{aligned} \tag{2.89}$$

And $J_1(m)$ and $J_2(m)$ from the Eq.2.88 and Eq.2.89 takes the form;

$$J_1(m) = \frac{2m^2}{m_h^2 - m_Z^2}\Big[1 + 2m^2 C_0(0, m_Z^2, m_h^2, m, m, m) + \frac{m_Z^2}{m_h^2 - m_Z^2}\{B_0(m_h^2, m, m) - B_0(m_Z^2, m, m)\}\Big], \tag{2.90}$$

$$J_2(m) = m^2 C_0(0, m_Z^2, m_h^2, m, m, m). \tag{2.91}$$

C_0 and B_0 are Passarino-Veltman functions[57–59] expressed as;

$$C_0(0, 0, m_h^2, m, m, m) = \frac{-2}{m_h^2} f\left(\frac{4m^2}{m_h^2}\right), \tag{2.92}$$

$$C_0(0, m_Z^2, m_h^2, m, m, m) = \frac{-2}{m_h^2 - m_Z^2}\left[f\left(\frac{4m^2}{m_h^2}\right) - f\left(\frac{4m^2}{m_Z^2}\right)\right], \tag{2.93}$$

And the function $f(x)$ takes the form;

$$f(x) = \begin{cases} [\arcsin(1/\sqrt{x})]^2, & \text{if } x \geq 1, \\ -\frac{1}{4}[\ln \frac{1+\sqrt{1-x}}{1-\sqrt{1-x}} - i\pi]^2, & \text{if } x < 1 \end{cases}. \tag{2.94}$$

2.4.6 SM Higgs branching ratios

Branching ratio is a very useful parameter when talking about the decay of particles. In simple terms, it is the ratio of individual decay modes with respect to the total decay mode of the particle. So, in the case of the SM Higgs, the ratio of the individual decays to the total width of the Higgs yields the branching faction,

$$BR\,(h \to XX) = \frac{\Gamma\,(h \to XX)}{\Gamma^h_{tot}} \tag{2.95}$$

where Γ^h_{tot} is the total width. Table 2.2 shows the predicted branching fractions for the125 GeV SM Higgs boson in the order of size, taken from [51, 60].

Table 2.2: Predicted branching ratios (BRs) for a 125 GeV SM Higgs boson, in order of size.

Decay mode	BR	Notes (as of early 2014)
$b\bar{b}$	58%	Observed at about 2σ at CMS
WW^*	22%	Observed at 4σ
gg	8.6%	
$\tau\tau$	6.3%	Observed at 1–2 σ
$c\bar{c}$	2.9%	
ZZ^*	2.6%	Discovery mode (in $ZZ^* \to 4\mu$, $2\mu 2e$, $4e$)
$\gamma\gamma$	0.23%	Discovery mode
$Z\gamma$	0.15%	
$\mu\mu$	0.022%	
Γ_{tot}	4.1 MeV	

2.4.7 Production cross section of the SM Higgs

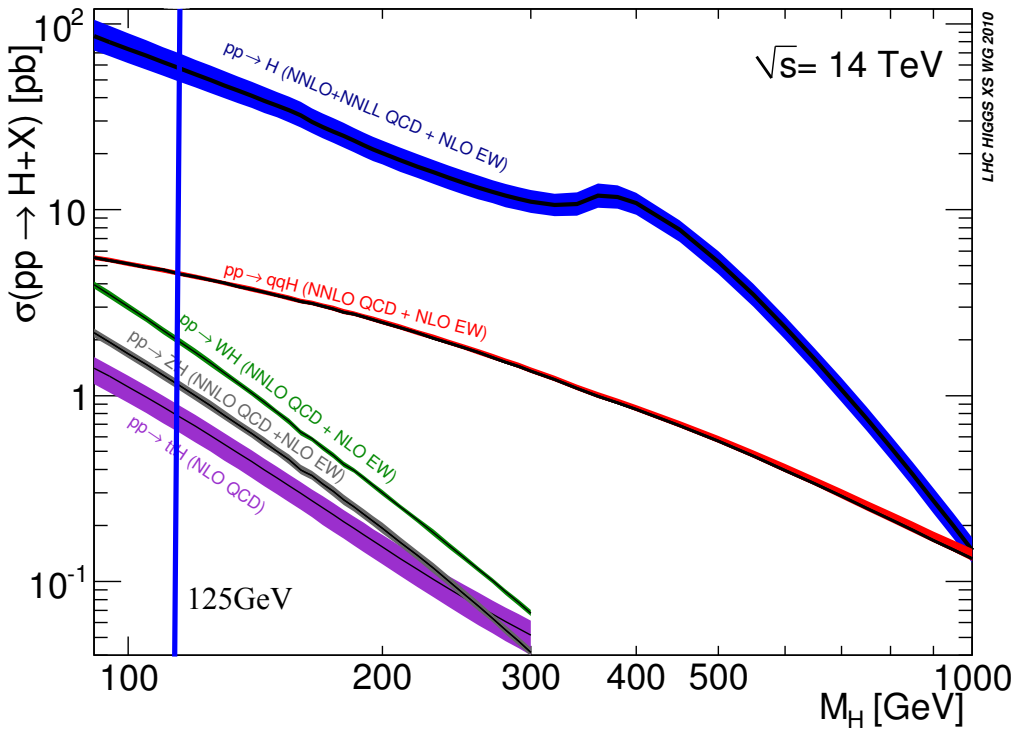

Figure 2.4: LHC cross sections for SM Higgs at $\sqrt{s} = 14$TeV

Fig. 2.4 represents the LHC production cross sections for the SM Higgs at $\sqrt{s} = 14\text{TeV}$ [61]. From Fig. 2.4, the biggest production is the gluon fusion mechanism. Although, the SM Higgs boson has no tree level with gluon directly, the gluon fusion mechanism still dominates since the scalar Higgs boson is produced via a loop in which top quarks run in the loop. It is crucial to note that although all quarks can in principle contribute to the SM Higgs production, the top and bottom quarks give the biggest contributions when it comes to the production of the SM Higgs bosons since the top and bottom quarks have large Yukawa couplings to the SM Higgs boson and the loop function in Eq. 2.94 is non-zero. The second dominant production for the SM Higgs comes from the vector boson fusion. Here, each of the two quarks can radiate a vector boson and since at tree level the Higgs couples with $W^+_\mu W^-_\nu$ and $Z_\mu Z_\nu$ as seen in equations 2.39 and 2.44 respectively, we conclude that these produced vector bosons interact with the SM Higgs boson. Besides, we can produce the SM Higgs via a WH or ZH associated production [62]. Finally, we can also produce the SM Higgs in association with a top-quark pair. The ATLAS experiment at the LHC presents this production channel in [63]. No detail discussion for the last two production channels is given in this thesis since the contributions from these channels are smaller and could be negligible as compared to the gluon-gluon fusion and vector boson fusion.

Chapter 3

The Two Higgs Doublet Model

3.1 Introduction

With the discovery of a new particle [9, 10] at the LHC whose properties were observed to be closer to that of the SM, it is clear that models describing an extended Higgs sector will be significantly constrained by data. In particular, it is important to assess under these constraints all possibilities for other Higgs like states that may have escaped detection at run-1 of the LHC. The two Higgs doublet models (2HDMs) are an especially simple and appealing framework for such considerations. In this chapter, we present the type II CP conserving 2HDM, where we discuss the Higgs scalar potential in different bases. Also, we discuss the interactions of the Higgs scalars with gauge bosons and fermions and finally summarize both theoretical and experimental constraints in the 2HDM.

3.2 The Two Higgs Doublet Model

We describe the Two Higgs Doublet Model (2HDM), where extensive studies have been carried out recently in [64–80] . In the 2HDM, we have two isospin doublet scalar fields Φ_1 and Φ_2 with hyperchare $Y = \frac{1}{2}$. The scalar Lagrangian $\mathcal{L}_{\rm S}$ which introduces the kinetic

terms of the Higgs doublets and their scalar potential is given by

$$\mathcal{L}_S = \sum_{i=1}^{2} (D_\mu \Phi_i)^\dagger (D^\mu \Phi_i) - V_{\text{2HDM}} \ , \tag{3.1}$$

with the the covariant derivative

$$D_\mu = \partial_\mu - \frac{i}{2} g \sum_{a=1}^{3} \sigma^a W_\mu^a - \frac{i}{2} g' B_\mu \tag{3.2}$$

where W_μ^a and B_μ are the gauge fields of the $SU(2)_L$ and $U(1)_Y$ respectively, g and g' are the corresponding coupling constants of the gauge groups and σ^a are the Pauli matrices. The most general Higgs potential is given by

$$\begin{aligned} V_{\text{2HDM}} = {} & m_1^2 |\Phi_1|^2 + m_2^2 |\Phi_2|^2 - (m_3^2 \Phi_1^\dagger \Phi_2 + \text{h.c.}) \\ & + \frac{1}{2}\lambda_1 |\Phi_1|^4 + \frac{1}{2}\lambda_2 |\Phi_2|^4 + \lambda_3 |\Phi_1|^2 |\Phi_2|^2 + \lambda_4 |\Phi_1^\dagger \Phi_2|^2 \\ & + \frac{1}{2}[\lambda_5 (\Phi_1^\dagger \Phi_2)^2 + \lambda_6 |\Phi_1|^2 \Phi_1^\dagger \Phi_2 + \lambda_7 |\Phi_2|^2 \Phi_1^\dagger \Phi_2 + \text{h.c.}], \end{aligned} \tag{3.3}$$

where m_1, m_2 and λ_1 - λ_4 are real parameters while m_3 and λ_5 - λ_7 are complex in general. The Higgs doublets can be parameterized as

$$\Phi_1 = \begin{pmatrix} w_1^+ \\ \frac{1}{\sqrt{2}} (v_1 + h_1 + i z_1) \end{pmatrix}, \qquad \Phi_2 = \begin{pmatrix} w_2^+ \\ \frac{1}{\sqrt{2}} (v_2 + h_2 + i z_2) \end{pmatrix} \tag{3.4}$$

In this thesis, we study the 2HDM with a softly-broken discrete Z_2 symmetry. Under the Z_2 symmetry, we suppose that the Higgs doublets are translated into $\Phi_1 \to +\Phi_1$ and $\Phi_2 \to -\Phi_2$. We impose this symmetry condition in order to avoid tree-level Higgs mediated flavour changing neutral currents[64, 81–87]. The Z_2 invariant Higgs potential can be written as

$$\begin{aligned} V_{\text{2HDM}}^{Z_2} = {} & m_1^2 |\Phi_1|^2 + m_2^2 |\Phi_2|^2 - m_3^2 (\Phi_1^\dagger \Phi_2 + \text{h.c.}) \\ & + \frac{1}{2}\lambda_1 |\Phi_1|^4 + \frac{1}{2}\lambda_2 |\Phi_2|^4 + \lambda_3 |\Phi_1|^2 |\Phi_2|^2 + \lambda_4 |\Phi_1^\dagger \Phi_2|^2 + \frac{1}{2}\lambda_5 [(\Phi_1^\dagger \Phi_2)^2 + \text{h.c.}], \end{aligned} \tag{3.5}$$

where λ_6 and λ_7 in Eq. (3.3) are forbidden by the Z_2 symmetry. In the Z_2 invariant Higgs potential, there are six real parameters and two complex parameters. We now turn to discuss the Higgs scalar potential in different bases.

3.2.1 The Higgs scalar potential in different bases

There are several different bases which can be employed to specify the parameters of the Higgs sector in the two Higgs doublet model. Despite the fact that some of these bases are less used, each of them possess unique advantages. Table 3.1 below shows a full list of input parameters for the Higgs potential in different bases and their parametrization choices.

Table 3.1: Input parameters for the Higgs potential in different bases and parametrizations

Type	Free parameters
General basis	λ_1, λ_2, λ_3, λ_4, λ_5, λ_6, λ_7, m_{12}^2, $\tan\beta$
Physical basis	m_h, m_H, m_A, $m_{H^\pm}$, $\sin(\beta-\alpha)$, λ_6, λ_7, m_{12}^2, $\tan\beta$
Higgs Hunter's Guide basis	Λ_1, Λ_2, Λ_3, Λ_4, Λ_5,Λ_6, $\tan\beta$
Higgs basis	Z_1, Z_2, Z_3, Z_4, Z_5,Z_6, Z_7, $m_{H^\pm}$

- **General basis[88, 89]**

The general basis is a widely used basis when studying the theoretical framework of the 2HDM. For a CP conserving 2HDM where $\lambda_6 = \lambda_7 = 0$, the most general Higgs scalar potential in Eq. (3.3) yields the Z_2 invariant Higgs potential in Eq. (3.5). Hence, from Eq. (3.5), the parameters of the scalar potential are chosen such that the minimum of the scalar potential respects the $\mathrm{U}(1)_{EM}$ gauge symmetry. Then, the scalar field vacuum expectations values take the forms

$$\langle\Phi_1\rangle = \frac{1}{\sqrt{2}}\begin{pmatrix} 0 \\ v_1 \end{pmatrix}, \qquad \langle\Phi_2\rangle = \frac{1}{\sqrt{2}}\begin{pmatrix} 0 \\ e^{i\xi}v_2 \end{pmatrix}. \tag{3.6}$$

If the parameters are real, the phase factor ξ could still be non zero if the vacuum breaks the CP spontaneously. However, if we consider a case where the CP is not broken spontaneously, the parameter choices for which this happens can be avoided and hence the phase factor ξ is

taken to be $\xi = 0$. So, by minimizing the scalar potential that is to say that by just taking the derivative of the scalar potential with respect to the two doublets complex scalar fields $\langle\Phi_1\rangle$ and $\langle\Phi_2\rangle$, then the squared mass matrices m_1^2 and m_2^2 can be eliminated to obtain the following expressions;

$$m_1^2 = m_3^2 \tan\beta - \frac{v^2}{2}(\lambda_1 \cos^2\beta + \bar{\lambda}\sin^2\beta), \tag{3.7}$$

$$m_2^2 = m_3^2 \cot\beta - \frac{v^2}{2}(\lambda_1 \sin^2\beta + \bar{\lambda}\cos^2\beta), \tag{3.8}$$

where $\bar{\lambda} = \lambda_3 + \lambda_4 + \lambda_5$ and

$$v^2 \equiv v_1^2 + v_2^2 = \frac{4m_W^2}{g^2} = (246\ \text{GeV})^2\,. \tag{3.9}$$

Now, after EWSB, there remain 8 degrees of freedom. Therefore, counting up the fields, we have two complex charged scalars $w_1^\pm$ and $w_2^\pm$, two CP even real scalars h_1 and h_2, and two CP odd real scalars z_1 and z_2. Of the original 8 degrees of freedom, three Goldstone bosons are absorbed by the $W^\pm$ and Z via electroweak symmetry breaking, just like what happens in the SM. The remaining five physical Higgs particles are: two CP even scalars ($h, H,$ with $m_h \leq m_H$), a CP odd scalar A and charged Higgs pair $H^\pm$. The masses of $H^\pm$ and A can be calculated as

$$m_{H^\pm}^2 = M^2 - \frac{v^2}{2}(\lambda_4 + \lambda_5), \quad m_A^2 = M^2 - v^2\lambda_5, \tag{3.10}$$

where M, the soft breaking Z_2 symmetry parameter is given by

$$M^2 = \frac{m_3^2}{\sin\beta\cos\beta}. \tag{3.11}$$

The mass matrix for the neutral CP-even scalar states is

$$V_{\text{2HDM}}^{\text{CP-even}} = \frac{1}{2}(h_1', h_2') \begin{pmatrix} M_{11}^2 & M_{12}^2 \\ M_{12}^2 & M_{22}^2 \end{pmatrix} \begin{pmatrix} h_1' \\ h_2' \end{pmatrix}, \tag{3.12}$$

where matrix elements are

$$M_1^2 = v^2(\lambda_1 \cos^4\beta + \lambda_2 \sin^4\beta) + \frac{v^2}{2}\bar{\lambda}\sin^2 2\beta, \tag{3.13}$$

$$M_2^2 = M^2 + v^2 \sin^2\beta\cos^2\beta(\lambda_1 + \lambda_2 - 2\bar{\lambda}), \tag{3.14}$$

$$M_{12}^2 = \frac{v^2}{2}\sin 2\beta(-\lambda_1\cos^2\beta + \lambda_2\sin^2\beta) + \frac{v^2}{2}\sin 2\beta\cos 2\beta\bar{\lambda}. \tag{3.15}$$

To diagonalize the mass matrix for the CP-even scalar states, we introduce the mixing angle α as:

$$\begin{pmatrix} h_1' \\ h_2' \end{pmatrix} = R(\alpha-\beta)\begin{pmatrix} H \\ h \end{pmatrix}. \tag{3.16}$$

The mass eigenvalues are

$$m_{H,h}^2 = \frac{1}{2}\left[M_1^2 + M_2^2 \pm \sqrt{(M_1^2+M_2^2)^2 + 4M_{12}^2}\right]. \tag{3.17}$$

The mixing angle $\alpha - \beta$ is expressed in terms of the mass matrix elements in Eq. (3.2.1)

$$\tan 2(\alpha-\beta) = \frac{2M_{12}^2}{M_1^2 - M_2^2}. \tag{3.18}$$

- **Physical basis[88, 90, 91]**

Another useful basis in the 2HDM is the physical basis. The physical basis parametrization is useful for phenomenological studies. As the name implies, in the physical basis, the input parameters are described by the 4 physical scalar boson masses: $m_{H^\pm}$, m_A, m_H, m_h, two mixing angles α and β, the VEV v, and the soft-breaking scale of the Z_2 symmetry M. In this basis, we rewrite the quartic couplings $\lambda_1 - \lambda_5$ in terms of the physical parameters as

$$\lambda_1 = \frac{1}{v^2\cos^2\beta}\left[-\sin^2\beta M^2 + \cos^2\alpha m_H^2 + \sin^2\alpha m_h^2\right], \tag{3.19}$$

$$\lambda_2 = \frac{1}{v^2\sin^2\beta}\left[-\cos^2\beta M^2 + \sin^2\alpha m_H^2 + \cos^2\alpha m_h^2\right], \tag{3.20}$$

$$\lambda_3 = -\frac{M^2}{v^2} + \frac{2m_{H^\pm}^2}{v^2} + \frac{1}{v^2}\frac{\sin 2\alpha}{\sin 2\beta}(m_H^2 - m_h^2), \tag{3.21}$$

$$\lambda_4 = \frac{1}{v^2}(M^2 + m_A^2 - 2m_{H^\pm}^2), \tag{3.22}$$

$$\lambda_5 = \frac{1}{v^2}(M^2 - m_A^2). \tag{3.23}$$

- **Higgs Hunter's Guide basis[88, 89, 92]**

The Higgs Hunter's guide basis is an alternative approach to parametrize the Higgs scalar potential in the 2HDM which was originally introduced in [92]. In the HHG basis, the most general gauge invariant Higgs potential of the CP conserving 2HDM under a discrete symmetry $\Phi_1 \to -\Phi_2$ is given by;

$$\begin{aligned}\mathcal{V} = {} & \Lambda_1\left(\Phi_1^\dagger\Phi_1 - V_1^2\right)^2 + \Lambda_2\left(\Phi_2^\dagger\Phi_2 - V_2^2\right)^2 + \Lambda_3\left[\left(\Phi_1^\dagger\Phi_1 - V_1^2\right) + \left(\Phi_2^\dagger\Phi_2 - V_2^2\right)\right]^2 \\ & + \Lambda_4\left[(\Phi_1^\dagger\Phi_1)(\Phi_2^\dagger\Phi_2) - (\Phi_1^\dagger\Phi_2)(\Phi_2^\dagger\Phi_1)\right] + \Lambda_5\left[\Re(\Phi_1^\dagger\Phi_2) - V_1V_2\cos\xi\right]^2 \\ & + \Lambda_6\left[\Im(\Phi_1^\dagger\Phi_2) - V_1V_2\sin\xi\right]^2\end{aligned} \tag{3.24}$$

where the Λ_i are real parameters. The vacuum expectation values of the 2HDM fields $V_{1,2}$ are related to the $v_{1,2}$ of Eq. (3.3) by $V_{1,2} = v_{1,2}/\sqrt{2}$. From Appendix A of [89], the conversion from these Λ_i to the λ_i and m_{ij}^2 of Eq. (3.3) is:

$$
\begin{aligned}
\lambda_1 &= 2(\Lambda_1 + \Lambda_3)\,, \\
\lambda_2 &= 2(\Lambda_2 + \Lambda_3)\,, \\
\lambda_3 &= 2\Lambda_3 + \Lambda_4\,, \\
\lambda_4 &= -\Lambda_4 + \tfrac{1}{2}(\Lambda_5 + \Lambda_6)\,, \\
\lambda_5 &= \tfrac{1}{2}(\Lambda_5 - \Lambda_6 - i\Lambda_7)\,, \\
\lambda_6 &= \lambda_7 = 0 \\
m_{11}^2 &= -2V_1^2\Lambda_1 - 2(V_1^2 + V_2^2)\Lambda_3\,, \\
m_{22}^2 &= -2V_2^2\Lambda_2 - 2(V_1^2 + V_2^2)\Lambda_3\,, \\
m_{12}^2 &= V_1V_2(\Lambda_5\cos\xi - i\Lambda_6\sin\xi - \tfrac{i}{2}e^{i\xi}\Lambda_7)\,.
\end{aligned}
\tag{3.25}
$$

The CP-conserving case is most easily obtained by setting $\xi = 0$ and $\Lambda_7 = 0$. In the CP-conserving limit, we inversely convert Eq.3.25 and solve for the Λ_i $(i = 1, \ldots, 6)$. The result is:

$$
\begin{aligned}
\Lambda_1 &= \tfrac{1}{2}\left[\lambda_1 - \bar{\lambda} + 2m_3^2/(v^2\sin\beta\cos\beta)\right]\,, \\
\Lambda_2 &= \tfrac{1}{2}\left[\lambda_2 - \bar{\lambda} + 2m_3^2/(v^2\sin\beta\cos\beta)\right]\,, \\
\Lambda_3 &= \tfrac{1}{2}\left[\bar{\lambda} - 2m_3^2/(v^2\sin\beta\cos\beta)\right]\,, \\
\Lambda_4 &= 2m_3^2/(v^2\sin\beta\cos\beta) - \lambda_4 - \lambda_5\,, \\
\Lambda_5 &= 2m_3^2/(v^2\sin\beta\cos\beta)\,, \\
\Lambda_6 &= 2m_3^2/(v^2\sin\beta\cos\beta) - 2\lambda_5\,,
\end{aligned}
\tag{3.26}
$$

where $v^2\sin\beta\cos\beta = 2V_1V_2$. The mass of the pseudoscalar and charged Higgs bosons can be calculated as

$$
m_A^2 = \Lambda_6 V^2 \quad \text{and} \quad m_{H^\pm}^2 = \Lambda_4 V^2 \tag{3.27}
$$

Where $V^2 \equiv V_1^2 + V_2^2 = (174\text{GeV})^2$. By inverting the relations in Eq. (3.26), one can obtain

the $\Lambda' s$ in terms of the Higgs masses and the angles α and β [12]

$$\begin{aligned}
\Lambda_1 &= \frac{1}{4\cos^2\beta v^2}\left(\cos^2\alpha m_H^2 + \sin^2\alpha M_h^2\right) - \frac{\sin 2\alpha}{\sin 2\beta}\frac{m_H^2 - m_h^2}{4v^2} + \frac{\Lambda_5}{4}\left(1 - \frac{\sin^2\beta}{\cos^2\beta}\right) \\
\Lambda_2 &= \frac{1}{4\sin^2\beta v^2}\left(\sin^2\alpha m_H^2 + \cos^2\alpha m_h^2\right) - \frac{\sin 2\alpha}{\sin 2\beta}\frac{m_H^2 - m_h^2}{4v^2} + \frac{\Lambda_5}{4}\left(1 - \frac{\cos^2\beta}{\sin^2\beta}\right) \\
\Lambda_3 &= \frac{\sin 2\alpha}{\sin 2\beta}\frac{m_H^2 - m_h^2}{4v^2} - \frac{\Lambda_5}{4}; \qquad \Lambda_4 = \frac{m_{H^\pm}^2}{v^2}; \qquad \Lambda_6 = \frac{m_A^2}{v^2}
\end{aligned} \tag{3.28}$$

- **Higgs basis[67, 88, 93, 94]**

For a non CP conserving 2HDM, the gauge invariant scalar potential in the Higgs basis takes almost the same form as in Eq. (3.3) but with new coefficients,

$$\begin{aligned}
\mathcal{V} &= Y_1 H_1^\dagger H_1 + Y_2 H_2^\dagger H_2 + [Y_3 H_1^\dagger H_2 + \text{h.c.}] + \tfrac{1}{2}Z_1 (H_1^\dagger H_1)^2 \\
&+ \tfrac{1}{2}Z_2 (H_2^\dagger H_2)^2 + Z_3 (H_1^\dagger H_1)(H_2^\dagger H_2) + Z_4 (H_1^\dagger H_2)(H_2^\dagger H_1) \\
&+ \left\{\tfrac{1}{2}Z_5 (H_1^\dagger H_2)^2 + \left[Z_6 (H_1^\dagger H_1) + Z_7 (H_2^\dagger H_2)\right] H_1^\dagger H_2 + \text{h.c.}\right\}
\end{aligned} \tag{3.29}$$

where Y_1, Y_2 and $Z_1, \ldots, Z_4$ are real whereas Y_3, Z_5, Z_6 and Z_7 can be complex . With new coefficients, we can define new Higgs doublet fields,

$$H_1 = \begin{pmatrix} H_1^+ \\ H_1^0 \end{pmatrix} \equiv \frac{v_1 e^{-i\xi_1}\Phi_1 + v_2 e^{-i\xi_2}\Phi_2}{v}\,, \qquad H_2 = \begin{pmatrix} H_2^+ \\ H_2^0 \end{pmatrix} \equiv \frac{-v_2 e^{i\xi_2}\Phi_1 + v_1 e^{i\xi_1}\Phi_2}{v}\,. \tag{3.30}$$

From [67], the the real coefficients of the scalar potential in the Higgs basis for an explicitly CP-conserving 2HDM are given by

$$Y_1 = m_{11}^2 c_\beta^2 + m_{22}^2 s_\beta^2 - m_{12}^2 s_{2\beta}\cos\xi\,, \tag{3.31}$$

$$Y_2 = m_{11}^2 s_\beta^2 + m_{22}^2 c_\beta^2 + m_{12}^2 s_{2\beta}\cos\xi\,, \tag{3.32}$$

$$Z_1 = \lambda_1 c_\beta^4 + \lambda_2 s_\beta^4 + \tfrac{1}{2}(\lambda_3 + \lambda_4 + \lambda_5\cos 2\xi)s_{2\beta}^2 + 2s_{2\beta}(\lambda_6 c_\beta^2 + \lambda_7 s_\beta^2)\cos\xi\,, \tag{3.33}$$

$$Z_2 = \lambda_1 s_\beta^4 + \lambda_2 c_\beta^4 + \tfrac{1}{2}(\lambda_3 + \lambda_4 + \lambda_5\cos 2\xi)s_{2\beta}^2 - 2s_{2\beta}(\lambda_6 s_\beta^2 + \lambda_7 c_\beta^2)\cos\xi\,, \tag{3.34}$$

$$Z_3 = \tfrac{1}{4}(\lambda_1 + \lambda_2 - 2\lambda_3 - 2\lambda_4 - 2\lambda_5\cos 2\xi)s_{2\beta}^2 + \lambda_3 - (\lambda_6 - \lambda_7)s_{2\beta}c_{2\beta}\cos\xi\,, \tag{3.35}$$

$$Z_4 = \tfrac{1}{4}(\lambda_1 + \lambda_2 - 2\lambda_3 - 2\lambda_4 - 2\lambda_5\cos 2\xi)s_{2\beta}^2 + \lambda_4 - (\lambda_6 - \lambda_7)s_{2\beta}c_{2\beta}\cos\xi\,, \tag{3.36}$$

Also, the complex coefficients of the scalar potential in the Higgs basis are given by [67] :

$$Y_3 = -e^{-i\xi}\left[\tfrac{1}{2}(m_{11}^2 - m_{22}^2)s_{2\beta} + m_{12}^2 c_{2\beta}\cos\xi + i m_{12}^2 \sin\xi\right], \tag{3.37}$$

$$Z_5 = e^{-2i\xi}\Big\{\tfrac{1}{4}\big[\lambda_1 + \lambda_2 - 2(\lambda_3 + \lambda_4 + \lambda_5\cos 2\xi)\big]s_{2\beta}^2 + \lambda_5\cos 2\xi - (\lambda_6 - \lambda_7)s_{2\beta}c_{2\beta}\cos\xi$$
$$+ i\big[\lambda_5 c_{2\beta}\sin 2\xi - (\lambda_6 - \lambda_7)s_{2\beta}\sin\xi\big]\Big\}, \tag{3.38}$$

$$Z_6 = e^{-i\xi}\Big\{-\tfrac{1}{2}\big[\lambda_1 c_\beta^2 - \lambda_2 s_\beta^2 - (\lambda_3 + \lambda_4 + \lambda_5\cos 2\xi)c_{2\beta}\big]s_{2\beta} + (\lambda_6 c_\beta c_{3\beta} + \lambda_7 s_\beta s_{3\beta})\cos\xi$$
$$+ i\big[\tfrac{1}{2}\lambda_5 s_{2\beta}\sin 2\xi + (\lambda_6 c_\beta^2 + \lambda_7 s_\beta^2)\sin\xi\big]\Big\}, \tag{3.39}$$

$$Z_7 = e^{-i\xi}\Big\{-\tfrac{1}{2}\big[\lambda_1 s_\beta^2 - \lambda_2 c_\beta^2 + (\lambda_3 + \lambda_4 + \lambda_5\cos 2\xi)c_{2\beta}\big]s_{2\beta} + (\lambda_6 s_\beta s_{3\beta} + \lambda_7 c_\beta c_{3\beta})\cos\xi$$
$$+ i\big[-\tfrac{1}{2}\lambda_5 s_{2\beta}\sin 2\xi + (\lambda_6 s_\beta^2 + \lambda_7 c_\beta^2)\sin\xi\big]\Big\}, \tag{3.40}$$

In the Higgs basis, we give new definitions for α and β; $c_\beta = \cos\beta$, $s_\beta = \sin\beta$, α is defined to be the rotation angle which diagonalizes the mass matrix of the neutral CP even states and ξ is expressed in terms of the relative phase factor as $e^{i\xi}$. If $\sin\xi = 0$, then Y_3, Z_5, Z_6 and Z_7 are all real and the scalar potential and the vacuum are CP-conserving. The physical charged Higgs boson is the charged component of the Higgs-basis doublet H_2, and its mass is given by

$$m_{H^\pm}^2 = Y_2 + \tfrac{1}{2}Z_3 v^2\,. \tag{3.41}$$

For the 3 physical neutral Higgs boson, their mass-eigenstates can be examined by simply diagonalizing a 3×3 real symmetric squared-mass matrix that is defined in the Higgs basis [93, 94]

$$\mathcal{M}^2 = \begin{pmatrix} Z_1 v^2 & Z_6 v^2 & 0 \\ Z_6 v^2 & Y_2 + \frac{1}{2}(Z_3 + Z_4 + Z_5)v^2 & 0 \\ 0 & 0 & Y_2 + \frac{1}{2}(Z_3 + Z_4 - Z_5)v^2 \end{pmatrix} \tag{3.42}$$

The CP-odd Higgs boson $A = \sqrt{2}\,\mathrm{Im}\; H_2^0$ with squared mass can be identified as;

$$m_A^2 = Y_2 + \tfrac{1}{2}(Z_3 + Z_4 - Z_5)v^2\,. \tag{3.43}$$

The upper 2×2 matrix block given in equation 3.42 is the CP-even Higgs squared-mass matrix,

$$\mathcal{M}_H^2 = \begin{pmatrix} Z_1 v^2 & Z_6 v^2 \\ Z_6 v^2 & m_A^2 + Z_5 v^2 \end{pmatrix}\,, \tag{3.44}$$

To diagonalize $\mathcal{M}_H^2$, we define the CP-even mass eigenstates, h and H (with $m_h \leq m_H$) by

$$\begin{pmatrix} H \\ h \end{pmatrix} = \begin{pmatrix} c_{\beta-\alpha} & -s_{\beta-\alpha} \\ s_{\beta-\alpha} & c_{\beta-\alpha} \end{pmatrix} \begin{pmatrix} \sqrt{2}\;\mathrm{Re}\; H_1^0 - v \\ \sqrt{2}\,\mathrm{Re}\; H_2^0 \end{pmatrix}\,, \tag{3.45}$$

The squared masses of h and H are then given by,

$$m_{H,h}^2 = \tfrac{1}{2}\left\{ m_A^2 + (Z_1 + Z_5)v^2 \pm \sqrt{\left[m_A^2 + (Z_5 - Z_1)v^2\right]^2 + 4Z_6^2 v^4}\;\right\}. \tag{3.46}$$

The following identity therefore holds,

$$|Z_6|v^2 = \sqrt{\left(m_H^2 - Z_1 v^2\right)\left(Z_1 v^2 - m_h^2\right)}\,. \tag{3.47}$$

Hence, diagonalizing $\mathcal{M}_H^2$ yields the following expressions:

$$Z_1 v^2 = m_h^2 s_{\beta-\alpha}^2 + m_H^2 c_{\beta-\alpha}^2\,, \tag{3.48}$$

$$Z_6 v^2 = (m_h^2 - m_H^2) s_{\beta-\alpha} c_{\beta-\alpha}\,, \tag{3.49}$$

$$m_A^2 + Z_5 v^2 = m_H^2 s_{\beta-\alpha}^2 + m_h^2 c_{\beta-\alpha}^2\,, \tag{3.50}$$

Equation 3.49 implies that:

$$Z_6 s_{\beta-\alpha} c_{\beta-\alpha} \leq 0\,. \tag{3.51}$$

Using the fact that $\beta - \alpha$ is defined modulo π, we can restrict the values to

$$0 \leq \beta - \alpha \leq \pi\,. \tag{3.52}$$

And finally, $c_{\beta-\alpha}$ and $s_{\beta-\alpha}$ can be derived from equations 3.48 and 3.49, where the signs of the corresponding quantities are fixed by equations 3.51 and 3.52:

$$c_{\beta-\alpha} = -\operatorname{sgn}(Z_6)\sqrt{\frac{Z_1 v^2 - m_h^2}{m_H^2 - m_h^2}} = \frac{-Z_6 v^2}{\sqrt{(m_H^2 - m_h^2)(m_H^2 - Z_1 v^2)}}\,, \tag{3.53}$$

$$s_{\beta-\alpha} = \sqrt{\frac{m_H^2 - Z_1 v^2}{m_H^2 - m_h^2}} = \frac{|Z_6| v^2}{\sqrt{(m_H^2 - m_h^2)(Z_1 v^2 - m_h^2)}}\,. \tag{3.54}$$

3.2.2 Gauge boson mass generation

Both the W and Z boson masses receive contributions via the gauge-kinetic [1] terms of the two Higgs doublets. From Eq. (3.1), we can write the kinetic term as

$$\begin{aligned} \mathcal{L} &= \sum_{i=1}^{2} (D_\mu \Phi_i)^\dagger (D^\mu \Phi_i) \\ &= \left(\mathcal{D}_\mu \Phi_1\right)^\dagger \left(\mathcal{D}^\mu \Phi_1\right) + \left(\mathcal{D}_\mu \Phi_2\right)^\dagger \left(\mathcal{D}^\mu \Phi_2\right) \end{aligned} \tag{3.55}$$

From [51], the part of Eq. (3.55) above involving only h^0, H^0, and the vevs is

$$\begin{aligned} \mathcal{L} &= \frac{1}{2}(\partial_\mu h_1)(\partial^\mu h_1) + \frac{1}{2}(\partial_\mu h_2)(\partial^\mu h_2) \\ &\quad + \frac{1}{4} g^2 \left[(h_1 + v_1)^2 + (h_2 + v_2)^2\right] W_\mu^+ W^{-\mu} \\ &\quad + \frac{1}{8}(g^2 + g'^2) \left[(h_1 + v_1)^2 + (h_2 + v_2)^2\right] Z_\mu Z^\mu \end{aligned} \tag{3.56}$$

From the first line of Eq. (3.56), the unitary transformation from the (h_1, h_2) basis to the (h, H) basis gives the proper kinetic terms for the physical states:

$$\mathcal{L} = \frac{1}{2}(\partial_\mu h)(\partial^\mu h) + \frac{1}{2}(\partial_\mu H)(\partial^\mu H) \tag{3.57}$$

[1] Unlike the potential term which we can describe in various bases and parametrizations, the kinetic term of the scalar Lagrangian in Eq. (3.1) is same for all the bases, hence no need to discuss the kinetic terms in their respective basis.

The masses of the W and Z bosons come from the terms involving no scalar fields in the second and third lines of Eq. (3.56):

$$\begin{aligned} m_W^2 &= \frac{g^2}{4}(v_1^2+v_2^2) = \frac{g^2v^2}{4}, \\ m_Z^2 &= \frac{g^2+g'^2}{4}(v_1^2+v_2^2) = \frac{(g^2+g'^2)v^2}{4}, \end{aligned} \tag{3.58}$$

Where the two vevs in the 2HDM are related to that of the SM as, $v_1^2+v_2^2=v^2$.

3.2.3 Fermion mass generation

In contrast to the SM Yukawa Lagrangian, the 2HDM Yukawa Lagrangian brings some interesting properties. The main difference is that, in the most general Yukawa Lagrangian, flavour changing neutral currents (FCNC) arise at the tree-level [95–97] . The Yukawa interaction for the Higgs field is

$$\mathcal{L}_{\rm 2HDM}^{Y} = -\Big[\bar{Q}_L(Y_{d1}\Phi_1+Y_{d2}\Phi_2)d_R + \bar{Q}_L(Y_{u1}\tilde{\Phi}_1+Y_{u2}\tilde{\Phi}_2)u_R + \bar{L}_L(Y_{e1}\Phi_1+Y_{e2}\Phi_2)e_R + \text{h.c.}\Big], \tag{3.59}$$

where $Y_{u1,d1,e1}$ and $Y_{u2,d2,e2}$ are the 3×3 complex matrices and $\tilde{\Phi}_i = i\tau_2\Phi_i^\dagger$, $(i=1,2)$.
From Eq. 3.59, looking at the down-type quark mass terms:

$$\begin{aligned} \mathcal{L}_{\rm Yukawa} &= -\left(Y_{ij}^{d1}\Phi_1^\dagger + Y_{ij}^{d2}\Phi_2^\dagger\right) d_{Ri}Q_{Lj} + \text{h.c.} \\ &= -\left(Y_{ij}^{d1}\frac{v_1}{\sqrt{2}} + Y_{ij}^{d2}\frac{v_2}{\sqrt{2}}\right) d_{Ri}d_{Lj} + \text{h.c.}, \end{aligned} \tag{3.60}$$

This implies that the down-type quark mass matrix is

$$\mathcal{M}_{ij}^{d} = \left(Y_{ij}^{d1}\frac{v_1}{\sqrt{2}} + Y_{ij}^{d2}\frac{v_2}{\sqrt{2}}\right). \tag{3.61}$$

This is just a general complex 3×3 matrix, which can be diagonalized in the same way as in the SM. Diagonalizing $\mathcal{M}^d_{ij}$ diagonalizes the particular linear combination of Y^{d1} and Y^{d2} given by

$$Y^{d1}_{ij} \cos\beta + Y^{d2}_{ij} \sin\beta, \tag{3.62}$$

which is in fact the coefficient of the down-type quark coupling to Φ_H in the Higgs basis. On the other hand, diagonalizing $\mathcal{M}^d_{ij}$ does not generally diagonalize the orthogonal linear combination of y^{d1} and y^{d2},

$$-y^{d1}_{ij} \sin\beta + y^{d2}_{ij} \cos\beta, \tag{3.63}$$

which is the coefficient of the down-type quark coupling to Φ_h in the Higgs basis.

3.2.4 Classes of Two Higgs Doublet Model

There are 4 independent Z_2 charge assignments [98, 99] on quarks and charged leptons as summarized in Table 3.2 below. In the type-I 2HDM, all quarks and charged leptons obtain their masses from the vev of Φ_2. In the type-II 2HDM, masses of up type quarks are generated by the vev of Φ_2, while those of down type quarks and charged leptons are acquired by that of Φ_1. The Higgs sector of the MSSM is a special 2HDM whose Yukawa interactions is of type II. In the ℓ-specific (type-X), all quarks couple to Φ_2 while charged leptons couple to Φ_1. The last one is the Flipped (type-Y) where all down type quarks couple to Φ_1 whereas both up type quarks and charged leptons couple to Φ_2.

Table 3.2: Yukawa couplings for the Four classes of 2HDM

	Type-I	Type-II	ℓ-specific (Type-X)	Flipped (Type-Y)
Up-type	Φ_2	Φ_2	Φ_2	Φ_2
Down-type	Φ_2	Φ_1	Φ_2	Φ_1
Leptons	Φ_2	Φ_1	Φ_1	Φ_2

3.3 Theoretical and experimental constraints

From the scalar potential in Eq. (3.3), the free parameters could be constrained by both theoretical requirements and experimental measurements. The former mainly includes vacuum stability and tree level unitarity when there is a spontaneous breaking of the electroweak symmetry. We adopt the results in [100, 101] for unitarity contraints. Imposing tree-level unitarity constraints [70, 102–104], one can show the upper bounds of values for certain combinations of the Higgs quartic couplings. Also, we force the potential to be perturbative by demanding that all the quartic couplings of the scalar potential obey $|\lambda_i| \leq 8\pi$ for all i [105]. Moreover, the vacuum stability conditions ensure that the potential is bounded from below. We impose these conditions to the physical basis whose input parameters are mainly the physical mass states $(m_h, m_H, m_A, m_{H^\pm})$, $\tan\beta$, and the mixing angle α. To ensure that this condition is imposed, we require the parameters satisfy the conditions as [106, 107].

$$\begin{aligned} &\lambda_1 > 0\,, \qquad \lambda_2 > 0\,, \lambda_3 + \sqrt{\lambda_1\lambda_2} > 0, \quad \sqrt{\lambda_1\lambda_2} + \lambda_3 + \lambda_4 - |\lambda_5| > 0, \\ &2|\lambda_6 + \lambda_7| \leq \frac{1}{2}(\lambda_1 + \lambda_2) + \lambda_3 + \lambda_4 + \lambda_5\,. \end{aligned} \tag{3.64}$$

Next, we show the constraints from experimental measurements. The self energy of the W and Z bosons receives contribution from the neutral CP even and the charged Higgs bosons via the loop effects. Hence, the parameters involved could be constrained by the precision measurements of the oblique parameters denoted by S, T and U [108]. The electroweak oblique parameters S, T, U [109] constitute a sensitive probe of new physics coupling to the EW gauge bosons. The 2HDM contributions to the Peskin-Takeuchi oblique parameters[108] are presented in [110] and [111] as:

$$
\begin{aligned}
\Delta S &= \frac{1}{\pi\, m_Z^2}\Big\{\Big[\mathcal{B}_{22}(m_Z^2\,;m_H^2\,,m_A^2)-\mathcal{B}_{22}(m_Z^2\,;m_{H^\pm}^2\,,m_{H^\pm}^2)\Big] \\
&\quad+\Big[\mathcal{B}_{22}(m_Z^2\,;m_h^2\,,m_A^2)-\mathcal{B}_{22}(m_Z^2\,;m_H^2\,,m_A^2)+\mathcal{B}_{22}(m_Z^2\,;m_Z^2\,,m_H^2)-\mathcal{B}_{22}(m_Z^2\,;m_Z^2\,,m_h^2) \\
&\quad-m_Z^2\mathcal{B}_0(m_Z\,;m_Z\,,m_H^2)+m_Z^2\mathcal{B}_0(m_Z\,;m_Z\,,m_h^2)\Big]\cos^2(\beta-\alpha)\Big\}\,, \qquad (3.65)\\
\Delta T &= \frac{1}{16\pi\, m_W^2\, s_W^2}\Big\{\Big[F(m_{H^\pm}^2\,,m_A^2)+F(m_{H^\pm}^2\,,m_H^2)-F(m_A^2\,,m_H^2)\Big] \\
&\quad+\Big[F(m_{H^\pm}^2\,,m_h^2)-F(m_{H^\pm}^2\,,m_H^2)-F(m_A^2\,,m_h^2)+F(m_A^2\,,m_H^2) \\
&\quad+F(m_W^2\,,m_H^2)-F(m_W^2\,,m_h^2)-F(m_Z^2\,,m_H^2)+F(m_Z^2\,,m_h^2) \\
&\quad+4m_Z^2\overline{B}_0(m_Z^2\,,m_H^2\,,m_h^2)-4m_W^2\overline{B}_0(m_W^2\,,m_H^2\,,m_h^2)\Big]\cos^2(\beta-\alpha)\Big\}\,, \qquad (3.66)\\
\Delta U &= -\Delta S+\frac{1}{\pi m_W^2}\Big\{\Big[\mathcal{B}_{22}(m_W^2,m_A^2,m_{H^\pm}^2)-2\mathcal{B}_{22}(m_W^2,m_{H^\pm}^2,m_{H^\pm}^2)+\mathcal{B}_{22}(m_W^2,m_H^2,m_{H^\pm}^2)\Big] \\
&\quad+\Big[\mathcal{B}_{22}(m_W^2,m_h^2,m_{H^\pm}^2)-\mathcal{B}_{22}(m_W^2,m_H^2,m_{H^\pm}^2)+\mathcal{B}_{22}(m_W^2,m_W^2,m_H^2)-\mathcal{B}_{22}(m_W^2,m_W^2,m_h^2) \\
&\quad-m_W^2\mathcal{B}_0(m_W^2,m_W^2,m_H^2)+m_W^2\mathcal{B}_0(m_W^2,m_W^2,m_h^2)\Big]\cos^2(\beta-\alpha)\Big\}\,, \qquad (3.67)
\end{aligned}
$$

where

$$\mathcal{B}_{22}(q^2;m_1^2,m_2^2)\equiv B_{22}(q^2;m_1^2,m_2^2)-B_{22}(0;m_1^2,m_2^2)\,, \qquad (3.68)$$

$$\mathcal{B}_0(q^2;m_1^2,m_2^2)\equiv B_0(q^2;m_1^2,m_2^2)-B_0(0;m_1^2,m_2^2)\,, \qquad (3.69)$$

The functions B_{22} and B_0 are defined in [112] and m_k are the masses of the neutral Higgs h_k $(k=1,2,3)$.

And the function $\mathcal{F}$ is defined by

$$\mathcal{F}(m_1^2,m_2^2)\equiv\tfrac{1}{2}(m_1^2+m_2^2)-\frac{m_1^2m_2^2}{m_1^2-m_2^2}\ln\left(\frac{m_1^2}{m_2^2}\right)\,. \qquad (3.70)$$

Now, taking $m_h=125$ GeV, $m_t=173.3$ GeV and assuming that $U=0$, the accepted ranges for values of S and T are found by [113] to be,

$$\Delta S=0.06\pm0.09\,,\quad \Delta T=0.10\pm0.07\,, \qquad (3.71)$$

where the correlation factor is $\rho = +0.91$, $\Delta S = S^{\rm 2HDM} - S^{\rm SM}$ and $\Delta T = T^{\rm 2HDM} - T^{\rm SM}$, and their explicit expressions can be found in [89]. Also from [114, 115], we see that in the limit where $m_{H^\pm} = m_{A^0}$ or $m_{H^\pm} = m_{H^0}$, ΔT vanishes. The next set of constraints come from the signal strength measurements. By observing the scalar boson at $m_h \approx 125$ GeV to be SM like, searches for the Higgs boson by the ATLAS and CMS experiments at the LHC can impose strong bounds on the free parameters. The signal strength μ is defined as the ratio of the Higgs signal in the 2HDM to the SM prediction and it is given by:

$$\mu_j^X = \frac{[\sigma_j(h) \times Br(h \to X)]^{\rm 2HDM}}{[\sigma_j(h) \times Br(h \to X)]^{\rm SM}} \tag{3.72}$$

where $\sigma_j(h)$ represents the production cross section of the Higgs by channel j and $Br(h \to X)$ denotes the branching ratio for $h \to X$. At the LHC, while there are several channels available for the Higgs boson production, we are only interested in the gluon fusion production (ggF) mechanism because it is the dominant production as shown in Fig. 2.4. So, in order for us to consider the constrains from current data at the LHC, we analyze the scaling factors κ which show the deviations of the Higgs coupling from the SM and are defined as;

$$\kappa_V \equiv \frac{g_{hVV}^{\rm 2HDM}}{g_{hVV}^{\rm SM}}, \qquad \kappa_f \equiv \frac{y_{hff}^{\rm 2HDM}}{y_{hff}^{\rm SM}}, \tag{3.73}$$

where g_{hVV} and y_{hff} are the couplings of the Higgs to gauge bosons and fermions respectively, and f represents top, bottom quarks, and tau leptons. For the loop induced channels, the scaling factors are defined by

$$\begin{aligned} \kappa_\gamma^2 &\equiv \frac{\Gamma(h \to \gamma\gamma)^{\rm 2HDM}}{\Gamma(h \to \gamma\gamma)^{\rm SM}}, \qquad \kappa_g^2 \equiv \frac{\Gamma(h \to g\,g)^{\rm 2HDM}}{\Gamma(h \to g\,g)^{\rm SM}}, \\ \kappa_{Z\gamma}^2 &\equiv \frac{\Gamma(h \to Z\gamma)^{\rm 2HDM}}{\Gamma(h \to Z\gamma)^{\rm SM}}, \qquad \kappa_h^2 \equiv \frac{\Gamma(h)^{\rm 2HDM}}{\Gamma(h)^{\rm SM}}, \end{aligned} \tag{3.74}$$

where $\Gamma(h \to XY)$ denotes the partial decay width for $h \to XY$. In our numerical estimations, we use $m_h = 125.09$ GeV which is in agreement with latest LHC results at $\sqrt{s} = 13$ TeV [116–118].

3.3.1 Constraints on $\cos(\beta-\alpha)$ and $\tan\beta$ in the 2HDM Type II

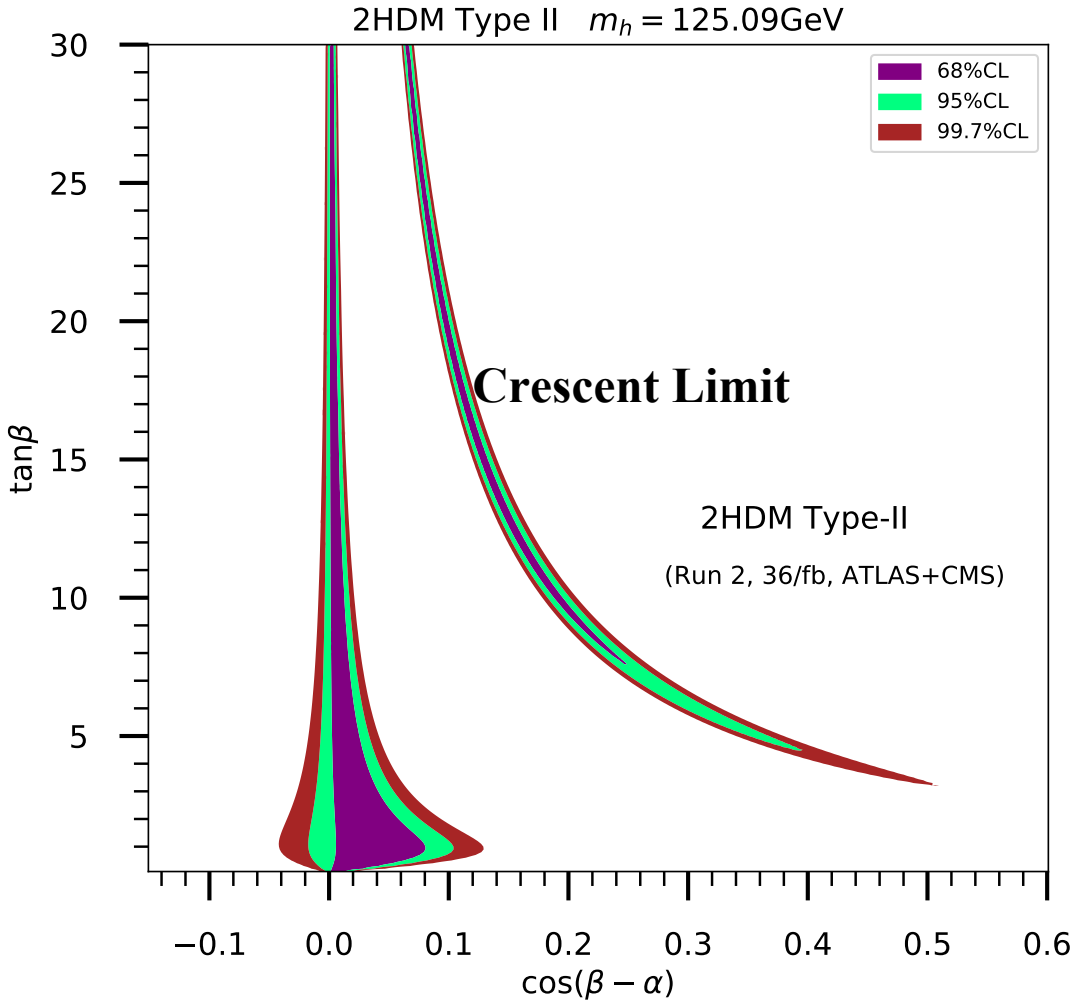

Figure 3.1: Constraints on $\cos(\beta-\alpha)$ and $\tan\beta$ in the 2HDM Type II

Fig. 3.1 above shows the constraints from signal strength measurements of the 125GeV Higgs boson on the $\cos(\beta-\alpha)$ and $\tan\beta$ plane in the 2HDM Type II. Searches at the LHC target different modes of production and decays of the Higgs boson. Higgs production and decay modes constraint the Higgs couplings to vector bosons and to third generation quarks. The main decay modes which are easily accessible at the LHC are $h \to \gamma\gamma$, $h \to ZZ^* \to 4l$, $h \to WW^* \to 2l2\nu$, $h \to b\bar{b}$ and $h \to \tau\tau$, where $l = e, \mu$. These decays can provide vital information on the Higgs coupling to vectors when considering the decays into ZZ^*, WW^* and $\gamma\gamma$ as well as to third generation fermions from the decays into $b\bar{b}$ and $\tau\tau$. Usually, the

results of the SM Higgs searches are given in terms of signal strengths μ which have been defined in Eq. (3.72). In this thesis, the signal strength measurements are carried out for the type-II 2HDM where the light Higgs is considered as the SM like and is set to a mass of 125.09GeV. Identifying the lighter CP even state with the observed one fixes the coupling structure of the model. Also, we neglect the charged Higgs contributions to $\gamma\gamma$. With these assumptions, the $\cos(\beta-\alpha)$ and $\tan\beta$ plane in Fig 3.1 is a viable parameter space region where H, A and $H^{\pm}$ decays can occur. Finally, from Fig. 3.1, we predict that, in the crescent limit, when kinematically accessible $H \to hh$, $A \to Zh$ and $H^{\pm} \to W^{\pm}h$ should become high priorities in searching for additional Higgs bosons.

3.3.2 Numerical Analysis and Benchmark scenarios

We use the physical basis in which the input parameters are the physical Higgs masses $(m_h, m_H, m_A, m_{H^{\pm}})$, $\tan\beta$, and the mixing angle α, all supplemented by the Z_2 soft-breaking parameter m_3^2. With these inputs, $\lambda_{1,2,3,4,5}$ as well as m_1^2 and m_2^2 are determined. To choose benchmark scenarios for our phenomenological analysis, we follow constraints on the $\cos(\beta-\alpha)$ and $\tan\beta$ plane in the 2HDM Type II shown in Fig. 3.1 above. Table 3.3, 3.4 and 3.5 below shows 3 benchmark scenarios for the heavy Higgs, which we refer to as in the exact decoupling, near the decoupling and the crescent limit.

Table 3.3: Benchmark points for heavy Higgs searches in the decoupling limit

Scenario A (Decoupling limit)				
	m_h (GeV)	m_H (TeV)	$c_{\beta-\alpha}$	$\tan\beta$
A.1	125	$0.2-1.5$	0.0	1
A.2	125	$0.2-1.5$	0.0	7.8
A.3	125	$0.2-1.5$	0.0	15
A.4	125	$0.2-1.5$	0.0	20

Table 3.4: Benchmark points for heavy Higgs searches near the decoupling limit

Scenario B (Near the decoupling limit)				
	m_h (GeV)	m_H (TeV)	$c_{\beta-\alpha}$	$\tan\beta$
B.1	125	$0.2 - 1.5$	0.004	1
B.2	125	$0.2 - 1.5$	0.004	7.8
B.3	125	$0.2 - 1.5$	0.004	15
B.4	125	$0.2 - 1.5$	0.004	20

Table 3.5: Benchmark points for heavy Higgs searches in the crescent limit

Scenario C (Crescent limit)				
	m_h (GeV)	m_H (TeV)	$c_{\beta-\alpha}$	$\tan\beta$
C.1	125	$0.2 - 1.5$	0.35	5
C.2	125	$0.2 - 1.5$	0.24	7.8
C.3	125	$0.2 - 1.5$	0.13	15
C.4	125	$0.2 - 1.5$	0.1	20

From Table 3.3 , 3.4 and 3.5 , we choose similar benchmark points for A and $H^{\pm}$ in the 2HDM. Phenomenological analysis for A and $H^{\pm}$ with respect to similar benchmark scenarios have been discussed in Chapters 5 and 6 of this thesis.

Chapter 4

Heavy Higgs Bosons in the Two Higgs Doublet Model

We present in this Chapter a phenomenological analysis of the CP even Higgs boson within the type II two Higgs doublet model. We begin with a brief overview of 2HDM Yukawa interactions, the decays, and the production of the heavy Higgs. Using constraints from both the ATLAS and CMS collaborations, we choose viable values within the $\tan\beta$ and $\cos(\beta-\alpha)$ plane for our analysis, as indicated in the previous Chapter. Additionally, we impose explicit theoretical constraints on the heavy Higgs mass and then perform a scan over a range of $0.2-1.5$TeV. We finally present possible avenues for detecting the heavy Higgs as the objectives of this thesis.

4.1 Yukawa interaction of H

Table 4.1 below summarizes the tree-level couplings of H to up and down type quarks, leptons, and massive gauge bosons relative to the SM Higgs boson couplings as functions of α and β in the type II Yukawa interactions of the two Higgs doublet model.

Table 4.1: The Yukawa factors in the Type II - 2HDM for heavy Higgs

H couplings $\frac{y_{2HDM}}{y_{SM}}$	2HDM Type II
C_V^H	$\cos(\beta-\alpha)$
C_u^H	$\cos(\beta-\alpha) - \frac{\sin(\beta-\alpha)}{\tan\beta}$
C_d^H	$\cos(\beta-\alpha) + \tan\beta\sin(\beta-\alpha)$
C_l^H	$\cos(\beta-\alpha) + \tan\beta\sin(\beta-\alpha)$

For couplings involving two or more scalars, the coupling of heavy Higgs scalar H to two SM-like scalars h, g_{Hhh} is given by [119, 120];

$$g_{Hhh} = \frac{\cos(\beta-\alpha)}{v}\Bigg\{\left(\frac{6m_{12}^2}{\sin 2\beta} - m_H^2 - 2m_h^2\right) \left(\cos 2(\beta-\alpha) - \frac{\sin 2(\beta-\alpha)}{\tan 2\beta}\right) - \frac{2m_{12}^2}{\sin 2\beta}\Bigg\}, \tag{4.1}$$

This coupling is very relevant as it controls the rates of three processes that may be kinematically allowed when $m_h < m_A \sim m_H \sim m_{H^\pm}$. Unlike the other couplings involving SM vectors or fermions, the triple Higgs coupling, g_{Hhh} depends on additional parameters beyond the physical masses and mixing angles. And it should be noted clearly that the expression for g_{Hhh} above is for a CP conserving 2HDM where $\lambda_6 = \lambda_7 = 0$.

4.2 Heavy Higgs Decay

In this section, we will discuss the decay rates of the heavy Higgs within the context of the 2HDM. We evaluate the decay rates, total widths, and the branching ratios with the help of 2HDMC. First, we show results in the decoupling limit where $\cos(\beta-\alpha) = 0$ or $\sin(\beta-\alpha) = 1$. In this limit, the lighter Higgs state(h) becomes the SM Higgs boson, with the same mass at leading order excluding loop induced channels. Also, in this limit, the heavier Higgs (H) does not decay into boson pairs, but it mainly decays into a pair of fermions. We also discuss results for H near the decoupling limit and within the crescent limit. In these limits, when kinematically allowed, the heavy Higgs may decay into two SM

Higgs.

4.2.1 Decay of the heavy Higgs into fermions

The partial decay width for the heavy Higgs into a pair of fermions can be calculated at tree-level as;

$$\Gamma\left(H \to f\bar{f}\right) = \frac{\sqrt{2}G_F m_f^2 m_H}{8\pi}\left(C_f^H\right)^2 N_f \left(1 - \frac{4m_f^2}{m_H^2}\right)^{3/2} \tag{4.2}$$

where G_F is the Fermi coupling constant, m_f is the mass of fermion, m_H is the heavier Higgs mass, N_f is the number of color factors and C_f^H describes the Yukawa interaction of Higgs to fermions. The number of color factors, N_f is 3 for quarks and 1 for leptons. And the mixing factors in the Yukawa interactions C_f^H are usually expressed in terms of the mass eigenstates of the Higgs bosons which can be found in Table 4.1.

4.2.2 Decay of the heavy Higgs into Gauge Bosons

The partial decay width of H decaying into a pair of gauge bosons WW or ZZ is;

$$\Gamma\left(H \to VV\right) = \sqrt{2}G_F \frac{m_H^3}{32\pi}\left(C_V^H\right)^2 \delta_V \left[1 - \frac{4m_V^2}{m_H^2} + \frac{12m_V^2}{m_H^4}\right]\left(\sqrt{1 - \frac{4m_V^2}{m_H^2}}\right) \tag{4.3}$$

Where δ_V is 2 for W bosons and 1 for Z bosons. However, if kinematically allowed, the heavy Higgs can decay into other scalar bosons like the charged Higgs ($H^\pm$) or the CP odd Higgs (A) plus a vector boson V, that is W or Z bosons. When the mass of the heavy Higgs (m_H) is greater than the mass of the other scalar boson (m_{Sc}) plus the mass of the vector bosons (m_V), $m_H > m_{Sc} + m_V$, then the partial decay widths $\Gamma\left(H \to H^\pm W^\pm\right)$ and $\Gamma\left(H \to AZ\right)$ can be computed as;

$$\Gamma\left(H \to H^\pm W^\pm\right) = \sqrt{2}G_F \frac{m_H^3}{8\pi}\left(\sin(\beta - \alpha)\right)^2 \left(1 + \frac{m_{H^\pm}^4}{m_H^4} + \frac{m_W^4}{m_H^4} - \frac{2m_{H^\pm}^2 m_W^2}{m_H^4} - \frac{2m_{H^\pm}^2}{m_H^2} - \frac{2m_W^2}{m_H^2}\right)^{3/2} \tag{4.4}$$

$$\Gamma\left(H \to AZ\right) = \sqrt{2} G_F \frac{m_H^3}{8\pi} \left(\sin(\beta-\alpha)\right)^2 \left(1 + \frac{m_A^4}{m_H^4} + \frac{m_Z^4}{m_H^4} - \frac{2m_A^2 m_Z^2}{m_H^4} - \frac{2m_A^2}{m_H^2} - \frac{2m_A^2}{m_H^2}\right)^{3/2} \tag{4.5}$$

On the other hand, when the mass of the other decaying scalar boson (m_{Sc}) plus the mass of the vector bosons (m_V) is greater than the heavy Higgs mass (m_H), then the heavy Higgs H decays into either $H^\pm$ or A and the off-shell V. The partial widths $\Gamma\left(H \to H^\pm W^{\pm *}\right)$ and $\Gamma\left(H \to AZ^*\right)$ can also be computed as;

$$\Gamma\left(H \to H^\pm W^{\pm *}\right) = \frac{9 G_F^2 m_W^4}{16\pi^3} \left(\sin(\beta-\alpha)\right)^2 m_H G\left(\frac{m_{H^+}^2}{m_H^2}, \frac{m_W^2}{m_H^2}\right) \tag{4.6}$$

$$\Gamma\left(H \to AZ^*\right) = \frac{3 G_F^2 m_Z^4}{32\pi^3} \left(\sin(\beta-\alpha)\right)^2 m_H \left(7 - \frac{40}{3}\sin\theta_W^2 + \frac{160}{9}\sin\theta_W^4\right) G\left(\frac{m_A^2}{m_H^2}, \frac{m_Z^2}{m_H^2}\right) \tag{4.7}$$

where the function $G\left(x,y\right)$ in both equations above can be expressed as;

$$\begin{aligned} G\left(x,y\right) = \frac{1}{12y}\Bigg\{ & 2\left(-1+x\right)^3 - 9\left(-1+x^2\right)y + 6\left(-1+x\right)y^2 \\ & + 6\left(1+x-y\right)y\sqrt{-\lambda\left(x,y\right)}\left[\tan^{-1}\left(\frac{-1+x-y}{\sqrt{-\lambda\left(x,y\right)}}\right)\right] + \left[\tan^{-1}\left(\frac{-1+x+y}{\sqrt{-\lambda\left(x,y\right)}}\right)\right] \\ & - 3\left[1+\left(x-y\right)^2 - 2y\right] y\log(x)\Bigg\} \end{aligned} \tag{4.8}$$

And the function $\lambda\left(x,y\right)$ is given as;

$$\lambda\left(x,y\right) = 1 + x^2 + y^2 - 2xy - 2x - 2y \tag{4.9}$$

4.2.3 Decay rates for the loop-induced decay modes

The partial decay width for the loop-induced decay modes of the heavy Higgs into photons, $\Gamma(H \to \gamma\gamma)$ can be computed as;

$$\Gamma(H \to \gamma\gamma) = \frac{\sqrt{2} G_F \alpha_{em}^2 m_H^3}{64\pi^3} \Big| I_{H^\pm}(m_H) + \sum_f Q_f^2 N_c^f C_f^H I_f(m_H) + C_V^H I_W(m_H) \Big|^2 \quad (4.10)$$

where the loop functions are

$$I_f(m_H) = -\frac{4m_f^2}{m_H^2}\left[1 - \frac{m_H^2}{2}\left(1 - \frac{4m_f^2}{m_H^2}\right) C_0(0,0,m_H^2,m_f,m_f,m_f)\right], \quad (4.11)$$

$$I_W(m_H) = 1 + \frac{6m_W^2}{m_H^2} - 6m_W^2\left(1 - \frac{2m_W^2}{m_H^2}\right) C_0(0,0,m_H^2,m_f,m_f,m_f), \quad (4.12)$$

$$I_{H^\pm}(m_{\mathcal{H}}) = \frac{v\lambda_{\varphi H^+H^-}}{m_{\mathcal{H}}^2}[1 + 2m_{H^+}^2 C_0(0,0,m_{\mathcal{H}}^2; m_{H^+}^2, m_{H^+}^2, m_{H^+}^2)], \quad (4.13)$$

And the decay into gluons, $\Gamma(H \to gg)$ is given by

$$\Gamma(H \to gg) = \frac{\sqrt{2} G_F \alpha_s^2 m_H^3}{128\pi^3} \Big| \sum_{f=q} C_f^H I_f(m_H) \Big|^2 \quad (4.14)$$

The function C_0 as seen in the above decay is given by

$$C_0\left(0,0,m_H^2; m_f^2, m_f^2, m_f^2\right) = \frac{-2}{m_H^2} f\left(\frac{4m_f^4}{m_H^2}\right) \quad (4.15)$$

The function $f(x)$ takes the form; $f(x) = \begin{cases} \left[\arcsin\left(1/\sqrt{x}\right)\right]^2, & \text{if } x \geq 1 \\ -\frac{1}{4}\left[\ln\frac{1+\sqrt{1-x}}{1-\sqrt{1-x}} - i\pi\right]^2, & \text{if} x < 1 \end{cases}$

4.2.4 Decay of the heavy Higgs to SM-like Higgs hh

The partial decay width of the heavier Higgs boson to SM Higgs can be determined by inferring the tree-level decay width for $m_H > 2m_h$,

$$\Gamma[H \to hh] \;=\; \frac{9\,\zeta^2 m_h^4}{32\pi v^2 m_H} \sqrt{1 - \frac{4m_h^2}{m_H^2}}\,. \quad (4.16)$$

Where ζ defines the coupling ratio $g_{Hhh}/g_{hhh}^{\rm sm}$ which characterizes the relative strength of the Hhh coupling as compared to the triple Higgs coupling in the SM and it is written as;

$$\zeta = \frac{g_{Hhh}}{g_{hhh}^{\rm sm}} = \frac{(8m_{12}^2/\sin 2\beta - m_H^2 - 2m_h^2)}{3m_h^2}\cos(\beta-\alpha) + \mathcal{O}\left(\cos^2(\beta-\alpha)\right) \tag{4.17}$$

From equation 4.17 above, $g_{hhh}^{\rm sm}$ represents the cubic Higgs coupling in the SM which takes the form;

$$g_{hhh}^{\rm sm} = \frac{-3m_h^2}{v} \tag{4.18}$$

4.3 Heavy Higgs Production

At the LHC, the heavy Higgs is mainly produced via the gluon fusion process $gg \to H$. We can also produce heavy Higgs in different ways. These other production processes include the vector boson fusion $pp \to Hqq'$, the vector boson associated production $pp \to HV$, and the top associated production $gg \to Ht\bar{t}$. A detailed discussion on the Higgs pair production via gluon fusion processes in the 2HDM can be found in [121]. Ref. [122] studied the production of the heavy Higgs boson and its decay into top quarks in the strong coupling regime. The studies in [122] focussed on the total decay widths of the heavy Higgs by considering the type II 2HDM where three favorable parameter scenarios were chosen for the heavy Higgs bosons mass above the $t\bar{t}$ threshold and unsuppressed Yukawa coupling to the top quarks. Ref. [123] describes the code SusHi which calculates the cross sections in gluon fusion and bottom quark annihilation in the SM, 2HDM and MSSM. Cross sections for gluon fusion at leading order (LO), next to leading order (NLO), next-to-next-to-leading (NNLO) expressions are explicitly given in this reference. In this thesis, we adopt the following method to determine the appropriate production cross-section of the heavy Higgs. The LHC Higgs Cross Section Working Group presented in [61, 124] the case of the SM Higgs boson production where, they calculated the NLO production cross sections for gluon fusion, vector-boson fusion, and production in association to vector bosons or top quarks. For the 2HDM, the ratio of the LO production partial widths is computed in each production channel for both h and H relative to the SM Higgs boson of the same mass, and the couplings as functions of α and β. The

SM Higgs production cross sections at NLO in each production rates are then rescaled by these factors to obtain an estimate for the NLO cross sections. The α and β dependent cross section for gluon fusion production cross section of the heavy Higgs H is given by [125];

$$\sigma_{\mathrm{NLO}}\left(gg \to H\right)\Big|_{\alpha,\beta} = \sigma_{\mathrm{NLO}}\left(gg \to h_{\mathrm{sm}}\right) \frac{\Gamma_{\mathrm{LO}}\left(H \to gg\right)\Big|_{\alpha,\beta}}{\Gamma_{\mathrm{LO}}\left(h_{\mathrm{sm}} \to gg\right)} \tag{4.19}$$

Fig. 4.1 below shows the gluon fusion production cross-section of the heavy Higgs in the decoupling limit where $\cos(\beta - \alpha) = 0$ at four different values of $\tan\beta$. This represents the production cross sections of heavy Higgs with masses from 200GeV to 1.5TeV at center of mass energy of 14TeV. The cross sections are obtained at NLO using the default SusHi[123] and LHAPDF [126, 127]. We see here that the total production cross section ranges from about 22.5pb for $m_H = 200$GeV to about 2×10^{-2}pb for $m_H = 1.5$TeV for $\tan\beta = 1$ in the decoupling limit. In the decoupling limit of 2HDMs, the lightest Higgs boson has SM like couplings, and its production follows precisely that of the SM Higgs boson. For the heavy Higgs boson, the production rates depend on m_H and strongly on $\tan\beta$. For instance, for small values, $\tan\beta \approx 1$, the dominant contribution comes from the top quark loops as the $g_{t\bar{t}}$ couplings, $g_{Htt} \propto 1/\tan\beta$ are strong. At higher values of $\tan\beta$, $\tan\beta \geq 10$, the couplings to top quarks are strongly suppressed while those to bottom quarks, $g_{Hbb} \propto \tan\beta$ are enhanced. This makes the bottom quark loop contribution to $gg \to H$ become the dominant one, while it was about 10% less in the SM case.

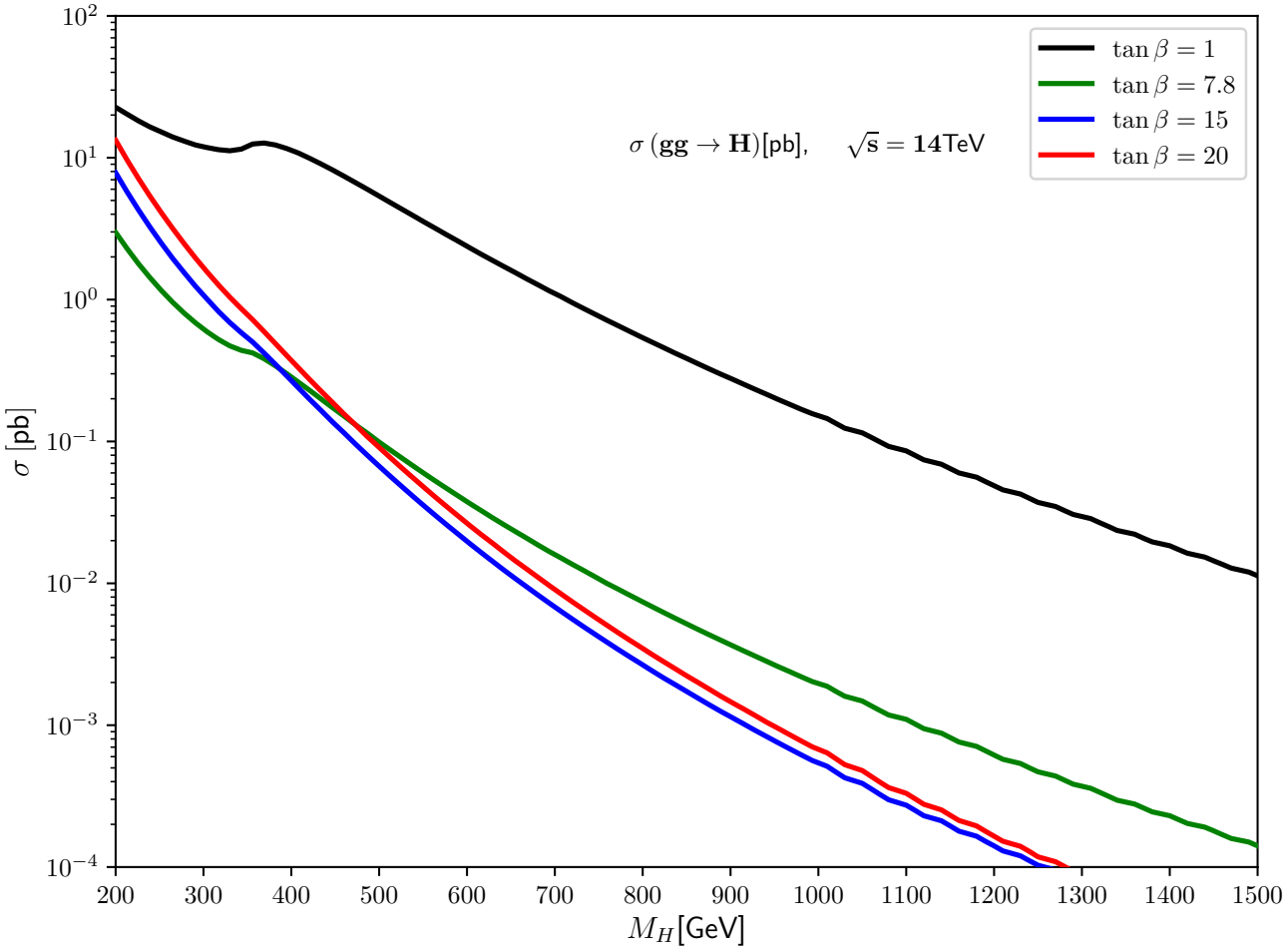

Figure 4.1: 2HDM Type II: σ_{ggH} in the decoupling limit for $\tan\beta = 1, 7.8, 15$ and 20 at NLO

At small to intermediate values, $\tan\beta \approx 3 - 10$, we see that the suppression of the top coupling $g_{t\bar{t}}$ is more effective already while the bottom coupling g_{Hbb} is not yet enhanced, resulting in production cross sections that are smaller than in those in the SM. As can be seen clearly in figure 4.1 below, in an attempt to compare the results to the case of the SM Higgs, the production rates for the 2HDM type II Heavier Higgs are smaller than for SM Higgs like at low $\tan\beta$ when the suppressed top quark loop is still dominant and much larger at high $\tan\beta$ values when the bottom quark loop is strongly enhanced. They are pretty small for $\tan\beta \approx 7.8$ when there is maximal g_{Htt} suppression and minimal g_{Hbb} enhancement.

4.4 Decay channels for the Heavy Higgs

We present in this section our results for the decay channels of the heavy Higgs. In our analysis, we constrain the mass of the heavy Higgs, such that the masses of the charged and pseudoscalar Higgs are smaller than that of the heavy Higgs masses. We impose these constraints to allow the heavy Higgs to decay into SM particles only. The imposed constraints follow the expressions;

$$m_H = m_{H^\pm} + 50\text{GeV}; \qquad m_H = m_A + 50\text{GeV} \tag{4.20}$$

Also, a detailed analysis on the phenomenology of the heavy Higgs is performed in three different scenarios determined by the parameter space, which is allowed by constraints coming from the requirement that the light Higgs boson in this model, h, is SM-like. The first part focuses on the decoupling limit where $\cos(\beta - \alpha) = 0$. In this limit, the lighter CP even Higgs boson h has the same coupling as the 125.09GeV SM Higgs boson. In this limit, the heavy Higgs can't decay into any two neutral or charged scalar bosons since its coupling to such bosons is directly proportional to $\cos(\beta - \alpha)$. The second part focuses on the phenomenological analysis of heavy Higgs near the decoupling limit, where we choose $\cos(\beta - \alpha)$ to be 0.004. And finally, for the third part, we present analysis in the crescent limit, which we believe to be the most promising limit for new physics discoveries. In both the second and the third scenarios, one would expect the heavy Higgs to decay into two SM Higgs. We also present results for the production cross sections times the branching ratios of the heavy Higgs, for distinct $\cos(\beta - \alpha)$ values at $\tan\beta$ values; $\tan\beta = 1, 7.8, 15$ and 20. The $\tan\beta$ parameter can be determined using measurements from the branching ratios, total width measurements of extra Higgs bosons and the precision measurements [128] of the SM Higgs branching ratios.

4.4.1 σ_{ggH} times branching ratios vrs m_H in the decoupling limit

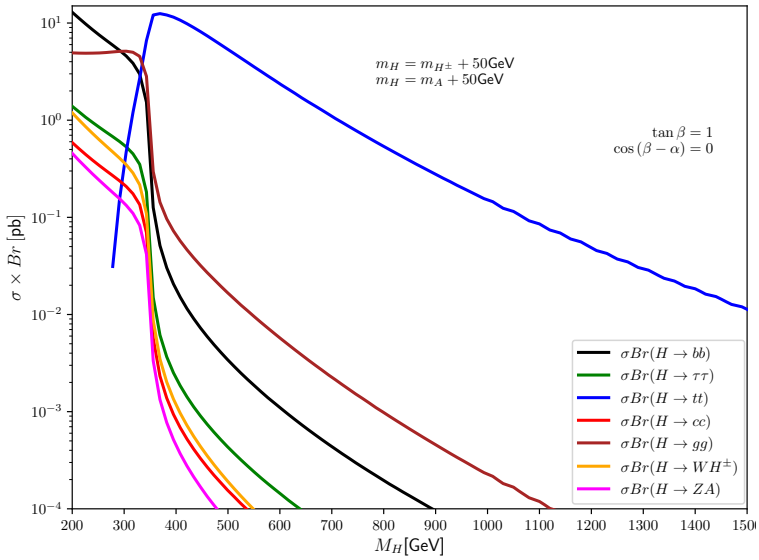

Figure 4.2: σ_{ggH} times branching ratios vrs m_H at $\cos(\beta - \alpha) = 0$, for $\tan\beta = 1$

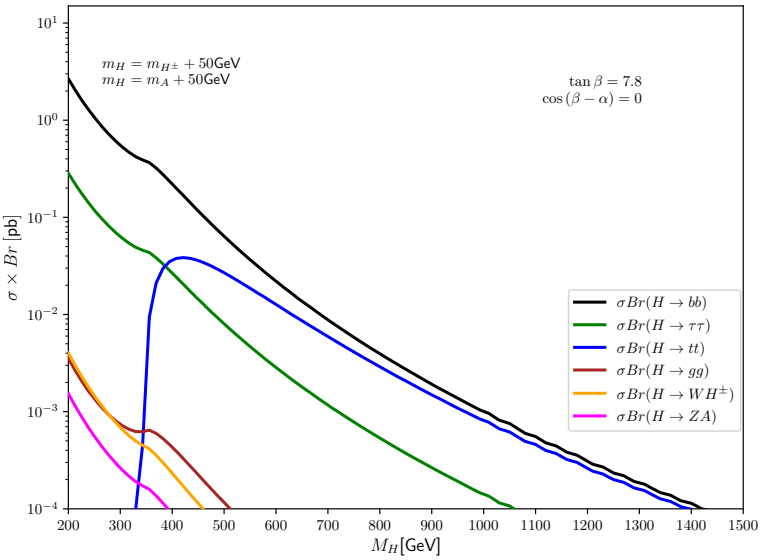

Figure 4.3: σ_{ggH} times branching ratios vrs m_H at $\cos(\beta - \alpha) = 0$, for $\tan\beta = 7.8$

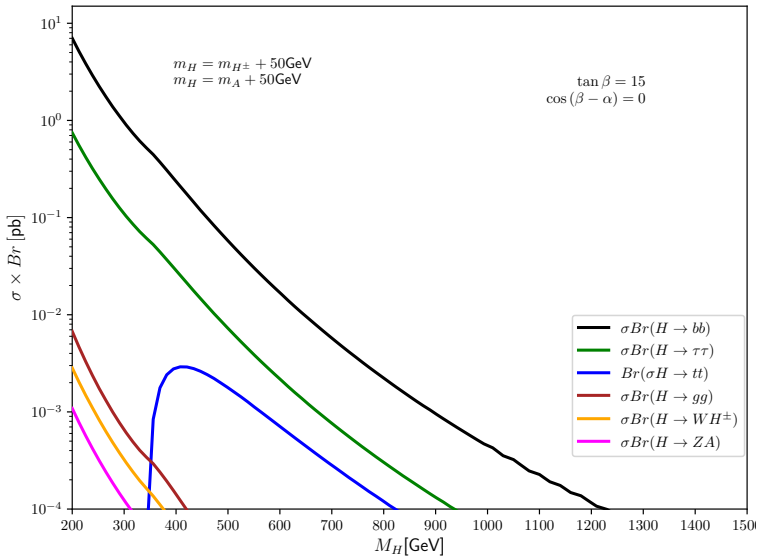

Figure 4.4: σ_{ggH} times branching ratios vrs m_H at $\cos(\beta - \alpha) = 0$, for $\tan\beta = 15$

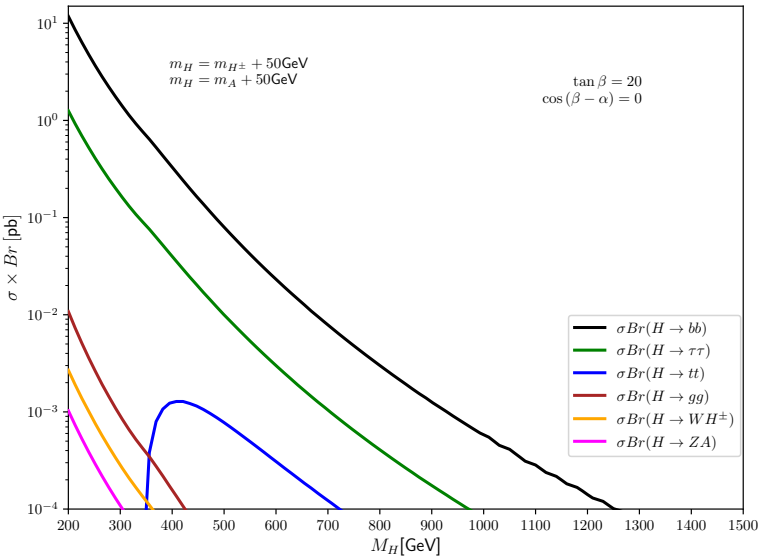

Figure 4.5: σ_{ggH} times branching ratios vrs m_H at $\cos(\beta - \alpha) = 0$, for $\tan\beta = 20$

From Figs. 4.2 , 4.3 , 4.4 and 4.5 above, it can be seen that in the decoupling limit, the best channels from the decay of the heavy Higgs are some fermionic channels $H \to b\bar{b}, H \to t\bar{t}, H \to c\bar{c}, H \to \tau\tau$ and a loop induced channel $H \to gg$ for all chosen values of $\tan\beta$. The $H \to c\bar{c}$ channel is seen to be suppressed and quickly disappears for $\tan\beta = 7, 8, 15$, and 20, whereas, the $H \to t\bar{t}$ remains visible for higher values of $\tan\beta$. This is because the decay rate is proportional to the square of the fermion mass as m_f^2, hence heavier top quarks is enhanced as compared to lighter charm quark. From our results, it was also noticed that in the decoupling limit, the decay of the heavy Higgs into vector bosons vanishes. We also discuss the influence of $\tan\beta$ on the heavy Higgs. As seen in Fig. 4.2, for $\tan\beta = 1$, the $H \to t\bar{t}$ channel opens up whereas it closes up gradually for $\tan\beta = 7.8, 15$ and 20. This is because the heavy couplings to $t\bar{t}$ is highly enhanced for low $\tan\beta$ values whereas it is suppressed for high $\tan\beta$. Another reason is that comparing equations 4.2 and 4.3 we see that in equation 4.3, the partial decay widths for $h \to VV$ grows rapidly as m_h^3 whiles in equation 4.2, $h \to t\bar{t}$ grows only as m_h. This is exactly what one would expect in the minimal supersymmetric models for $\tan\beta \leq 3$ [129–133]. This is the same for the type II 2HDM where from Table 4.1, we observe that the top loop is suppressed by the square of the Yukawa coupling $C_{tt}^H \propto \frac{1}{\tan\beta}$ if $\tan\beta$ is not close to 1. It can be concluded from the above results that the $H \to t\bar{t}$ will surely be more favourable for the type II 2HDM in the low $\tan\beta$ regimes. Finally, there is a continuous enhancement for $H \to b\bar{b}$ and $H \to \tau\tau^-$ as $\tan\beta$ is increased. This is true since down type quarks and charged leptons couple to the same doublet in the type II 2HDM, hence this is enhanced by the square of the coupling C_{bb}^H or $C_{\tau\tau}^H \propto \tan\beta$ for $\tan\beta > 1$.

4.4.2 σ_{ggH} times branching ratios vrs m_H near the decoupling limit

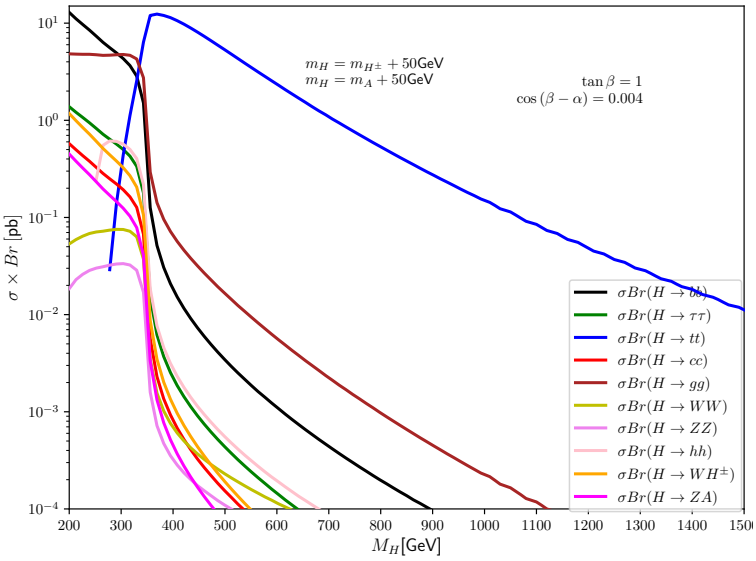

Figure 4.6: σ_{ggH} times branching ratios vrs m_H at $\cos(\beta-\alpha) = 0.004$, for $\tan\beta = 1$

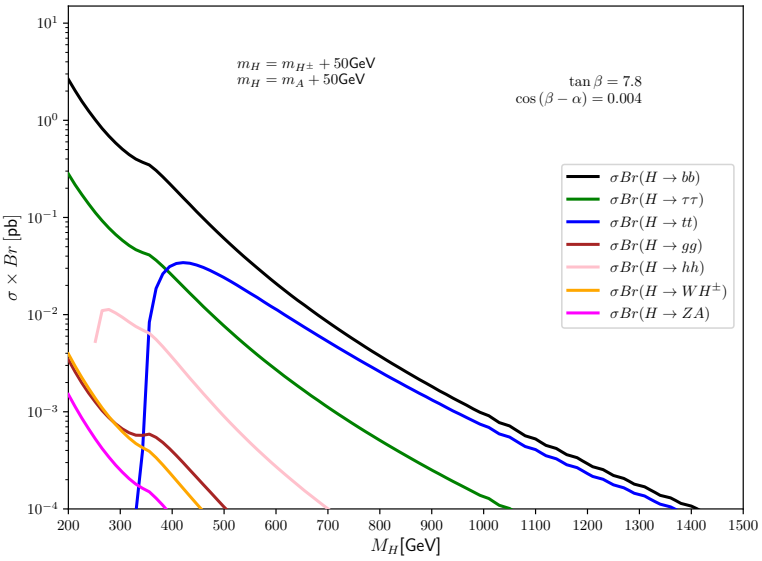

Figure 4.7: σ_{ggH} times branching ratios vrs m_H at $\cos(\beta-\alpha) = 0.004$, for $\tan\beta = 7.8$

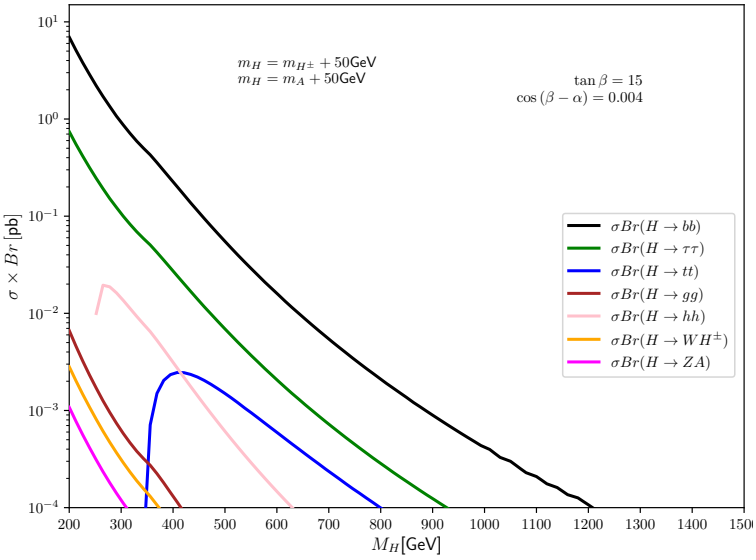

Figure 4.8: σ_{ggH} times branching ratios vrs m_H at $\cos(\beta-\alpha) = 0.004$, for $\tan\beta = 15$

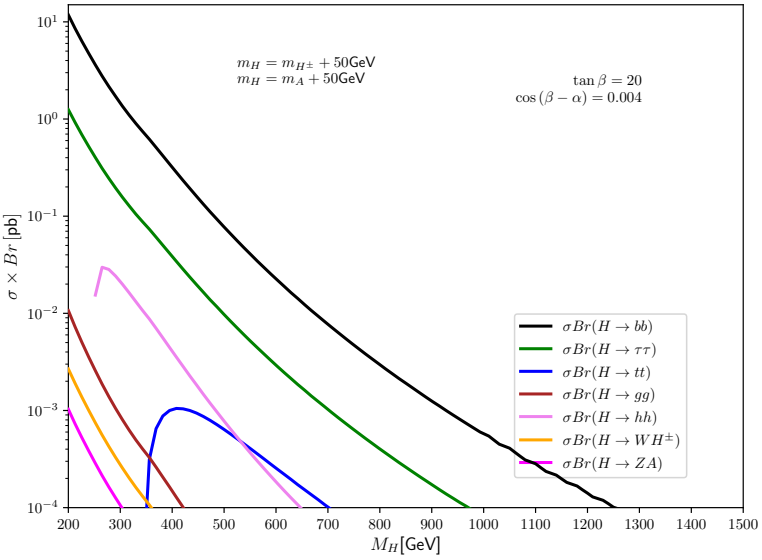

Figure 4.9: σ_{ggH} times branching ratios vrs m_H at $\cos(\beta-\alpha) = 0.004$, for $\tan\beta = 20$

4.4.3 σ_{ggH} times branching ratios vrs m_H in the crescent limit

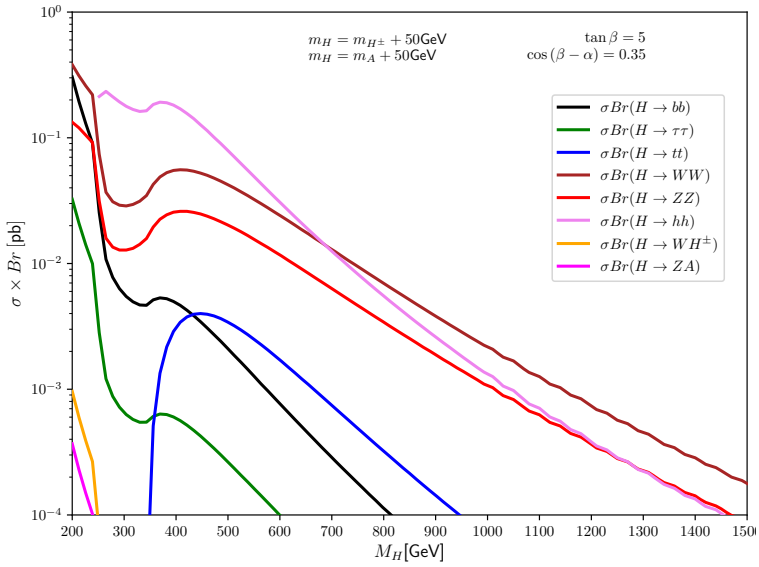

Figure 4.10: σ_{ggH} times branching ratios vrs m_H at 2σ for $\tan\beta = 5$

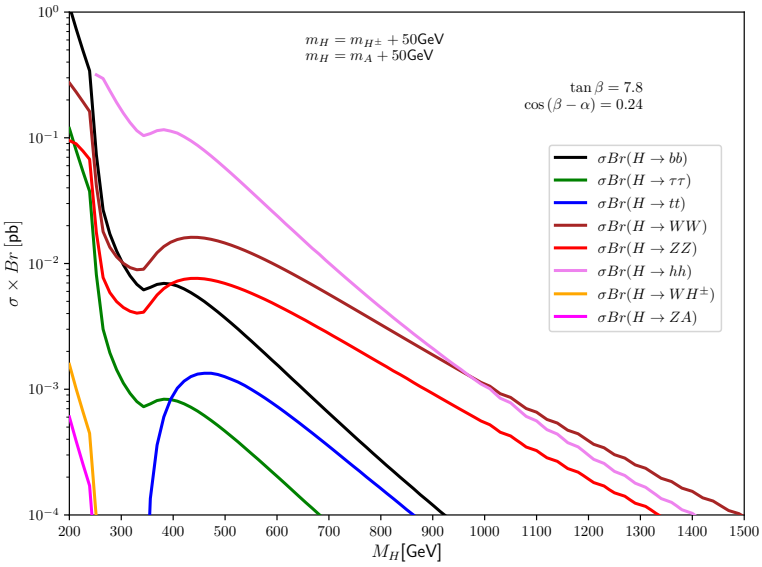

Figure 4.11: σ_{ggH} times branching ratios vrs m_H at 1σ for $\tan\beta = 7.8$

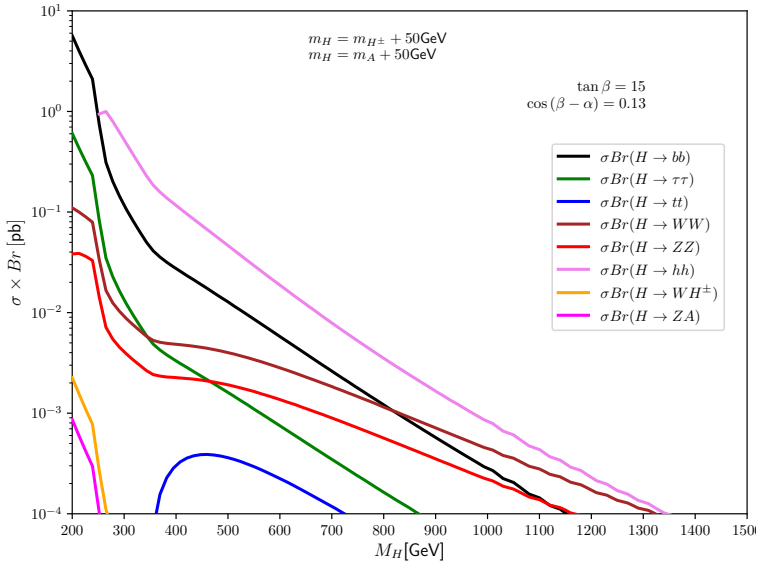

Figure 4.12: σ_{ggH} times branching ratios vrs m_H at 1σ for $\tan\beta = 15$

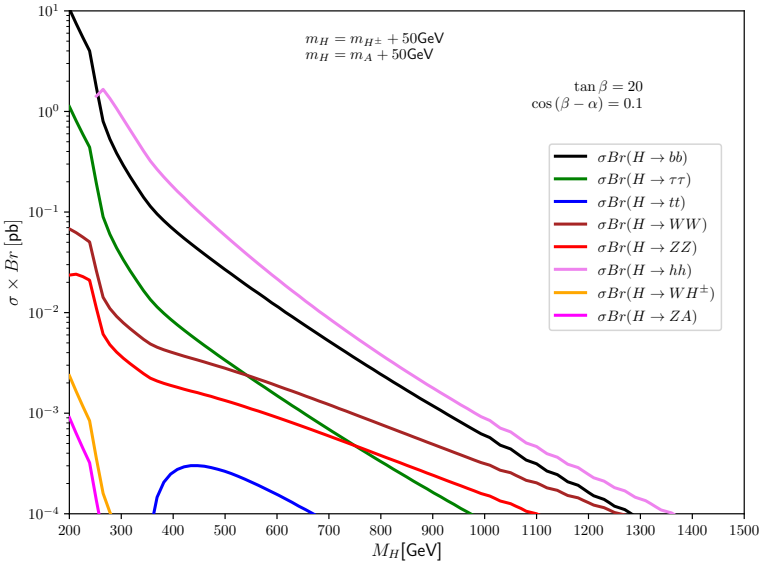

Figure 4.13: σ_{ggH} times branching ratios vrs m_H at 1σ for $\tan\beta = 20$

Here, we discuss two interesting more limits, near the decoupling limit and the crescent limit. These two limits differ from the decoupling limit by providing an avenue for detecting the decays into gauge bosons and two SM Higgs particles. Figs. 4.6 , 4.7 , 4.8 , and 4.9 shows the production cross section times branching ratios vrs heavier Higgs masses for $\tan\beta = 1, 7.8, 15$ and 20 near the decoupling limit where $\cos(\beta-\alpha)$ is set to 0.004 whereas Figs. 4.10 , 4.11 , 4.12 , and 4.13 shows the same but for different $\cos(\beta-\alpha)$ values in the crescent limit. In these two limits, when kinematically allowed, the heavier Higgs can decay to two possible light Higgs scalars $H \to hh$ even when the couplings of the lightest Higgs are within a few percent of the SM Predictions [125, 134, 135].

Discussion for $\mathbf{H \to hh}$, $\mathbf{H \to WW, ZZ}$, and off-shell decay modes

From Eq. 4.16 , we see the partial decay width for the heavy Higgs to two SM Higgs whereas Eq.4.1 gives a simplified version for the g_{Hhh} coupling. The first thing to note is that the coupling is directly proportional to the Yukawa interaction as $g_{Hhh} \propto \cos(\beta-\alpha)$ which implies that in the exact decoupling limit, $g_{Hhh} \to 0$. This is the same for the vector boson couplings, g_{HVV}, hence when $\cos(\beta-\alpha) = 0$, neither $H \to hh$ nor $H \to VV$ would be available. Notwithstanding, for very small departures from the decoupling limit, these decays channels may be significant, and they may dominate the total width of H. This is because the partial decay width for both channels grows as $\Gamma(H \to VV), \Gamma(H \to hh) \propto \frac{m_H^3}{v^2}$. This is exactly what we notice in all the 8 figures above. In Figs. 4.6 to 4.13 , the $\Gamma(H \to WW)$, $\Gamma(H \to ZZ)$, $\Gamma(H \to hh)$ channels open up. However, near the decoupling limit at $\cos(\beta-\alpha) = 0.004$ for increasing values of $\tan\beta$, the channels $\Gamma(H \to ZZ)$ and $\Gamma(H \to WW)$ become negligible around 10^{-5} (hence invisible channels in Figs. 4.7, 4.8, and 4.9). But the $\Gamma(H \to hh)$ channel dominates in this regime. Of these two processes, $\Gamma(H \to hh)$ and $\Gamma(H \to VV)$, the respective couplings determine which one dominates. $\Gamma(H \to hh) \geq \Gamma(H \to VV)$ holds when kinematically allowed or opened. Since the g_{Hhh} coupling is non zero, $\Gamma(H \to hh)$ is enhanced as we move further away from the decoupling limit. We observe similar results in Figs. 4.7 , 4.8 , and 4.9 , where the decay growth

$\Gamma(H \to hh)$ is exactly the same except for Fig. 4.6 which deviates slightly. For the off-shell decay modes, we see that in the decoupling limit the decay mode $H \to W^*H^\pm$ is mostly enhanced whereas that that of the $H \to AZ^*$ is slightly suppressed with increasing $\tan\beta$ values. Therefore, $H \to W^*H^\pm$ channel slightly opens up as compared to the $H \to AZ^*$ channel. We observed similar results near the decoupling limit. Moreover, comparing Figs. 4.10 and 4.11 , we noticed that, at $\cos(\beta-\alpha) = 0.35$ and $\cos(\beta-\alpha) = 0.24$, the $\Gamma(H \to hh)$ growth occurs at a heavy Higgs mass of around 1.05TeV and 1TeV respectively. Furthermore, our results show that at larger values of $\tan\beta$ far away from the decoupling limit, $\Gamma(H \to hh) >> \Gamma(H \to VV)$ due to the $\tan\beta$ enhancement of $\Gamma(H \to hh)$. In [125], $\Gamma(H \to hh)$ was singled out as very significant channel in determining the most favourable search for heavier Higgs as m_H is varied, since it implies that $BR(H \to VV)$ maybe small even when the partial width is appreciable. This is true because the $\tan\beta$ enhanced coupling of the heavy Higgs H to bottom quarks rapidly leads to $\Gamma\left(H \to b\bar{b}\right)$ dominating the total width as seen clearly in Figs. 4.6 to 4.13 shown above. This is valid for CP conserving 2HDM ($\lambda_6 = \lambda_7 = 0$), where near the decoupling limit the leading contribution to the g_{Hhh} coupling are not enhanced by $\tan\beta$ and the enhanced terms of $\tan\beta$ first arise from $\mathcal{O}(\cos^2(\beta-\alpha))$ [125, 136–139]. Besides, when λ_6 and λ_7 are non zero, $H \to hh$ dominates the total width even in cases where fermion decays are parametrically enhanced [125]. In conclusion, our results show that the crescent limit is a promising limit to search for heavy Higgs decays into both gauge bosons and two SM-like Higgs states.

Chapter 5

Pseudoscalar Higgs Bosons in the Two Higgs Doublet Model

We present in this chapter all analytical expressions for the partial decay widths of the pseudoscalar Higgs(A). We briefly discuss the Yukawa interactions of A. We finally present all phenomenological findings of the pseudoscalar Higgs in this chapter.

5.1 2HDM Type II: Yukawa interaction of A

We present the Yukawa interactions of the CP-odd Higgs (A) to fermions, leptons and gauge bosons in the Type II 2HDM. In addition to the coupling of the pseudoscalar Higgs involving only one scalar, we shall be interested in three couplings involving two or more couplings most importantly the coupling of the SM Higgs h to the pseudoscalar A and a Z boson, g_{hZA}. The couplings of two scalars, h, and A to an SM vector boson Z can be written in terms of α and β as [125];

$$g_{hZA} = \frac{1}{2}\sqrt{g^2 + g'^2}\cos(\beta - \alpha) \tag{5.1}$$

Table 5.1 below shows the tree-level couplings of the pseudoscalar Higgs A to up and down type quarks, leptons, and massive gauge bosons as functions of α and β.

Table 5.1: Yukawa interactions of A.

CP-odd Higgs A couplings $\frac{y_{2HDM}}{y_{SM}}$	2HDM Type II
C_V^A	0
C_u^A	$\frac{1}{\tan\beta}$
C_d^A	$\tan\beta$
C_l^A	$\tan\beta$

5.2 Decay Rates of pseudoscalar Higgs, A

5.2.1 Decay rates to fermions

The partial decay width for pseudoscalar Higgs into a pair of fermions is given by

$$\Gamma\left(A \to f\bar{f}\right) = \frac{\sqrt{2}G_F m_f^2 m_A}{8\pi}\left(C_f^A\right)^2 N_f \left(1 - \frac{4m_f^2}{m_A^2}\right)^{1/2} \tag{5.2}$$

where m_A is the pseudoscalar Higgs mass, and C_f^H is the mixing factor of the Yukawa interaction of A to fermions. The remaining terms have been defined in subsection 4.2.1.

5.2.2 Decay rates to Bosons

In the CP conserving 2HDM, the decay rates of A into gauge bosons are zero at the tree level, since the C_V^A coupling is absent as shown in Table 5.1 above. The CP-odd Higgs A can decay into other scalar bosons such as $H^\pm$ or H plus an either $W^\pm$ or Z bosons when kinematically allowed. When m_A is greater than the mass of the other scalar boson (m_{Sc}) plus the mass of the vector bosons (m_V), $m_A > m_{Sc} + m_V$, then the partial decay widths $\Gamma\left(A \to H^\pm W^\pm\right)$ and $\Gamma\left(H \to HZ\right)$ can be computed as;

$$\Gamma\left(A \to H^\pm W^\pm\right) = \sqrt{2}G_F \frac{m_A^3}{8\pi}(C_V^A)^2 \left(1 + \frac{m_{H^\pm}^4}{m_A^4} + \frac{m_{W^\pm}^4}{m_A^4} - \frac{2m_{H^\pm}^2 m_{W^\pm}^2}{m_A^4} - \frac{2m_{H^\pm}^2}{m_A^2} - \frac{2m_{W^\pm}^2}{m_A^2}\right)^{\frac{3}{2}} \tag{5.3}$$

$$\Gamma\left(A \to HZ\right) = \sqrt{2} G_F \frac{m_A^3}{8\pi} (C_V^A)^2 \left(1 + \frac{m_H^4}{m_A^4} + \frac{m_Z^4}{m_A^4} - \frac{2m_H^2 m_Z^2}{m_A^4} - \frac{2m_H^2}{m_A^2} - \frac{2m_H^2}{m_A^2}\right)^{\frac{3}{2}} \tag{5.4}$$

Also, when $m_{Sc} + m_V$ is greater than m_H, then the CP-odd Higgs A decays into either $H^\pm$ or H and an off-shell V, that is $\Gamma\left(A \to H^\pm W^{\pm *}\right)$ and $\Gamma\left(A \to HZ^*\right)$. These decay patterns are given by

$$\Gamma\left(A \to H^\pm W^{\pm *}\right) = \frac{9 G_F^2 m_{W^\pm}^4}{16\pi^3} \left(C_V^A\right)^2 m_A G\left(\frac{m_{H^+}^2}{m_A^2}, \frac{m_{W^\pm}^2}{m_A^2}\right) \tag{5.5}$$

$$\Gamma\left(A \to HZ^*\right) = \frac{3 G_F^2 m_Z^4}{32\pi^3} \left(C_V^A\right)^2 m_A \left(7 - \frac{40}{3}\sin\theta_W^2 + \frac{160}{9}\sin\theta_W^4\right) G\left(\frac{m_H^2}{m_A^2}, \frac{m_Z^2}{m_A^2}\right) \tag{5.6}$$

where the function $G\left(x, y\right)$ and $\lambda\left(x, y\right)$ are defined in subsection 4.2.1.

5.2.3 Decay rates to $\gamma\gamma$ and gg

The loop induced decay modes of the CP-odd Higgs, $\Gamma\left(H \to \gamma\gamma\right)$ and $\Gamma\left(H \to gg\right)$ can be expressed as;

$$\Gamma\left(A \to \gamma\gamma\right) = \frac{\sqrt{2} G_F \alpha_{em}^2 m_A^3}{64\pi^3} \Big| \sum_f Q_f^2 N_c^f C_f^A I_f^A\left(m_A\right) \Big|^2 \tag{5.7}$$

$$\Gamma\left(A \to gg\right) = \frac{\sqrt{2} G_F \alpha_s^2 m_A^3}{128\pi^3} \Big| \sum_{f=q} C_f^A I_f^A\left(m_A\right) \Big|^2 \tag{5.8}$$

Where the loop function $I_f^A\left(m_A\right)$ is given by

$$I_f^A(m_A) = 2m_f^2 C_0(0, 0, m_h^2; m_f^2, m_f^2, m_f^2), \tag{5.9}$$

The function C_0 takes the form

$$C_0\left(0,0,m_H^2;m_f^2,m_f^2,m_f^2\right)=\frac{-2}{m_H^2}f\left(\frac{4m_f^4}{m_H^2}\right) \tag{5.10}$$

5.2.4 Decay rates to Zh

The partial decay width of A to Zh is given by [140];

$$\Gamma\left(A\to Zh\right)=\frac{g^2\lambda^{3/2}\cos^2\left(\beta-\alpha\right)}{64\pi m_Z^2 m_A^3\cos^2\theta_W} \tag{5.11}$$

Where

$$\lambda\left(x,y,z\right)=x^2+y^2+z^2-2xy-2yz-2zx \tag{5.12}$$

5.3 Pseudoscalar Higgs Production

Similarily to the production of the heavy Higgs, the pseudoscalar Higgs can be produced predominantly in the gluon fusion mechanism via loops involving primarily the heavy bottom and top quarks. The gluon fusion mechanism for A can be examined at a threshold of higher-order corrections taking into account softly broken gluon effects [141]. Also, the CP-odd Higgs boson can be produced in association with top-anti top pair [142–144]. An alternative way to produce the CP odd Higgs is via photon-photon collision taking into account one complete loop contributions [145]. The principle of CP invariance forbids the coupling of the CP-odd Higgs to gauge vector bosons, hence A cannot be produced in the vector boson fusion. The production rates of the CP odd Higgs depend strongly on m_A and $\tan\beta$. For our numerical analysis, we have employed NLO MSTW2008[141, 146] parton distribution functions to calculate the cross sections at a center of mass energy, $\sqrt{s}=14$TeV. We calculate NLO cross sections for A using SusHi program [123] such that the radiative corrections of the Higgs sector were carefully calculated at a fixed SM Higgs mass, $m_h=125.09$GeV. The

production cross section rate is given by

$$\sigma_{\mathrm{NLO}}\left(gg \to A\right)\Big|_{\alpha,\beta} = \sigma_{\mathrm{NLO}}\left(gg \to h_{\mathrm{sm}}\right) \frac{\Gamma_{\mathrm{LO}}\left(A \to gg\right)\Big|_{\alpha,\beta}}{\Gamma_{\mathrm{LO}}\left(h_{\mathrm{sm}} \to gg\right)} \tag{5.13}$$

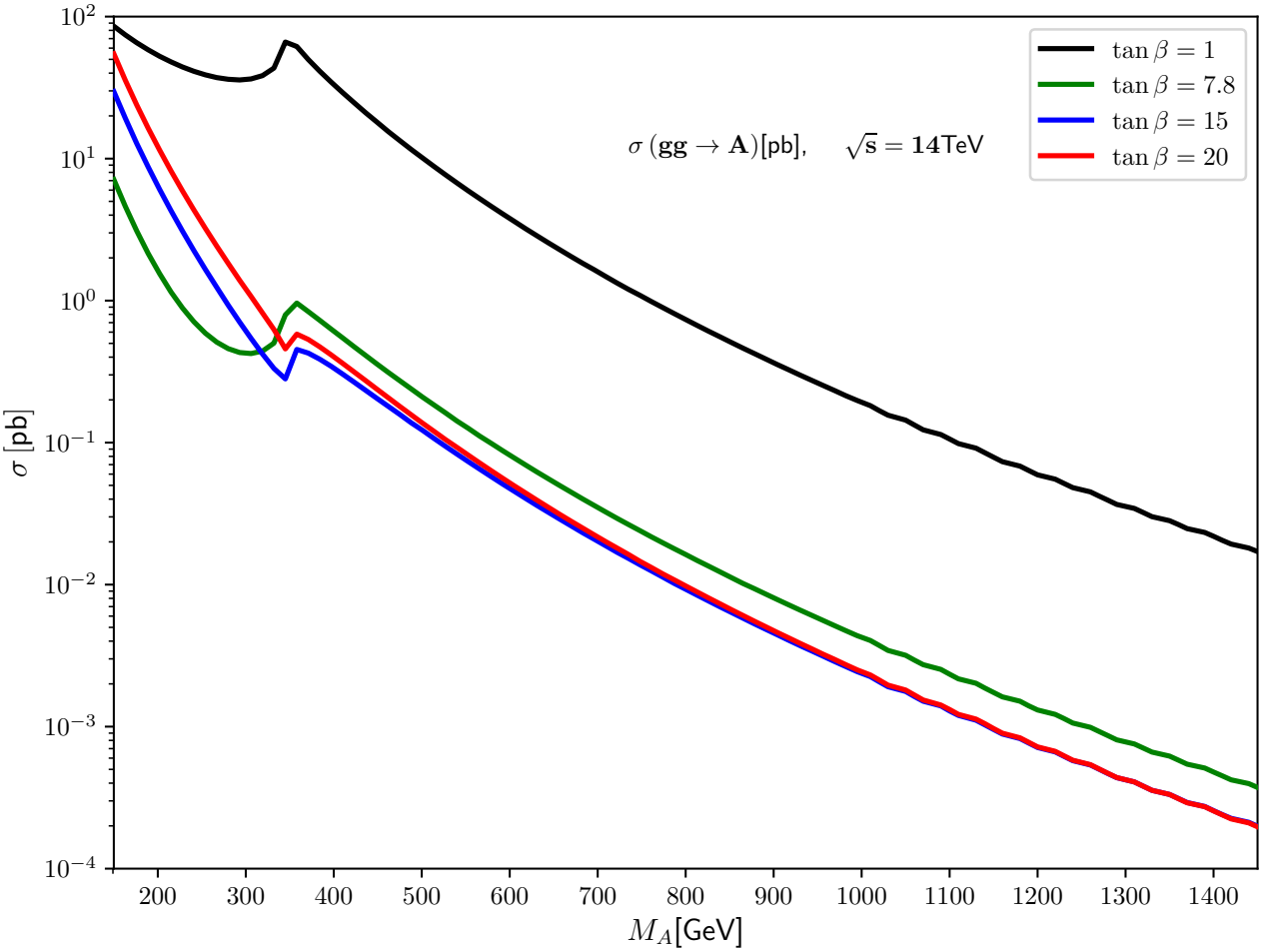

Figure 5.1: 2HDM Type II: σ_{ggA} in the decoupling limit for $\tan\beta = 1, 7.8, 15$ and 20

Fig. 5.1 shows the production cross section for A at the LHC with a center of mass energy of $\sqrt{s} = 14$TeV in the decoupling limit at $\tan\beta = 1, 7.8, 15$ and 20. From Fig. 5.1, for small values of $\tan\beta$, the dominant contributions to the cross sections come from the top quark loops as the g_{Att} couplings, $g_{Att} \propto \frac{1}{\tan\beta}$ are strong. At higher values of $\tan\beta$, the

coupling of A to the top quark loop g_{Att} becomes suppressed, while those to the bottom quarks g_{Abb} gets enhanced. For intermediate $\tan\beta$ values, $\tan\beta \approx 3-10$, the suppression of the g_{Att} coupling is already effective whereas the g_{Abb} is not yet significantly enhanced. We see also that the production cross sections for the CP odd state differs from that of the CP even state in the two Higgs doublet models since the couplings of the CP even H state to fermions are not exactly the same as those of the pseudoscalar state, A.

5.4 Decay channels for Pseudoscalar Higgs

We discuss the allowed channels of the CP odd Higgs in this section. We constraints the mass of the CP-odd Higgs such that;

$$m_H = m_{H^\pm} + 50\text{GeV}; \qquad m_A = m_H - 50\text{GeV} \tag{5.14}$$

Next, we present phenomenological analysis for the CP odd Higgs in the decoupling limit, near the decoupling limit, and in the crescent limit.

5.4.1 σ_{ggA} times branching ratios vrs m_A in the decoupling limit

Figs. 5.2 , 5.3 , 5.4 , 5.5 show the cross sections times branching fractions for the CP odd Higgs at $\sqrt{s} = 14\text{TeV}$. We focus our discussion on high and low $\tan\beta$ regimes. Values of $\tan\beta$ are of interest because the production and decay patterns of the 2HDM Higgs bosons depend significantly on $\tan\beta$ [133].

Low and High $\tan\beta$ regime

For extremely low values of $\tan\beta$, $\tan\beta = 1$, it can be seen from Fig. 5.2 that the production rates times the branching ratios are extremely high. Here, the couplings of A to the top quarks is enhanced, whereas that to the bottom quarks is suppressed. We conclude that $\tan\beta = 1$ is an excellent choice to see the dominant top quark in the loop. Our results show that at high $\tan\beta$ values, there is an enhancement in the couplings of the CP-odd

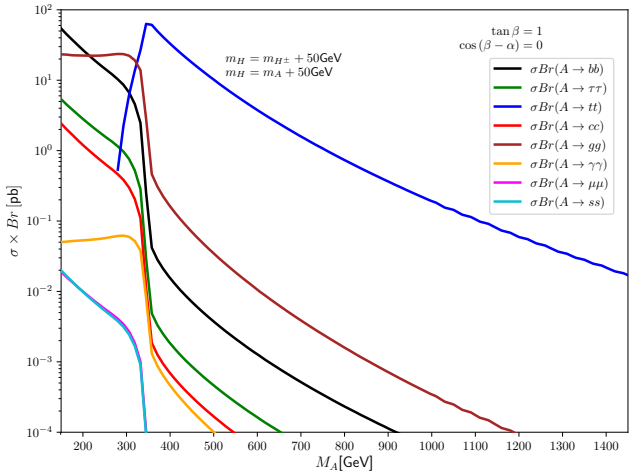

Figure 5.2: σ_{ggA} times branching ratios vrs m_A at $\cos(\beta-\alpha) = 0$ for $\tan\beta = 1$

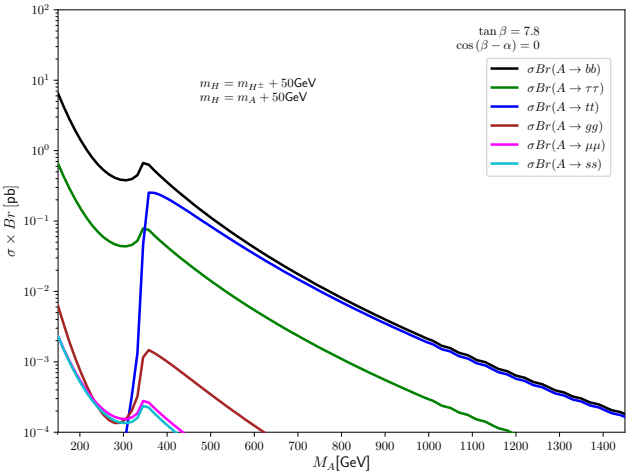

Figure 5.3: σ_{ggA} times branching ratios vrs m_A at $\cos(\beta-\alpha) = 0$ for $\tan\beta = 7.8$

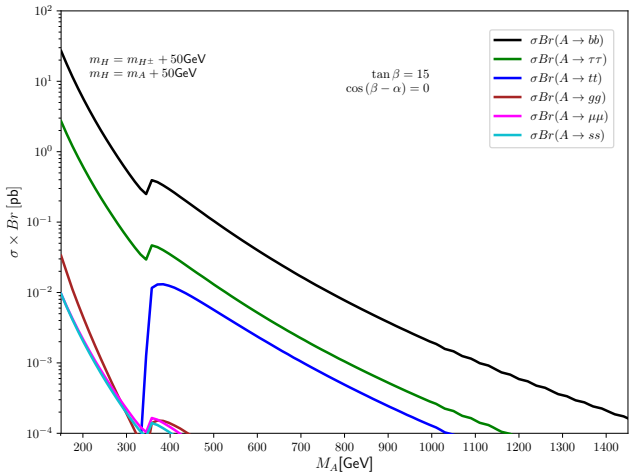

Figure 5.4: σ_{ggA} times branching ratios vrs m_A at $\cos(\beta-\alpha) = 0$ for $\tan\beta = 15$

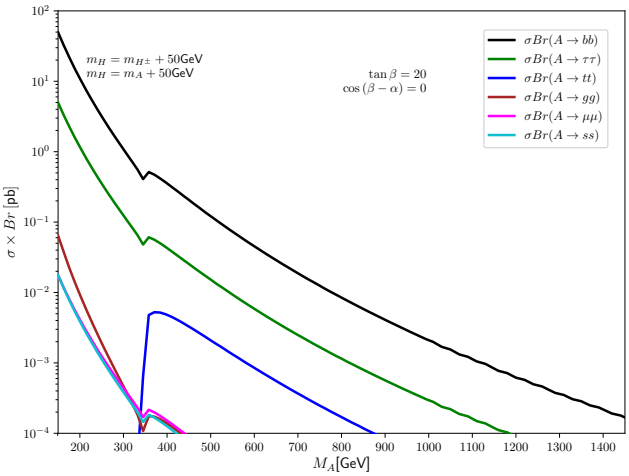

Figure 5.5: σ_{ggA} times branching ratios vrs m_A at $\cos(\beta-\alpha) = 0$ for $\tan\beta = 20$

Higgs to b quarks and τ leptons whereas that to top quarks is suppressed. This is because the couplings g_{Abb} and $g_{A\tau\tau}$ have the $\tan\beta$ dependence as $g_{Abb}, g_{A\tau\tau} \propto \tan\beta$ whereas that of $g_{At\bar{t}}$, is given as, $g_{At\bar{t}} \propto \frac{1}{\tan\beta}$. We also observe some clear channels for A, such as $A \to \mu\mu$, $A \to ss$ and a loop induced channel $A \to gg$. These channels are strongly enhanced for higher $\tan\beta$ values because the Yukawa interactions for strange quarks, and muons, are

directly proportional to $\tan\beta$. In summary, the decay pattern for the CP-odd Higgs is remarkably simple: the $t\bar{t}$ channel and all other decay modes are fully suppressed to a level where their branching ratios are negligible excluding the decay of the CP-odd Higgs into $\tau\tau$ and $b\bar{b}$ pairs. These exclusive channels are said to be the dominant channel at higher $\tan\beta$ regimes. Supposedly, the branching fractions of $Br\left(A \to \tau\tau\right)$ and $Br\left(A \to b\bar{b}\right)$ could be around approximately 10% and 90% respectively.

5.4.2 σ_{ggA} times branching ratios vrs m_A near the decoupling limit

When kinematically allowed, the CP-odd Higgs decays into a light Higgs scalar h and SM vector boson Z, $A \to Zh$. We observed the Z, $A \to Zh$ channel in this limit where $\cos(\beta-\alpha) \neq 0.004$. From equation 5.1, we see that the coupling of the CP-odd Higgs A to SM Higgs h and a vector boson away from the decoupling limit is strongly dependent on $\cos(\beta-\alpha)$. Figs. 5.6 , 5.7 , 5.8 , and 5.9 show cross sections times the branching ratios of A at $\cos(\beta-\alpha) = 0.004$. The results presented show that the $A \to Zh$ channel is enhanced at small values of $\tan\beta$, $\tan\beta = 1$, and is suppressed as $\tan\beta$ grows up. This case is valid because near the decoupling, the coupling of A to Zh approaches almost zero and we see from equation 5.11 that the partial decay width $\Gamma\left(A \to Zh\right)$ grows as $\Gamma\left(A \to Zh\right) \propto \frac{1}{\tan^2\beta}$. For $A \to ff$, similar analysis holds for the decoupling limit, since the couplings of A to fermions in both cases has the same $\tan\beta$ dependent. In conclusion, near the decoupling limit, the dominant decay modes for A are $A \to b\bar{b}$, $A \to gg$, $A \to \tau^+\tau^-$, $A \to Zh$ and $A \to t\bar{t}$. When kinematically available, $A \to Zh$ channel dominates at low values of $\tan\beta$ for $m_A < 2m_t$ but highly suppressed at high values of $\tan\beta$. Also, $A \to t\bar{t}$ becomes dominant at low values of $\tan\beta$ but it is suppressed relative to $A \to b\bar{b}$ at high values of $\tan\beta$ due to the reduction of g_{Att} and enhancement of g_{Abb}.

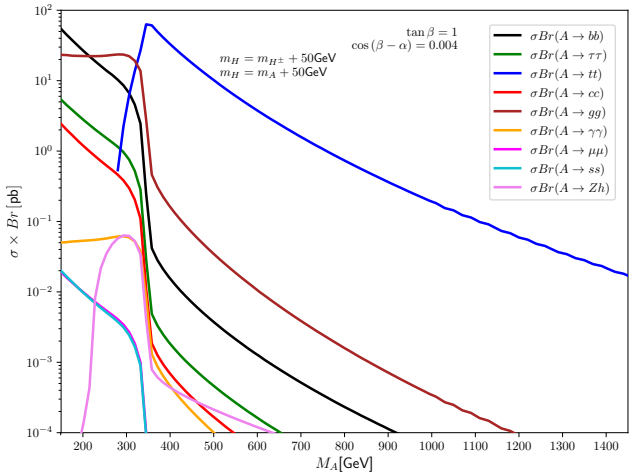

Figure 5.6: σ_{ggA} times branching ratios vrs m_A at $\cos(\beta-\alpha) = 0.004$ for $\tan\beta = 1$

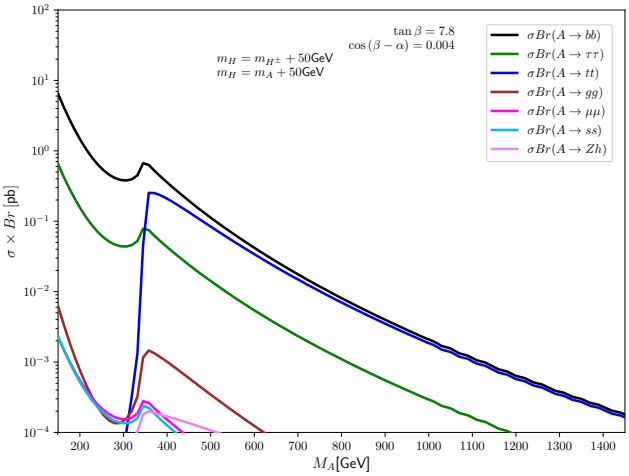

Figure 5.7: σ_{ggA} times branching ratios vrs m_A at $\cos(\beta-\alpha) = 0.004$ for $\tan\beta = 7.8$

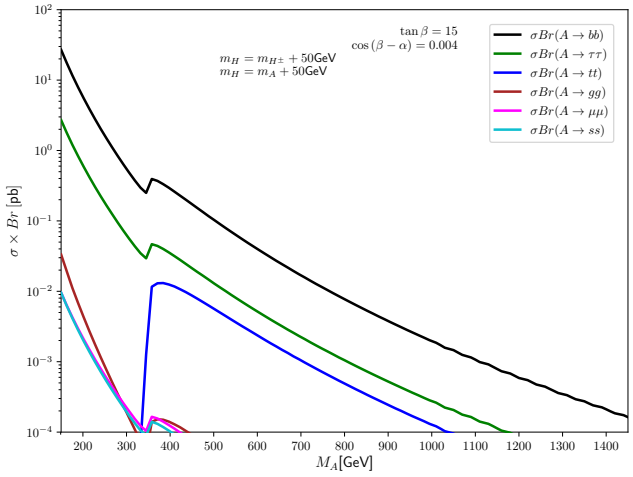

Figure 5.8: σ_{ggA} times branching ratios vrs m_A at $\cos(\beta-\alpha) = 0.004$ for $\tan\beta = 15$

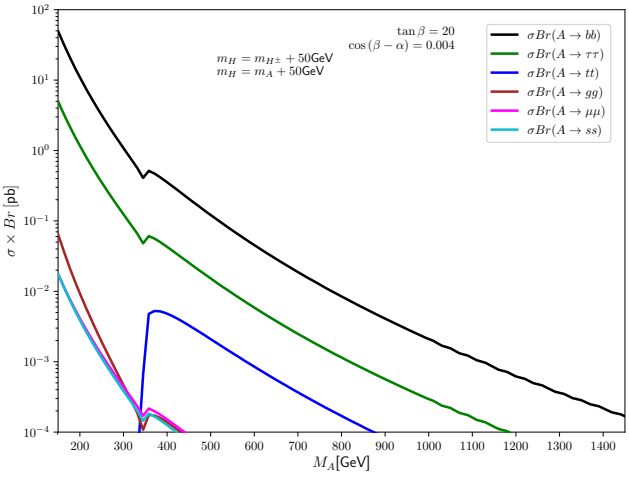

Figure 5.9: σ_{ggA} times branching ratios vrs m_A at $\cos(\beta-\alpha) = 0.004$ for $\tan\beta = 20$

5.4.3 σ_{ggA} times branching ratios vrs m_A in the crescent limit

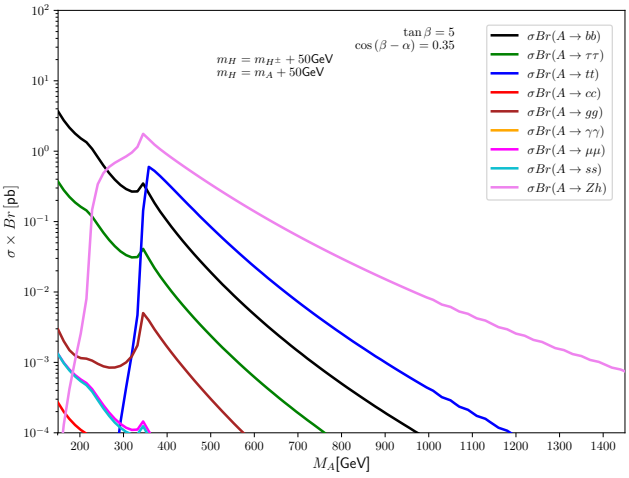

Figure 5.10: σ_{ggA} times branching ratios vrs m_A at 2σ for $\tan\beta = 5$

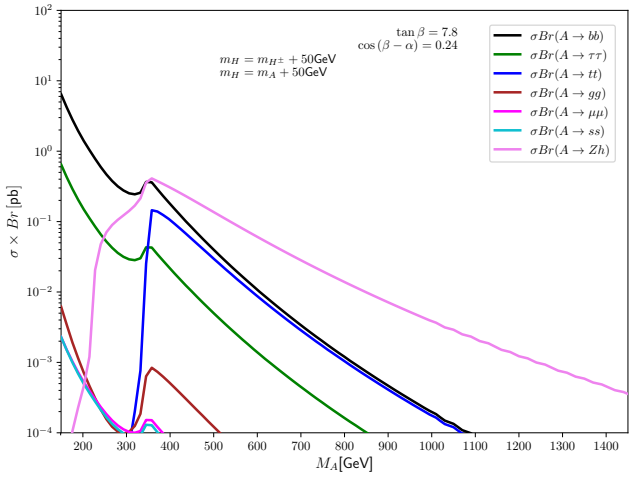

Figure 5.11: σ_{ggA} times branching ratios vrs m_A at 1σ for $\tan\beta = 7.8$

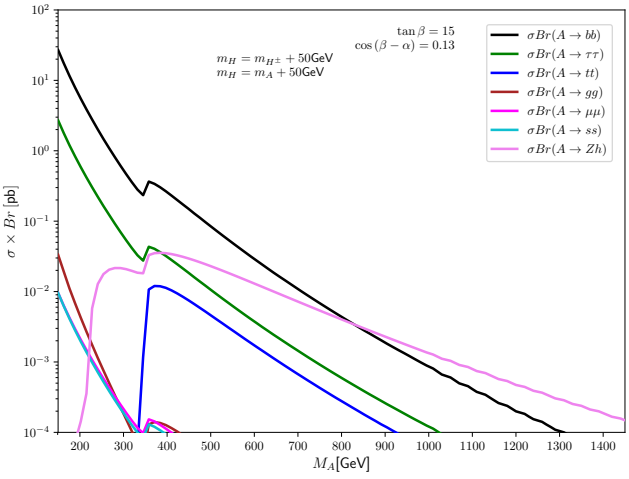

Figure 5.12: σ_{ggA} times branching ratios vrs m_A at 1σ for $\tan\beta = 15$

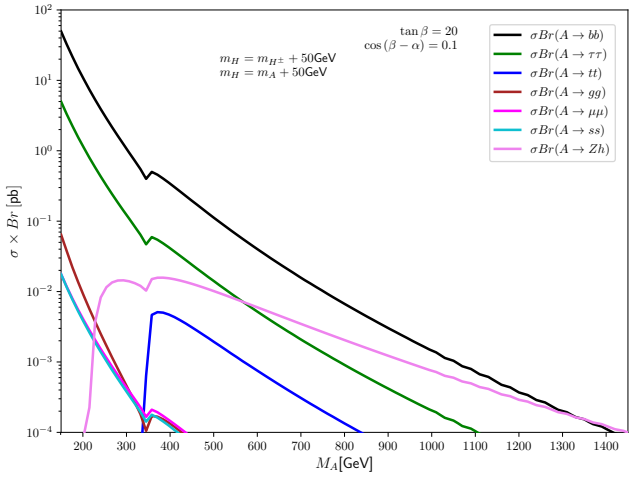

Figure 5.13: σ_{ggA} times branching ratios vrs m_A at 1σ for $\tan\beta = 20$

- **$A \to Zh$ search channel in the crescent limit**

This is a very important search channel of interest in this region. The coupling of A to Zh is directly proportional to $\cos(\beta - \alpha)$, which spans from about $0.2 - 0.6$ in the crescent limit as shown in Fig 3.1. Although the branching ratio $Br\,(A \to Zh)$ will be proportional to the square of this number, the magnitude is sufficient enough to make $Br\,(A \to Zh)$ the preferred channel for A decays within certain regions over the parameter space. That implies that for intermediate values of $\tan\beta$, $\tan\beta \approx 7.8$, the decay of A into Zh dominates over that of $t\bar{t}$ and $b\bar{b}$ as seen in Fig5.11. The $A \to Zh$ channel is predominantly enhanced for low $\tan\beta$ values and high $\cos(\beta - \alpha)$ values whereas it gets slightly suppresses for high $\tan\beta$ values and low $\cos(\beta - \alpha)$ values. The partial decay width for $\Gamma\,(A \to Zh)$ grows as $\frac{1}{\tan^2\beta}$. For the case of the fermionic channels, our analysis holds just like in and near the decoupling limit, since the coupling of the pseudoscalar Higgs to top quarks is proportional to $\frac{1}{\tan\beta}$, the coupling to bottom quarks grows with $\tan\beta$, and there is no dependence on $\cos\,(\beta - \alpha)$.

5.4.4 Comparative review on the $A \to Zh$ channel

There have been several studies for the $A \to Zh$ channel. The ATLAS [147–149] and CMS [150] collaborations at CERN searched for the $A \to Zh$ in di-photon, multi-leptons, and bottom anti-bottom quarks final states. According to [151, 152], searches in the di-photon channels are essentially important to constrain pseudoscalars below $m_A < 350$GeV. Moreover, the $pp \to A \to Zh$ was recently examined by [153] in the type II 2HDM, where the $A \to Zh$ decay channel was found to be dominant at moderate values of $\tan\beta$, even for m_A values above the threshold where the decay into a pair of top quarks is kinematically open. In [153], datasets were generated using ScannerS [154–157] and tree level theoretical constraints from the boundedness theory for some Higgs potential [13, 158] with perturbative unitarity[13] were imposed. Ref. [153] required the electroweak vacuum to be a global minimum of the tree-level Higgs potential outlined in [159] and finally passed the information obtained for the branching ratios, total decay widths and cross sections to HiggsBounds 4.3.1 [160–163] to check exclusion bounds from searches of additional Higgs.

Chapter 6

Charged Higgs Bosons in the Two Higgs Doublet Model

In this chapter, we investigate charged Higgs bosons phenomenology in the context of the Type II 2HDM. With constraints on the five scalar bosons masses and the parameter space coming from present LHC data, we search for new channels arising from the charged Higgs by studying its production and decays.

6.1 The Yukawa interaction of $H^{\pm}$

The Yukawa interaction for the charged Higgs boson $H^{\pm}$ in the Type II 2HDM is briefly outlined in this section. Table 6.1 below shows tree-level couplings of $H^{\pm}$ to up and down type quarks, leptons, and massive gauge bosons as functions of α and β.

Table 6.1: Mixing factors in Yukawa interactions of $H^{\pm}$

Charged Higgs $H^{\pm}$ couplings $\frac{y_{2HDM}}{y_{SM}}$	2HDM Type II
$C_V^{H^{\pm}}$	0
$C_u^{H^{\pm}}$	$\cot\beta$
$C_d^{H^{\pm}}$	$-\tan\beta$
$C_l^{H^{\pm}}$	$-\tan\beta$

From Table 6.1 above, we notice that the couplings of $H^{\pm}$ to the vector bosons are zero whereas that to the fermions are β dependent. However, if kinematically allowed, the charged Higgses $H^{\pm}$ may decay to an SM-like Higgs and a $W^{\pm}$ boson, $H^{\pm} \to W^{\pm}h$. The coupling of $H^{\pm} \to W^{\pm}h$, $g_{hW^{\pm}H^{\pm}}$ [125] can be written as:

$$g_{hW^{\pm}H^{\pm}} = \mp\frac{i}{2}g\cos\left(\beta-\alpha\right) \tag{6.1}$$

6.2 Decay rates of the charged Higgs bosons in the 2HDM

In this section, we present the analytic expression for the decays of the charged Higgs bosons.

6.2.1 Decay rates to fermions

If the mass of $H^{\pm}$ is larger than $m_t + m_b$, H^+ can decay into $t\bar{b}$ according to the decay rate:

$$\begin{aligned}\Gamma(H^+ \to t\bar{b}) = \sqrt{2}G_F\frac{m_{H^+}}{8\pi}\lambda\left(\frac{m_t^2}{m_{H^+}^2},\frac{m_b^2}{m_{H^+}^2}\right)^{1/2} \\ \times\left\{\left[m_b^2\left(C_d^{H^{\pm}}\right)^2+m_t^2\left(C_u^{H^{\pm}}\right)^2\right]\left(1-\frac{m_t^2+m_b^2}{m_{H^+}^2}\right)-\frac{4m_b^2m_t^2C_d^{H^{\pm}}C_u^{H^{\pm}}}{m_{H^+}^2}\right\},\end{aligned} \tag{6.2}$$

where the function $\lambda\left(x,y\right)$ is already defined in Eq. 4.9. For decay rates to gauge bosons, the decay rate for H^+ decaying into gauge bosons are zero at tree level since $C_V^{H^{\pm}} = 0$ as shown in Table 6.1.

6.2.2 Decay rates to scalar boson and a vector boson, V

If kinematically allowed, $H^\pm$ can decay into other scalar bosons plus a vector boson, $V = W$ or Z. Such decay rates can be evaluated as:

$$\Gamma(H^\pm \to hW^\pm) = \sqrt{2} G_F \frac{m_{H^+}^3}{8\pi} \left(\cos\left(\beta-\alpha\right)\right)^2 \lambda^{3/2}\left(\frac{m_h^2}{m_{H^+}^2}, \frac{m_W^2}{m_{H^+}^2}\right) \tag{6.3}$$

$$\Gamma(H^\pm \to HW^\pm) = \sqrt{2} G_F \frac{m_{H^+}^3}{8\pi} \left(\sin\left(\beta-\alpha\right)\right)^2 \lambda^{3/2}\left(\frac{m_H^2}{m_{H^+}^2}, \frac{m_W^2}{m_{H^+}^2}\right) \tag{6.4}$$

$$\Gamma(H^\pm \to AW^\pm) = \sqrt{2} G_F \frac{m_{H^+}^3}{8\pi} \lambda^{3/2}\left(\frac{m_A^2}{m_{H^+}^2}, \frac{m_W^2}{m_{H^\pm}^2}\right) \tag{6.5}$$

6.2.3 Decay rates to scalar boson and the off shell V

Also, if kinematically available, $H^\pm$ can decay into other scalar bosons and an off-shell V. These decay rates are given by

$$\Gamma(H^\pm \to hW^{\pm *}) = \frac{9 G_F^2 m_W^4}{16\pi^3} \left(\cos\left(\beta-\alpha\right)\right)^2 m_{H^+} G\left(\frac{m_h^2}{m_{H^+}^2}, \frac{m_W^2}{m_{H^+}^2}\right) \tag{6.6}$$

$$\Gamma(H^\pm \to HW^{\pm *}) = \frac{9 G_F^2 m_W^4}{16\pi^3} \left(\sin\left(\beta-\alpha\right)\right)^2 m_{H^+} G\left(\frac{m_H^2}{m_{H^+}^2}, \frac{m_W^2}{m_{H^+}^2}\right) \tag{6.7}$$

$$\Gamma(H^\pm \to AW^{\pm *}) = \frac{9 G_F^2 m_W^4}{16\pi^3} m_{H^+} G\left(\frac{m_A^2}{m_{H^+}^2}, \frac{m_W^2}{m_{H^+}^2}\right) \tag{6.8}$$

where the function $G(x,y)$ is given as

$$\begin{aligned} G(x,y) = \frac{1}{12y}\Bigg\{ & 2\left(-1+x\right)^3 - 9\left(-1+x^2\right) y + 6\left(-1+x\right) y^2 \\ & + 6\left(1+x-y\right) y \sqrt{-\lambda(x,y)} \left[\tan^{-1}\left(\frac{-1+x-y}{\sqrt{-\lambda(x,y)}}\right) + \tan^{-1}\left(\frac{-1+x+y}{\sqrt{-\lambda(x,y)}}\right)\right] \\ & - 3\left[1+(x-y)^2-2y\right] y \log x \Bigg\}. \end{aligned} \tag{6.9}$$

6.3 Charged Higgs Production

In this section, we discuss predictions for single charged Higgs production at a center of mass energy, $\sqrt{s} = 14$TeV for the Type II 2HDM. In hadronic collisions, there are several relevant charged Higgs production channels. We categorize these channels into two, namely the fermionic and bosonic channels. We can consider single charged Higgs production for the Type II 2HDM in the following ways;

(1) Fermionic channel, $gg \to H^+ b\bar{t}$

(2) Fermionic channel, $g\bar{b} \to H^+ \bar{t}$

(3) Bosonic channel, $gg \to H_j \to H^+ W^-$

The Feynman diagrams below show the production channels of the charged Higgs.

(1) $gg \to H^+ b\bar{t}$

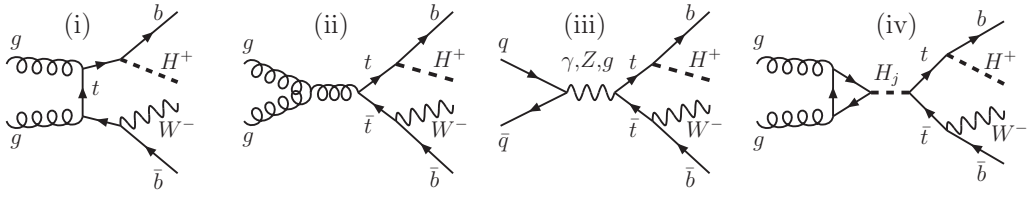

Figure 6.1: Feynman diagrams for $gg \to H^+ b\bar{t}$

.

(2) $g\bar{b} \to H^+\bar{t}$

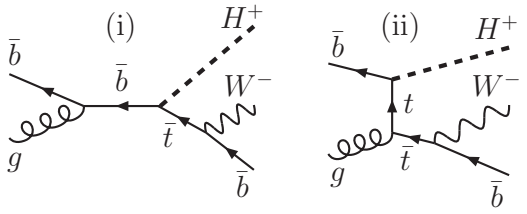

Figure 6.2: Feynman diagrams for $g\bar{b} \to H^+\bar{t}$

.

(3) $gg \to H_j \to H^+W^-$

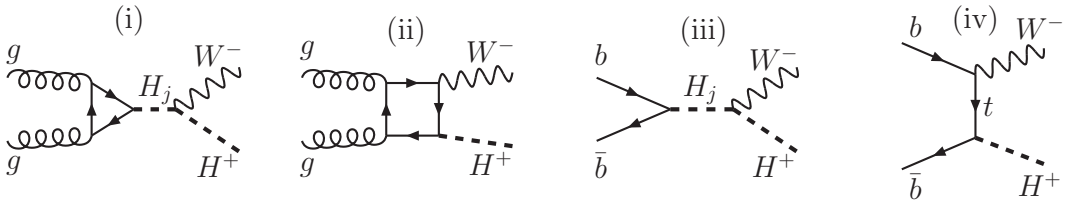

Figure 6.3: Feynman diagrams for $gg \to H_j \to H^+W^-$

.

6.4 Charged Higgs searches channels

The strategy to search for charged Higgs depends on its mass which predicts both the production and available decay modes. These search strategies can be grouped into low mass and high mass cross sections as briefly discussed below;

(1) **Low-mass cross-section**

If the mass of the charged Higgs boson satisfies $m_{H^+} < m_t - m_b$, where m_t is the top quark mass and m_b is the bottom quark mass, then H^+ could be produced via top decays, $t \to H^+b$. In this region, where m_{H^+} is below the tb threshold, the $H^+ \to \tau v$ decay mode is dominant for $\tan\beta > 1$.

(2) **High-mass cross-section**

The main contribution to the charged Higgs boson production at hadron colliders is via the twin processes, $gg \to tbH^+$ and $gb \to tH^+$ for $m_{H^+} > m_t$. We refer to these two processes as twin processes since they correspond to two different approximations describing the same basic processes. Hence for charged Higgs boson masses above the top quark masses, the twin processes are dominant due to the resummation of potentially large logarithms in the bottom quark parton density [164]. For high charged-Higgs masses, the decay into a top and bottom quarks, $H^+ \to t\bar{b}$ dominates. In this work, we evaluate the charged Higgs production cross sections with MadGraph 5 [165] for three significant channels at next-to-leading order, then we predict the most dominant H^+ production channel likely to be seen at the LHC. Our results in Figs. 6.4, C.1 and C.2 proves $pp \to H^+\bar{t}b$ to be the dominant production channel followed by $g\bar{b} \to H^+\bar{t}$ and $gg \to H^+W^-$ been the least channel. Both $pp \to H^+\bar{t}b$ and $g\bar{b} \to H^+\bar{t}$ occur for intermediate and higher H^+ mass range produced directly in association with a top and a bottom quark, leading to a cross section that is proportional to $\tan^2\beta$. From [166], the total cross section for the type II 2HDM can be parameterized by

$$\sigma_{H^\pm}^{\text{Type II}} \propto g_t^2\sigma_t \cot^2\beta + g_b\sigma_b \tan^2\beta + g_t g_b \sigma_{tb} \tag{6.10}$$

where g_t and g_b are the part of the Yukawa couplings proportional to the top and bottom quark masses respectively. We observe from our results in Figs. 6.4, C.1 and C.2 that for $\tan\beta \approx 1$, the Yukawa coupling to the top quark with $\frac{1}{\tan^2\beta}$ is enhanced whereas for intermediate and high $\tan\beta$ values, the coupling to the bottom quark with $\tan^2\beta$ is enhanced while that to the top quark is suppressed. This is true for all the three selected production channels since the production cross section according to Eq. 6.10 above is dependent on the masses of the scalar bosons and $\tan\beta$.

6.4.1 Cross sections rates in the decoupling limit

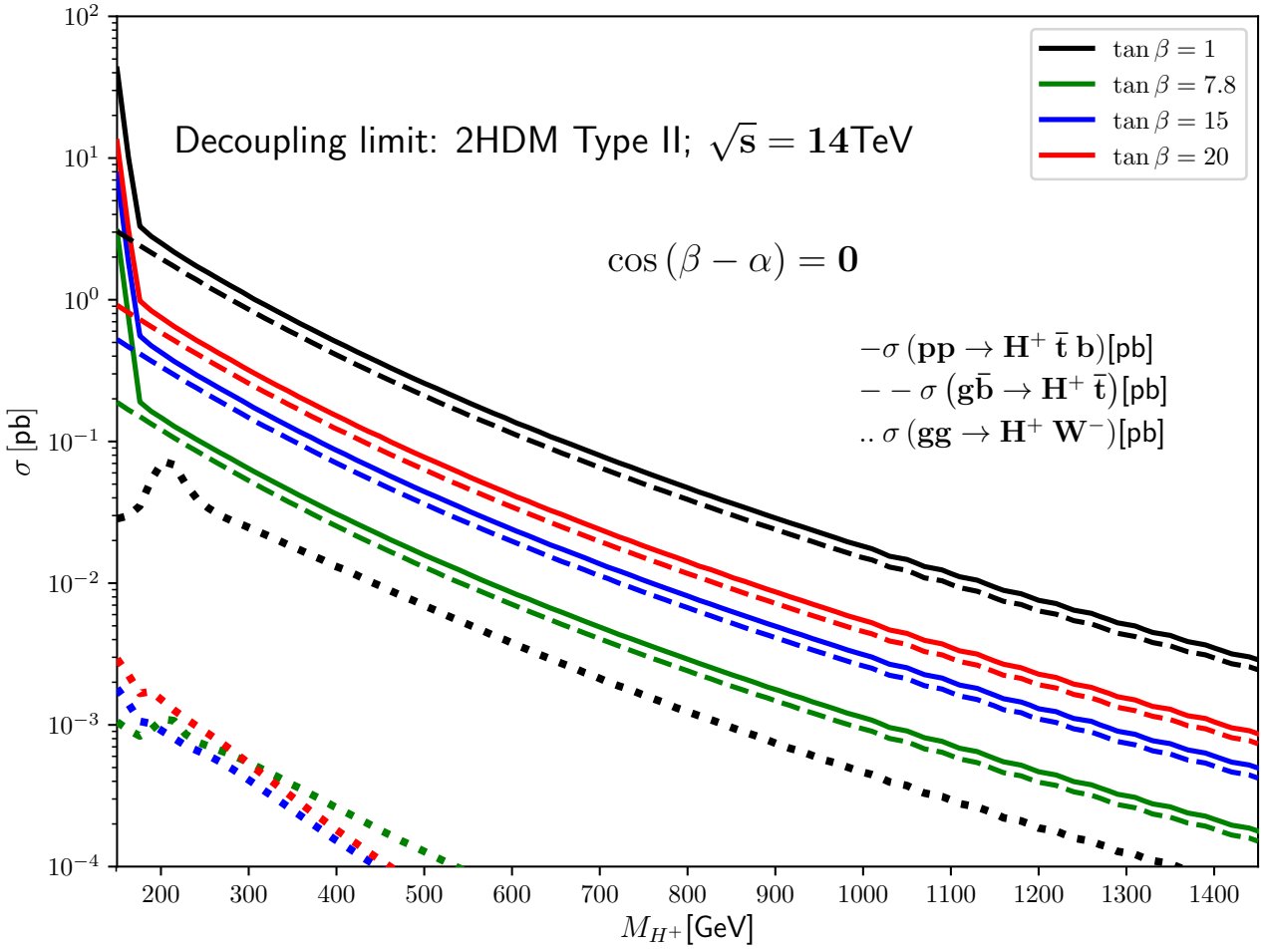

Figure 6.4: Cross section rates for charged Higgs in the decoupling limit

6.5 Production cross sections times branching fraction

We present in this section the production cross section times the branching fractions of the charged Higgs. We choose the $pp \to H^+\bar{t}b$ production channel for our analysis since it is the dominant channel. First, from Figs. 6.5, 6.6, 6.7 and 6.8, we show results in the decoupling limit at $\cos(\beta - \alpha) = 0$ and we found that above the top-bottom threshold (that is $m_{H^\pm} > m_t - m_b$), the dominant channel is $H^\pm \to t\bar{b}$ whereas $H^\pm \to \tau\nu_\tau$ dominates in a

region below the top-bottom threshold ($m_{H^\pm} < m_t - m_b$). The sub-dominant channels are the $H^\pm \to cb$ and $H^\pm \to cs$ followed by the leptonic channel $H^\pm \to \mu\nu_\mu$ being the least channel. Second, from Figs. 6.9, 6.10, 6.11 and 6.12, we present results near the decoupling limit at $\cos(\beta - \alpha) = 0.004$ and our results are very similar to that of the decoupling limit except for the $H^\pm \to hW$ channel which exists in the former and vanishes in the latter. The $H^\pm \to hW$ channel which exists at $\cos(\beta - \alpha) = 0.004$ is very small, about the orders of 10^{-7} and is not shown on the plots. Lastly, we show in Figs. 6.13, 6.14, 6.15 and 6.16 results far away from the decoupling limit. Here, the fermionic channel results follow similar pattern like in the decoupling and near the decoupling limit. However, we observe that another decay mode, $H^\pm \to hW^\pm$ opens up with a large branching ratio once the condition $\cos(\beta - \alpha) = 0$ is relaxed. The $H^\pm \to hW^\pm$ channel widely opens up for high $\cos(\beta - \alpha)$ values and gets suppressed for low $\cos(\beta - \alpha)$ values. This analysis is valid as it is guranteed by Eq. 6.1. In summary, we have shown that the dominant decay mode of charged Higgs in Type II model, as expected is in the $\bar{t}b$ channel, following the sub-dominant $\bar{\tau}\nu_\tau$ channel with Br $\sim 10 - 15$ %, followed by other suppressed modes such as, $H^+ \to \bar{b}c, c\bar{s}, \mu\nu_\mu$ and a new channel $H^\pm \to hW^\pm$ opens up for relaxed values of $\cos(\beta - \alpha)$.

6.5.1 Analyzing results in the decoupling limit

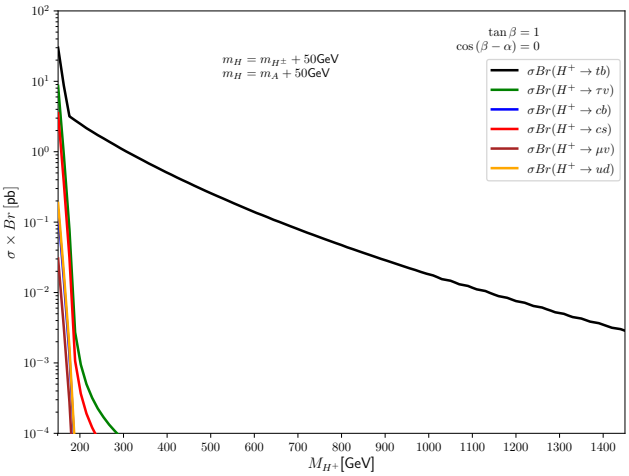

Figure 6.5: $\sigma\,(\mathbf{pp} \to \mathbf{H}^+\,\bar{\mathbf{t}}\,\mathbf{b})$[pb] times branching ratios vrs $m_{H^\pm}$ in the decoupling limit, for $\tan\beta = 1$

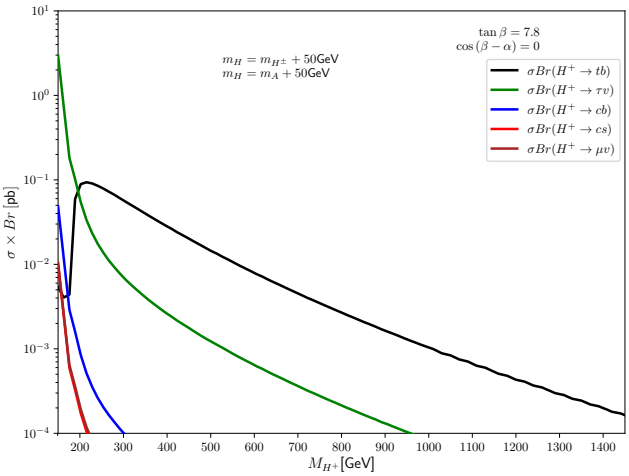

Figure 6.6: $\sigma\,(\mathbf{pp} \to \mathbf{H}^+\,\bar{\mathbf{t}}\,\mathbf{b})$[pb] times branching ratios vrs $m_{H^\pm}$ in the decoupling limit, for $\tan\beta = 7.8$

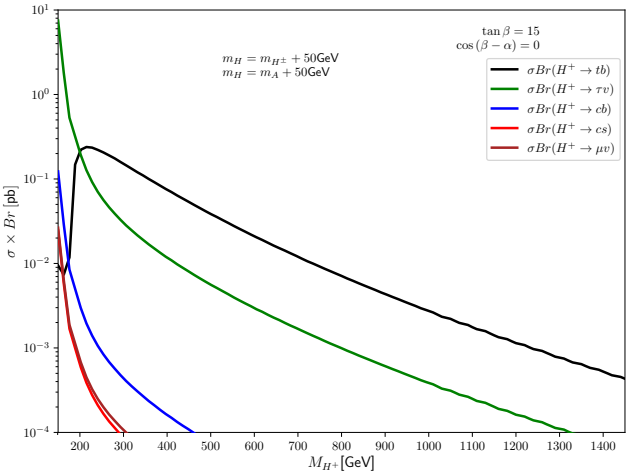

Figure 6.7: $\sigma\,(\mathbf{pp} \to \mathbf{H}^+\,\bar{\mathbf{t}}\,\mathbf{b})$[pb] times branching ratios vrs $m_{H^\pm}$ in the decoupling limit, for $\tan\beta = 15$

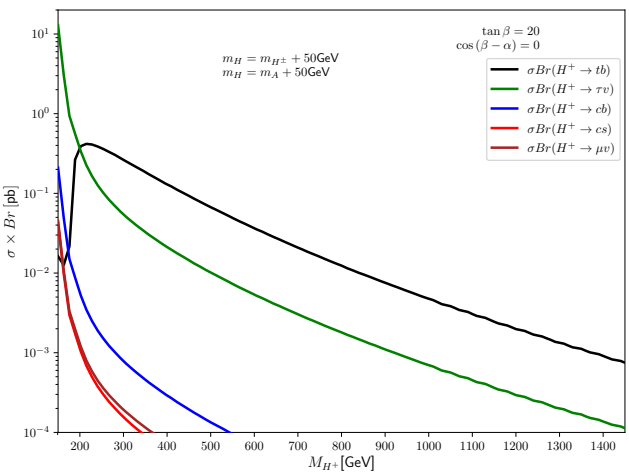

Figure 6.8: $\sigma\,(\mathbf{pp} \to \mathbf{H}^+\,\bar{\mathbf{t}}\,\mathbf{b})$[pb] times branching ratios vrs $m_{H^\pm}$ in the decoupling limit, for $\tan\beta = 20$

6.5.2 Analyzing results near the decoupling limit

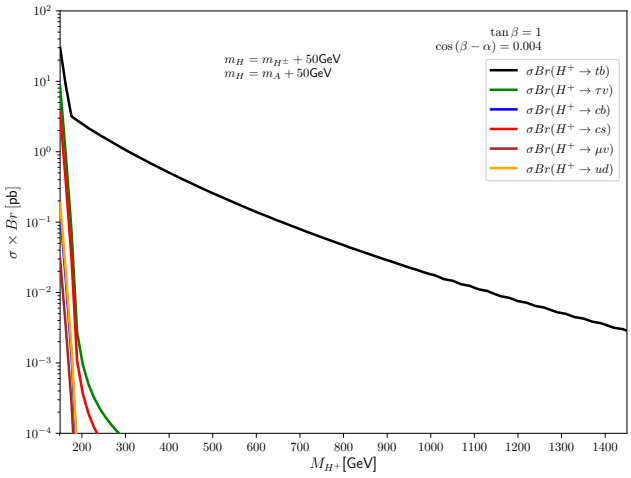

Figure 6.9: $\sigma\,(\mathbf{pp} \to \mathbf{H^+}\,\bar{\mathbf{t}}\,\mathbf{b})$[pb] times branching ratios vrs $m_{H^\pm}$ near the decoupling limit, for $\tan\beta = 1$

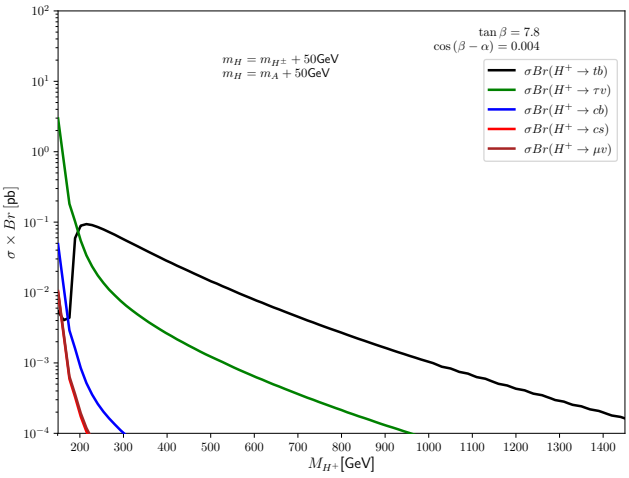

Figure 6.10: $\sigma\,(\mathbf{pp} \to \mathbf{H^+}\,\bar{\mathbf{t}}\,\mathbf{b})$[pb] times branching ratios vrs $m_{H^\pm}$ near the decoupling limit, for $\tan\beta = 7.8$

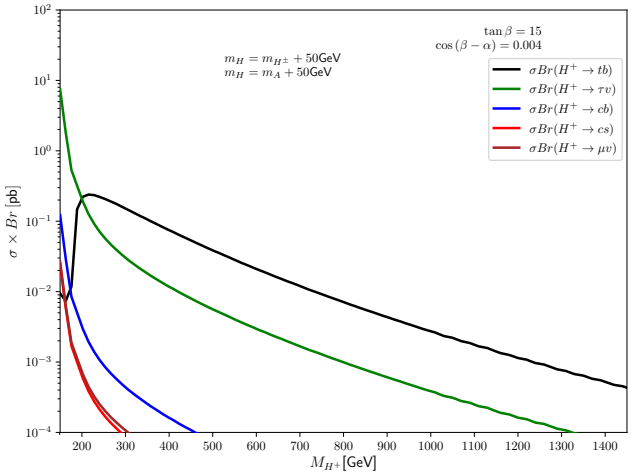

Figure 6.11: $\sigma\,(\mathbf{pp} \to \mathbf{H^+}\,\bar{\mathbf{t}}\,\mathbf{b})$[pb] times branching ratios vrs $m_{H^\pm}$ near the decoupling limit, for $\tan\beta = 15$

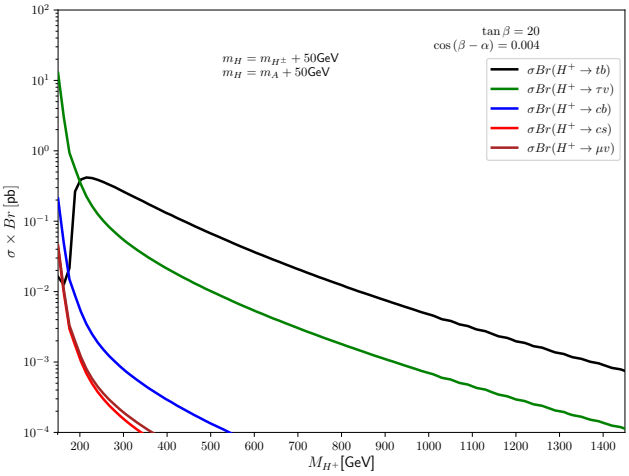

Figure 6.12: $\sigma\,(\mathbf{pp} \to \mathbf{H^+}\,\bar{\mathbf{t}}\,\mathbf{b})$[pb] times branching ratios vrs $m_{H^\pm}$ near the decoupling limit, for $\tan\beta = 20$

6.5.3 Analyzing results in the crescent limit

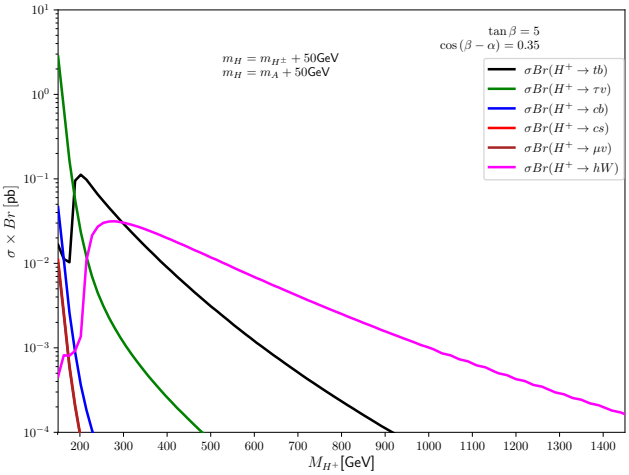

Figure 6.13: $\sigma\left(\mathbf{pp} \to \mathbf{H}^+\,\bar{\mathbf{t}}\,\mathbf{b}\right)$[pb] times branching ratios vrs $m_{H^\pm}$ in the crescent limit, for $\tan\beta = 5$

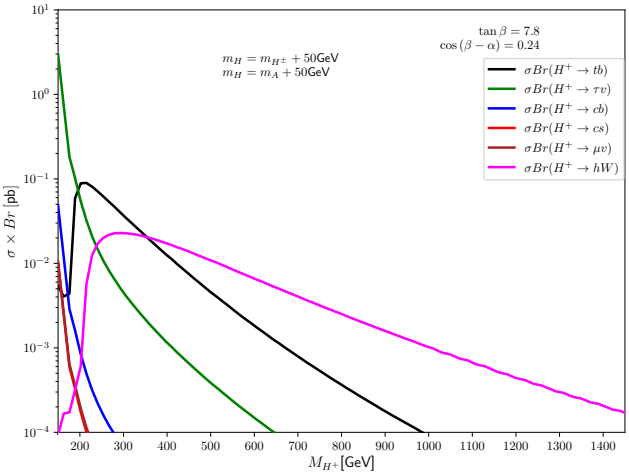

Figure 6.14: $\sigma\left(\mathbf{pp} \to \mathbf{H}^+\,\bar{\mathbf{t}}\,\mathbf{b}\right)$[pb] times branching ratios vrs $m_{H^\pm}$ in the crescent limit, for $\tan\beta = 7.8$

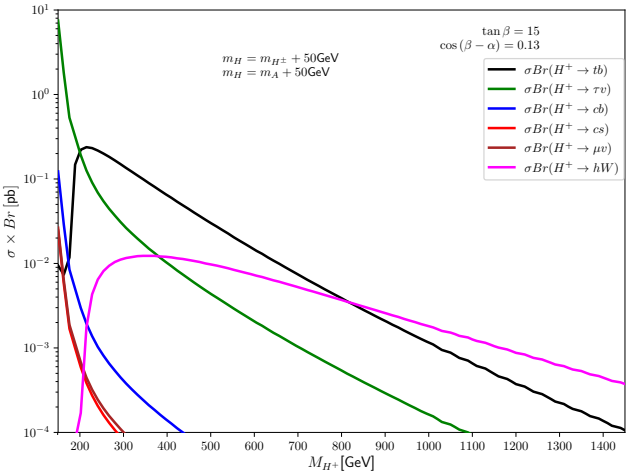

Figure 6.15: $\sigma\left(\mathbf{pp} \to \mathbf{H}^+\,\bar{\mathbf{t}}\,\mathbf{b}\right)$[pb] times branching ratios vrs $m_{H^\pm}$ in the crescent limit, for $\tan\beta = 15$

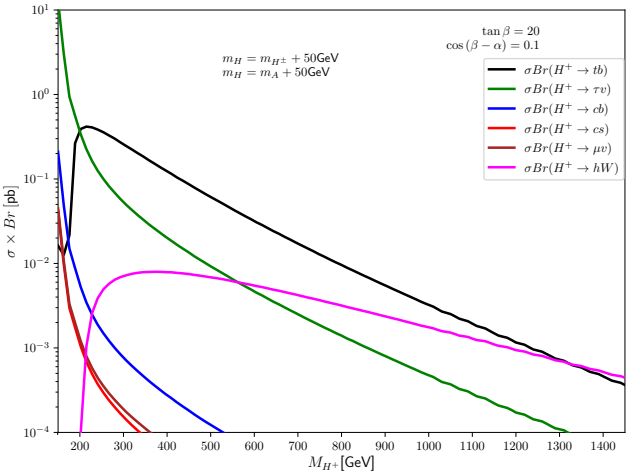

Figure 6.16: $\sigma\left(\mathbf{pp} \to \mathbf{H}^+\,\bar{\mathbf{t}}\,\mathbf{b}\right)$[pb] times branching ratios vrs $m_{H^\pm}$ in the crescent limit, for $\tan\beta = 20$

Chapter 7

Conclusions

After the observation of the 125-126GeV SM-like Higgs boson by the ATLAS and CMS collaborations, the next challenging task at the LHC should be to hunt for new phenomena beyond the SM. One way to achieve this is by looking for the direct production of new states. In this thesis, we have considered the production and decays of the heavy (H), CP odd (A), and charged ($H^{\pm}$) Higgs bosons within the type II 2HDM. We have chosen three areas of the type II 2HDM parameter space in the $\cos(\beta - \alpha)$ and the $\tan\beta$ plane where, our results showed that the area called the crescent shape which one would have thought to be an exclused region is a viable and highly significant region to search for the production of new states at a high energy scale around 1.5TeV. Signal strength measurements of the SM-like Higgs boson suggest that, in the context of the type II 2HDM, whereas certain decay channels vanish or become extremely low both in and near the decoupling limit, other promising channels were found to be in the crescent limit. A very concise summary of the most relevant findings or results described in this thesis is:

(1) Following the gluon fusion mechanism for the heavy Higgs, we found that for small $\tan\beta$ values, the dominant cross section rates contribution comes from the top quark loops as the $g_{t\bar{t}}$ couplings, $g_{Htt} \propto 1/\tan\beta$ are so strong. At higher values of $\tan\beta$, the couplings to top quarks are strongly suppressed while those to bottom quarks, $g_{Hbb} \propto \tan\beta$ are enhanced. We also found that in the decoupling limit, certain decay channels such as $H \to WW$ and $H \to ZZ$ vanish. These decay channels exist near

the decoupling limit but are subdominant. Interestingly, $H \to hh$, $H \to WW$ and $H \to ZZ$ become promising final states in the crescent limit. In all the three chosen limits, we established that while the $H \to t\bar{t}$ dominates in the low $\tan\beta$ regime and is suppressed in the high $\tan\beta$ regime, $H \to bb$ and $H \to \tau\tau$ follow the reverse way.

(2) Since the production of the CP odd Higgs also arises from the gluon fusion mechanism, we observed that in the low $\tan\beta$ regime, larger cross sections rates are from the top quark loops as the g_{Att} couplings, $g_{Att} \propto \frac{1}{\tan\beta}$ are so strong. In the high $\tan\beta$ regime, the coupling of A to the top quark loop g_{Att} are strongly suppressed while those to the bottom quarks g_{Abb} are enhanced. For extremely higher values of $\tan\beta$, our results showed that we get into the chiral limit, $m_A >> m_b$ for which the production rates for both the CP even and CP-odd states become approximately the same. We found that the dominant decay modes for A are $A \to b\bar{b}$, $A \to gg$, $A \to \tau^+\tau^-$, $A \to Zh$ and $A \to t\bar{t}$. The $A \to Zh$ is dominant in the crescent limit in the low $\tan\beta$ regime. For all the three limits, our results revealed that $A \to t\bar{t}$ becomes dominant at low values of $\tan\beta$ but it is suppressed relative to $A \to b\bar{b}$ at high values of $\tan\beta$ due to the reduction of g_{Att} and enhancement of g_{Abb}.

(3) For the charged Higgs bosons, the most dominant production channel was found to be the $pp \to H^+\bar{t}b$ state. Our results also showed that the dominant decay mode for the charged Higgs in type II 2HDM model, as expected is in the $\bar{t}b$ channel, following the sub-dominant ones $\bar{\tau}\nu_\tau$ channel with Br $\sim 10 - 15$ %, followed by other suppressed modes such as, $H^+ \to \bar{b}c, c\bar{s}, \mu\nu_\mu$ and a new channel $H^\pm \to hW^\pm$ opens up for larger values of $\cos(\beta - \alpha)$.

Our results suggest that $H \to hh$, $A \to Zh$ and $H^\pm \to W^\pm h$ should become high priorities in searching for additional Higgs bosons. Finally, our work focused on the simplest extension of the SM, the type II 2HDM. A possible avenue of research is to extend our work to the WEDM, a BSM scenario which allows excitations of the SM particles to propagate in an extra dimension.

References

[1] R. N. Cahn and G. Goldhaber, *The experimental foundations of particle physics*. Cambridge University Press, 2009.

[2] S. Braibant, G. Giacomelli, and M. Spurio, *Particles and fundamental interactions: an introduction to particle physics*. Springer Science & Business Media, 2011.

[3] D. H. Perkins and D. H. Perkins, *Introduction to high energy physics*. Cambridge University Press, 2000.

[4] H. Georgi and S. L. Glashow, "Unified weak and electromagnetic interactions without neutral currents," *Phys. Rev. Lett.*, vol. 28, pp. 1494–1497, May 1972.

[5] S. Weinberg, "The decay of the proton," *Sci. Am.*, vol. 244, no. 6, pp. 64–75, 1981.

[6] S. Matsuyama and H. Miyazawa, "Long range forces between hadrons," *Progress of Theoretical Physics*, vol. 61, no. 3, pp. 942–948, 1979.

[7] A. Pich, "The Standard Model of Electroweak Interactions," in *Proceedings, High-energy Physics. Proceedings, 18th European School (ESHEP 2010): Raseborg, Finland, June 20 - July 3, 2010*, pp. 1–50, 2012. [,1(2012)].

[8] P. W. Higgs, "Broken symmetries and the masses of gauge bosons," *Phys. Rev. Lett.*, vol. 13, pp. 508–509, Oct 1964.

[9] G. Aad *et al.*, "Observation of a new particle in the search for the Standard Model Higgs boson with the ATLAS detector at the LHC," *Phys. Lett.*, vol. B716, pp. 1–29, 2012.

[10] S. Chatrchyan *et al.*, "Observation of a New Boson at a Mass of 125 GeV with the CMS Experiment at the LHC," *Phys. Lett.*, vol. B716, pp. 30–61, 2012.

[11] J. D. Lykken, "Beyond the Standard Model," in *CERN Yellow Report CERN-2010-002, 101-109*, 2010.

[12] J. F. Gunion, H. E. Haber, G. L. Kane, and S. Dawson, "The Higgs Hunter's Guide," *Front. Phys.*, vol. 80, pp. 1–404, 2000.

[13] G. C. Branco, P. M. Ferreira, L. Lavoura, M. N. Rebelo, M. Sher, and J. P. Silva, "Theory and phenomenology of two-Higgs-doublet models," *Phys. Rept.*, vol. 516, pp. 1–102, 2012.

[14] H. P. Nilles, "Supersymmetry, Supergravity and Particle Physics," *Phys. Rept.*, vol. 110, pp. 1–162, 1984.

[15] R. Panek, *The 4 percent universe: Dark matter, dark energy, and the race to discover the rest of reality.* Houghton Mifflin Harcourt, 2011.

[16] M. S. Seigar, *Dark Matter in the Universe.* Morgan & Claypool Publishers, 2015.

[17] A. De Angelis and M. Pimenta, *Introduction to particle and astroparticle physics: multimessenger astronomy and its particle physics foundations.* Springer, 2018.

[18] D. Sokoloff, "Galaxy formation and evolution, by houjun mo, frank van den bosch and simon white," 2011.

[19] O. Engvold, R. Stabell, B. Czerny, and J. Lattanzio, "Astronomy and astrophysics, volume ii," *Astronomy and Astrophysics, Volume II. Edited by Oddbjørn Engvold, Rolf Stabell, Bozena Czerny and John Lattanzio. ISBN 978-1-84826-373-4 (e-Book Adobe Reader). ISBN 978-1-84826-823-4 (Print Volume). UK: UNESCO-EOLSS, 2012.*, 2012.

[20] E. Ma, "Verifiable radiative seesaw mechanism of neutrino mass and dark matter," *Phys. Rev.*, vol. D73, p. 077301, 2006.

[21] R. Barbieri, L. J. Hall, and V. S. Rychkov, "Improved naturalness with a heavy Higgs: An Alternative road to LHC physics," *Phys. Rev.*, vol. D74, p. 015007, 2006.

[22] A. D. Sakharov, "Violation of CP Invariance, C asymmetry, and baryon asymmetry of the universe," *Pisma Zh. Eksp. Teor. Fiz.*, vol. 5, pp. 32–35, 1967. [Usp. Fiz. Nauk161,no.5,61(1991)].

[23] G. W. Anderson and L. J. Hall, "Electroweak phase transition and baryogenesis," *Phys. Rev. D*, vol. 45, pp. 2685–2698, Apr 1992.

[24] W. Buchmuller, Z. Fodor, T. Helbig, and D. Walliser, "The weak electroweak phase transition," *Annals Phys.*, vol. 234, pp. 260–299, 1994.

[25] R. D. Peccei and H. R. Quinn, "Constraints imposed by CP conservation in the presence of pseudoparticles," *Phys. Rev. D*, vol. 16, pp. 1791–1797, Sep 1977.

[26] R. D. Peccei and H. R. Quinn, "CP conservation in the presence of pseudoparticles," *Phys. Rev. Lett.*, vol. 38, pp. 1440–1443, Jun 1977.

[27] C. Csaki, "The Minimal supersymmetric standard model (MSSM)," *Mod. Phys. Lett.*, vol. A11, p. 599, 1996.

[28] I. J. R. Aitchison, "Supersymmetry and the MSSM: An Elementary introduction," 2005.

[29] S. P. Martin, "A Supersymmetry primer," pp. 1–98, 1997. [Adv. Ser. Direct. High Energy Phys.18,1(1998)].

[30] D. Eriksson, J. Rathsman, and O. Stal, "2HDMC: Two-Higgs-Doublet Model Calculator Physics and Manual," *Comput. Phys. Commun.*, vol. 181, pp. 189–205, 2010.

[31] R. E. Maeder, *Programming in mathematica*. Addison-Wesley Longman Publishing Co., Inc., 1991.

[32] J. Bernon and B. Dumont, "Lilith: a tool for constraining new physics from Higgs measurements," *Eur. Phys. J.*, vol. C75, no. 9, p. 440, 2015.

[33] B. W. Kernighan and D. M. Ritchie, *The C programming language*. 2006.

[34] B. Stroustrup, *The C++ programming language*. Pearson Education India, 2000.

[35] R. Brun and F. Rademakers, "Root—an object oriented data analysis framework," *Nuclear Instruments and Methods in Physics Research Section A: Accelerators, Spectrometers, Detectors and Associated Equipment*, vol. 389, no. 1-2, pp. 81–86, 1997.

[36] C. Newham and B. Rosenblatt, *Learning the bash shell: Unix shell programming*. " O'Reilly Media, Inc.", 2005.

[37] W. Chun, *Core python programming*, vol. 1. Prentice Hall Professional, 2001.

[38] L. Wall *et al.*, "The perl programming language," 1994.

[39] M. Bustamante, L. Cieri, and J. Ellis, "Beyond the Standard Model for Montaneros," in *High-energy physics. Proceedings, 5th CERN-Latin-American School, Recinto Quirama, Colombia, March 15-28, 2009*, 2009.

[40] H. Georgi and S. L. Glashow, "Spontaneously broken gauge symmetry and elementary particle masses," *Phys. Rev. D*, vol. 6, pp. 2977–2982, Nov 1972.

[41] F. Englert and R. Brout, "Broken symmetry and the mass of gauge vector mesons," *Phys. Rev. Lett.*, vol. 13, pp. 321–323, Aug 1964.

[42] P. W. Higgs, "Broken Symmetries and the Masses of Gauge Bosons," *Phys. Rev. Lett.*, vol. 13, pp. 508–509, 1964. [,160(1964)].

[43] G. S. Guralnik, C. R. Hagen, and T. W. B. Kibble, "Global conservation laws and massless particles," *Phys. Rev. Lett.*, vol. 13, pp. 585–587, Nov 1964.

[44] G. 't Hooft, "Renormalizable Lagrangians for Massive Yang-Mills Fields," *Nucl. Phys.*, vol. B35, pp. 167–188, 1971. [,201(1971)].

[45] A. Djouadi, "The Anatomy of electro-weak symmetry breaking. I: The Higgs boson in the standard model," *Phys. Rept.*, vol. 457, pp. 1–216, 2008.

[46] Y. Nambu, "Quasiparticles and Gauge Invariance in the Theory of Superconductivity," *Phys. Rev.*, vol. 117, pp. 648–663, 1960. [,132(1960)].

[47] J. Goldstone, "Field Theories with Superconductor Solutions," *Nuovo Cim.*, vol. 19, pp. 154–164, 1961.

[48] A. Mohamadnejad, "Vacuum and Symmetry Breaking: New Approach," 2017.

[49] J. Goldstone, A. Salam, and S. Weinberg, "Broken Symmetries," *Phys. Rev.*, vol. 127, pp. 965–970, 1962.

[50] M. Gomez-Bock, M. Mondragon, M. Muhlleitner, M. Spira, and P. M. Zerwas, "Concepts of Electroweak Symmetry Breaking and Higgs Physics," in *High-energy physics. Proceedings, 4th Latin American CERN-CLAF School, Vina del Mar, Chile, February 18-March 3, 2007*, pp. 177–238, 2007.

[51] H. E. Logan, "TASI 2013 lectures on Higgs physics within and beyond the Standard Model," 2014.

[52] L. Reina, "TASI 2011: lectures on Higgs-Boson Physics," in *The Dark Secrets of the Terascale: Proceedings, TASI 2011, Boulder, Colorado, USA, Jun 6 - Jul 11, 2011*, pp. 39–106, 2013.

[53] M. J. D. Hamilton, "The Higgs boson for mathematicians. Lecture notes on gauge theory and symmetry breaking," 2015.

[54] A. De Angelis and M. J. M. Pimenta, "The higgs mechanism and the standard model of particle physics," in *Introduction to Particle and Astroparticle Physics*, pp. 361–420, Springer, 2015.

[55] M. Spira, "QCD effects in Higgs physics," *Fortsch. Phys.*, vol. 46, pp. 203–284, 1998.

[56] K. Yagyu, *Studies on Extended Higgs Sectors as a Probe of New Physics Beyond the Standard Model*. PhD thesis, Toyama U., 2012.

[57] D. Bardin, L. Kalinovskaya, V. Kolesnikov, and W. von Schlippe, "$J_{AW,WA}$ functions in Passarino - Veltman reduction," *Phys. Atom. Nucl.*, vol. 73, pp. 2048–2063, 2010.

[58] D. Y. Bardin, "Field theory and the standard model," 1999.

[59] N. Irges and F. Koutroulis, "Renormalization of the Abelian–Higgs model in the R_ξ and Unitary gauges and the physicality of its scalar potential," *Nucl. Phys.*, vol. B924, pp. 178–278, 2017. [Erratum: Nucl. Phys.B938,957(2019)].

[60] S. Dittmaier *et al.*, "Handbook of LHC Higgs Cross Sections: 2. Differential Distributions," 2012.

[61] J. R. Andersen *et al.*, "Handbook of LHC Higgs Cross Sections: 3. Higgs Properties," 2013.

[62] A. M. Sirunyan *et al.*, "Search for the associated production of the Higgs boson and a vector boson in proton-proton collisions at $\sqrt{s} = 13$ TeV via Higgs boson decays to τ leptons," *JHEP*, vol. 06, p. 093, 2019.

[63] M. Aaboud *et al.*, "Observation of Higgs boson production in association with a top quark pair at the LHC with the ATLAS detector," *Phys. Lett.*, vol. B784, pp. 173–191, 2018.

[64] J. Bernon, J. F. Gunion, H. E. Haber, Y. Jiang, and S. Kraml, "Scrutinizing the alignment limit in two-Higgs-doublet models: m_h=125 GeV," *Phys. Rev.*, vol. D92, no. 7, p. 075004, 2015.

[65] J. Bernon, B. Dumont, and S. Kraml, "Status of Higgs couplings after run 1 of the LHC," *Phys. Rev.*, vol. D90, p. 071301, 2014.

[66] L. Wang, F. Zhang, and X.-F. Han, "Two-Higgs-doublet model of type-II confronted with the LHC run-I and run-II data," *Phys. Rev.*, vol. D95, no. 11, p. 115014, 2017.

[67] H. E. Haber and O. Stål, "New LHC benchmarks for the $\mathcal{CP}$ -conserving two-Higgs-doublet model," *Eur. Phys. J.*, vol. C75, no. 10, p. 491, 2015. [Erratum: Eur. Phys. J.C76,no.6,312(2016)].

[68] J. Baglio, O. Eberhardt, U. Nierste, and M. Wiebusch, "Benchmarks for Higgs Pair Production and Heavy Higgs boson Searches in the Two-Higgs-Doublet Model of Type II," *Phys. Rev.*, vol. D90, no. 1, p. 015008, 2014.

[69] A. Pich and P. Tuzon, "Yukawa Alignment in the Two-Higgs-Doublet Model," *Phys. Rev.*, vol. D80, p. 091702, 2009.

[70] A. G. Akeroyd, A. Arhrib, and E.-M. Naimi, "Note on tree level unitarity in the general two Higgs doublet model," *Phys. Lett.*, vol. B490, pp. 119–124, 2000.

[71] A. Denner, R. Guth, W. Hollik, and J. Kühn, "Thez-width in the two higgs doublet model," *Zeitschrift für Physik C Particles and Fields*, vol. 51, no. 4, pp. 695–705, 1991.

[72] S. Davidson and H. E. Haber, "Basis-independent methods for the two-Higgs-doublet model," *Phys. Rev.*, vol. D72, p. 035004, 2005. [Erratum: Phys. Rev.D72,099902(2005)].

[73] N. G. Deshpande and X.-G. He, "Gluonic penguin B decays in Standard and two Higgs doublet Models," *Phys. Lett.*, vol. B336, pp. 471–476, 1994.

[74] Y. L. Wu and L. Wolfenstein, "Sources of CP violation in the two Higgs doublet model," *Phys. Rev. Lett.*, vol. 73, pp. 1762–1764, 1994.

[75] M. Aoki, S. Kanemura, K. Tsumura, and K. Yagyu, "Models of Yukawa interaction in the two Higgs doublet model, and their collider phenomenology," *Phys. Rev.*, vol. D80, p. 015017, 2009.

[76] M. Bauer, U. Haisch, and F. Kahlhoefer, "Simplified dark matter models with two Higgs doublets: I. Pseudoscalar mediators," *JHEP*, vol. 05, p. 138, 2017.

[77] A. Belyaev, G. Cacciapaglia, I. P. Ivanov, F. Rojas-Abatte, and M. Thomas, "Anatomy of the Inert Two Higgs Doublet Model in the light of the LHC and non-LHC Dark Matter Searches," *Phys. Rev.*, vol. D97, no. 3, p. 035011, 2018.

[78] A. Drozd, B. Grzadkowski, J. F. Gunion, and Y. Jiang, "Two-Higgs-Doublet Models and Enhanced Rates for a 125 GeV Higgs," *JHEP*, vol. 05, p. 072, 2013.

[79] H. Bélusca-Maïto, A. Falkowski, D. Fontes, J. C. Romão, and J. P. Silva, "Higgs EFT for 2HDM and beyond," *Eur. Phys. J.*, vol. C77, no. 3, p. 176, 2017.

[80] E. Accomando, D. Englert, J. Hays, and S. Moretti, "Voyage Across the 2HDM Type-II with Magellan," 2019.

[81] F. J. Botella, G. C. Branco, M. Nebot, and M. N. Rebelo, "Flavour Changing Higgs Couplings in a Class of Two Higgs Doublet Models," *Eur. Phys. J.*, vol. C76, no. 3, p. 161, 2016.

[82] K. Agashe and R. Contino, "Composite Higgs-Mediated FCNC," *Phys. Rev.*, vol. D80, p. 075016, 2009.

[83] M. E. Luke and M. J. Savage, "Flavor changing neutral currents in the higgs sector and rare top decays," *Phys. Lett.*, vol. 307, no. hep-ph/9303249, pp. 387–393, 1993.

[84] U. Haisch, "$\bar{B} \to X_s\gamma$: Standard Model and Beyond," 2008.

[85] F. Mahmoudi and O. Stal, "Flavor constraints on the two-Higgs-doublet model with general Yukawa couplings," *Phys. Rev.*, vol. D81, p. 035016, 2010.

[86] R. S. Gupta and J. D. Wells, "Next Generation Higgs Bosons: Theory, Constraints and Discovery Prospects at the Large Hadron Collider," *Phys. Rev.*, vol. D81, p. 055012, 2010.

[87] M. Jung, A. Pich, and P. Tuzon, "Charged-Higgs phenomenology in the Aligned two-Higgs-doublet model," *JHEP*, vol. 11, p. 003, 2010.

[88] Y. Jiang, *Higgs boson physics beyond the standard model.* University of California, Davis, 2015.

[89] J. F. Gunion and H. E. Haber, "The CP conserving two Higgs doublet model: The Approach to the decoupling limit," *Phys. Rev.*, vol. D67, p. 075019, 2003.

[90] M. Krause, M. Mühlleitner, and M. Spira, "2HDECAY - A program for the Calculation of Electroweak One-Loop Corrections to Higgs Decays in the Two-Higgs-Doublet Model Including State-of-the-Art QCD Corrections," 2018.

[91] S. Kanemura, Y. Okada, E. Senaha, and C. P. Yuan, "Higgs coupling constants as a probe of new physics," *Phys. Rev.*, vol. D70, p. 115002, 2004.

[92] P. H. Frampton, S. L. Glashow, and T. Yoshikawa, "Model of soft CP violation using scalars with quark number two," *Phys. Rev. Lett.*, vol. 87, p. 011801, 2001.

[93] G. C. Branco, L. Lavoura, and J. P. Silva, "CP Violation," *Int. Ser. Monogr. Phys.*, vol. 103, pp. 1–536, 1999.

[94] H. E. Haber and D. O'Neil, "Basis-independent methods for the two-Higgs-doublet model. II. The Significance of tanβ," *Phys. Rev.*, vol. D74, p. 015018, 2006. [Erratum: Phys. Rev.D74,no.5,059905(2006)].

[95] S. L. Glashow and S. Weinberg, "Natural Conservation Laws for Neutral Currents," *Phys. Rev.*, vol. D15, p. 1958, 1977.

[96] H. Georgi and D. V. Nanopoulos, "Suppression of Flavor Changing Effects From Neutral Spinless Meson Exchange in Gauge Theories," *Phys. Lett.*, vol. 82B, pp. 95–96, 1979.

[97] S. Gori, H. E. Haber, and E. Santos, "High scale flavor alignment in two-Higgs doublet models and its phenomenology," *JHEP*, vol. 06, p. 110, 2017.

[98] V. Barger, J. L. Hewett, and R. J. N. Phillips, "New constraints on the charged higgs sector in two-higgs-doublet models," *Phys. Rev. D*, vol. 41, pp. 3421–3441, Jun 1990.

[99] Y. Grossman, "Phenomenology of models with more than two Higgs doublets," *Nucl. Phys.*, vol. B426, pp. 355–384, 1994.

[100] A. Arhrib, "Unitarity constraints on scalar parameters of the standard and two Higgs doublets model," in *Workshop on Noncommutative Geometry, Superstrings and Particle Physics Rabat, Morocco, June 16-17, 2000*, 2000.

[101] J. Horejsi and M. Kladiva, "Tree-unitarity bounds for THDM Higgs masses revisited," *Eur. Phys. J.*, vol. C46, pp. 81–91, 2006.

[102] I. F. Ginzburg and I. P. Ivanov, "Tree-level unitarity constraints in the most general 2HDM," *Phys. Rev.*, vol. D72, p. 115010, 2005.

[103] I. F. Ginzburg and I. P. Ivanov, "Tree level unitarity constraints in the 2HDM with CP violation," 2003.

[104] B. Gorczyca and M. Krawczyk, "Tree-Level Unitarity Constraints for the SM-like 2HDM," 2011.

[105] A. Arhrib, R. Benbrik, and N. Gaur, "$H \to \gamma\gamma$ in Inert Higgs Doublet Model," *Phys. Rev.*, vol. D85, p. 095021, 2012.

[106] S. Kanemura, T. Kasai, and Y. Okada, "Mass bounds of the lightest CP even Higgs boson in the two Higgs doublet model," *Phys. Lett.*, vol. B471, pp. 182–190, 1999.

[107] P. M. Ferreira, R. Santos, and A. Barroso, "Stability of the tree-level vacuum in two Higgs doublet models against charge or CP spontaneous violation," *Phys. Lett.*, vol. B603, pp. 219–229, 2004. [Erratum: Phys. Lett.B629,114(2005)].

[108] M. E. Peskin and T. Takeuchi, "Estimation of oblique electroweak corrections," *Phys. Rev.*, vol. D46, pp. 381–409, 1992.

[109] I. F. Ginzburg and M. Krawczyk, "Symmetries of two Higgs doublet model and CP violation," *Phys. Rev.*, vol. D72, p. 115013, 2005.

[110] N. Chen, T. Han, S. Su, W. Su, and Y. Wu, "Type-II 2HDM under the Precision Measurements at the Z-pole and a Higgs Factory," *JHEP*, vol. 03, p. 023, 2019.

[111] H. E. Haber and D. O'Neil, "Basis-independent methods for the two-Higgs-doublet model III: The CP-conserving limit, custodial symmetry, and the oblique parameters S, T, U," *Phys. Rev.*, vol. D83, p. 055017, 2011.

[112] G. Passarino and M. J. G. Veltman, "One Loop Corrections for e+ e- Annihilation Into mu+ mu- in the Weinberg Model," *Nucl. Phys.*, vol. B160, pp. 151–207, 1979.

[113] M. Baak, J. Cúth, J. Haller, A. Hoecker, R. Kogler, K. Mönig, M. Schott, and J. Stelzer, "The global electroweak fit at NNLO and prospects for the LHC and ILC," *Eur. Phys. J.*, vol. C74, p. 3046, 2014.

[114] J. M. Gerard and M. Herquet, "A Twisted custodial symmetry in the two-Higgs-doublet model," *Phys. Rev. Lett.*, vol. 98, p. 251802, 2007.

[115] E. Cerveró and J.-M. Gérard, "Minimal violation of flavour and custodial symmetries in a vectophobic Two-Higgs-Doublet-Model," *Phys. Lett.*, vol. B712, pp. 255–260, 2012.

[116] A. M. Sirunyan *et al.*, "Measurements of properties of the Higgs boson decaying into the four-lepton final state in pp collisions at $\sqrt{s} = 13$ TeV," *JHEP*, vol. 11, p. 047, 2017.

[117] A. M. Sirunyan *et al.*, "Search for the Higgs boson decaying to two muons in proton-proton collisions at $\sqrt{s} = 13$ TeV," *Phys. Rev. Lett.*, vol. 122, no. 2, p. 021801, 2019.

[118] T. A. collaboration, "Study of the Higgs boson properties and search for high-mass scalar resonances in the $H \to ZZ^* \to 4\ell$ decay channel at $\sqrt{s} = 13$ TeV with the ATLAS detector," 2016.

[119] L.-C. Lü, C. Du, Y. Fang, H.-J. He, and H. Zhang, "Searching heavier Higgs boson via di-Higgs production at LHC Run-2," *Phys. Lett.*, vol. B755, pp. 509–522, 2016.

[120] K. Nakamura, K. Nishiwaki, K.-y. Oda, S. C. Park, and Y. Yamamoto, "Di-higgs enhancement by neutral scalar as probe of new colored sector," *Eur. Phys. J.*, vol. C77, no. 5, p. 273, 2017.

[121] B. Hespel, D. Lopez-Val, and E. Vryonidou, "Higgs pair production via gluon fusion in the Two-Higgs-Doublet Model," *JHEP*, vol. 09, p. 124, 2014.

[122] W. Bernreuther, P. Galler, C. Mellein, Z. G. Si, and P. Uwer, "Production of heavy Higgs bosons and decay into top quarks at the LHC," *Phys. Rev.*, vol. D93, no. 3, p. 034032, 2016.

[123] R. V. Harlander, S. Liebler, and H. Mantler, "SusHi: A program for the calculation of Higgs production in gluon fusion and bottom-quark annihilation in the Standard Model and the MSSM," *Comput. Phys. Commun.*, vol. 184, pp. 1605–1617, 2013.

[124] S. Dittmaier *et al.*, "Handbook of LHC Higgs Cross Sections: 1. Inclusive Observables," 2011.

[125] N. Craig, J. Galloway, and S. Thomas, "Searching for Signs of the Second Higgs Doublet," 2013.

[126] A. Buckley, J. Ferrando, S. Lloyd, K. Nordström, B. Page, M. Rüfenacht, M. Schönherr, and G. Watt, "LHAPDF6: parton density access in the LHC precision era," *Eur. Phys. J.*, vol. C75, p. 132, 2015.

[127] J. Baglio, A. Djouadi, and J. Quevillon, "Prospects for Higgs physics at energies up to 100 TeV," *Rept. Prog. Phys.*, vol. 79, no. 11, p. 116201, 2016.

[128] S. Kanemura, K. Tsumura, and H. Yokoya, "Determination of tan β from the Higgs boson decay at linear colliders," *Phys. Rev.*, vol. D88, p. 055010, 2013.

[129] A. Djouadi, "Implications of the Higgs discovery for the MSSM," *Eur. Phys. J.*, vol. C74, p. 2704, 2014.

[130] A. M. Sirunyan *et al.*, "Search for supersymmetry using Higgs boson to diphoton decays at $\sqrt{s} = 13$ TeV," 2019.

[131] A. Djouadi, J. Kalinowski, P. Ohmann, and P. M. Zerwas, "Heavy SUSY Higgs bosons at e^+e^- linear colliders," *Z. Phys.*, vol. C74, pp. 93–111, 1997.

[132] A. Djouadi, "SUSY Higgs boson decays," in *The Higgs puzzle - what can we learn from LEP-2, LHC, NLC and FMC? Proceedings, Ringberg Workshop, Tegernsee, Germany, December 8-13, 1996*, pp. 155–164, 1997.

[133] A. Djouadi and J. Quevillon, "The MSSM Higgs sector at a high M_{SUSY}: reopening the low tanβ regime and heavy Higgs searches," *JHEP*, vol. 10, p. 028, 2013.

[134] E. Bagnaschi *et al.*, "MSSM Higgs Boson Searches at the LHC: Benchmark Scenarios for Run 2 and Beyond," *Eur. Phys. J.*, vol. C79, no. 7, p. 617, 2019.

[135] C. Kilic, S. Najjari, and C. B. Verhaaren, "Discovering the Twin Higgs Boson with Displaced Decays," *Phys. Rev.*, vol. D99, no. 7, p. 075029, 2019.

[136] M. Gorbahn, S. Jager, U. Nierste, and S. Trine, "The supersymmetric Higgs sector and $B - \bar{B}$ mixing for large tan β," *Phys. Rev.*, vol. D84, p. 034030, 2011.

[137] P. M. Ferreira, J. F. Gunion, H. E. Haber, and R. Santos, "Probing wrong-sign Yukawa couplings at the LHC and a future linear collider," *Phys. Rev.*, vol. D89, no. 11, p. 115003, 2014.

[138] P. Bechtle, H. E. Haber, S. Heinemeyer, O. Stål, T. Stefaniak, G. Weiglein, and L. Zeune, "The Light and Heavy Higgs Interpretation of the MSSM," *Eur. Phys. J.*, vol. C77, no. 2, p. 67, 2017.

[139] L. Basso, A. Lipniacka, F. Mahmoudi, S. Moretti, P. Osland, G. M. Pruna, and M. Purmohammadi, "The CP-violating type-II 2HDM and Charged Higgs boson benchmarks," *PoS*, vol. Corfu2012, p. 029, 2013.

[140] C. A. Marin and B. Hoeneisen, "Mass constraints, production cross-sections, and decay rates in the two Higgs doublet model of type two," 2004.

[141] T. Ahmed, M. C. Kumar, P. Mathews, N. Rana, and V. Ravindran, "Pseudo-scalar Higgs boson production at threshold N^3 LO and N^3 LL QCD," *Eur. Phys. J.*, vol. C76, no. 6, p. 355, 2016.

[142] R. Frederix, S. Frixione, V. Hirschi, F. Maltoni, R. Pittau, and P. Torrielli, "Scalar and pseudoscalar Higgs production in association with a top–antitop pair," *Phys. Lett.*, vol. B701, pp. 427–433, 2011.

[143] S. Frixione and B. R. Webber, "Matching NLO QCD computations and parton shower simulations," *JHEP*, vol. 06, p. 029, 2002.

[144] S. Frixione, F. Stoeckli, P. Torrielli, B. R. Webber, and C. D. White, "The MCaNLO 4.0 Event Generator," 2010.

[145] M. Demirci, "Pseudoscalar Higgs boson pair production at a photon-photon collision in the two Higgs doublet model," 2019.

[146] A. D. Martin, W. J. Stirling, R. S. Thorne, and G. Watt, "Parton distributions for the LHC," *Eur. Phys. J.*, vol. C63, pp. 189–285, 2009.

[147] G. Aad *et al.*, "Search For Higgs Boson Pair Production in the $\gamma\gamma b\bar{b}$ Final State using pp Collision Data at $\sqrt{s} = 8$ TeV from the ATLAS Detector," *Phys. Rev. Lett.*, vol. 114, no. 8, p. 081802, 2015.

[148] G. Aad *et al.*, "Search for a CP-odd Higgs boson decaying to Zh in pp collisions at $\sqrt{s} = 8$ TeV with the ATLAS detector," *Phys. Lett.*, vol. B744, pp. 163–183, 2015.

[149] G. Aad *et al.*, "Search for Higgs boson pair production in the $b\bar{b}b\bar{b}$ final state from pp collisions at $\sqrt{s} = 8$ TeVwith the ATLAS detector," *Eur. Phys. J.*, vol. C75, no. 9, p. 412, 2015.

[150] V. Khachatryan *et al.*, "Searches for a heavy scalar boson H decaying to a pair of 125 GeV Higgs bosons hh or for a heavy pseudoscalar boson A decaying to Zh, in the final states with $h \to \tau\tau$," *Phys. Lett.*, vol. B755, pp. 217–244, 2016.

[151] M. Aaboud *et al.*, "Search for new phenomena in high-mass diphoton final states using 37 fb^{-1} of proton–proton collisions collected at $\sqrt{s} = 13$ TeV with the ATLAS detector," *Phys. Lett.*, vol. B775, pp. 105–125, 2017.

[152] V. Khachatryan *et al.*, "Search for high-mass diphoton resonances in proton–proton collisions at 13 TeV and combination with 8 TeV search," *Phys. Lett.*, vol. B767, pp. 147–170, 2017.

[153] P. M. Ferreira, S. Liebler, and J. Wittbrodt, "$pp \to A \to Zh$ and the wrong-sign limit of the two-Higgs-doublet model," *Phys. Rev.*, vol. D97, no. 5, p. 055008, 2018.

[154] P. M. Ferreira, R. Guedes, M. O. P. Sampaio, and R. Santos, "Wrong sign and symmetric limits and non-decoupling in 2HDMs," *JHEP*, vol. 12, p. 067, 2014.

[155] R. Coimbra, M. O. P. Sampaio, and R. Santos, "ScannerS: Constraining the phase diagram of a complex scalar singlet at the LHC," *Eur. Phys. J.*, vol. C73, p. 2428, 2013.

[156] R. Costa, M. Mühlleitner, M. O. P. Sampaio, and R. Santos, "Singlet Extensions of the Standard Model at LHC Run 2: Benchmarks and Comparison with the NMSSM," *JHEP*, vol. 06, p. 034, 2016.

[157] M. Muhlleitner, M. O. P. Sampaio, R. Santos, and J. Wittbrodt, "The N2HDM under Theoretical and Experimental Scrutiny," *JHEP*, vol. 03, p. 094, 2017.

[158] K. G. Klimenko, "On Necessary and Sufficient Conditions for Some Higgs Potentials to Be Bounded From Below," *Theor. Math. Phys.*, vol. 62, pp. 58–65, 1985. [Teor. Mat. Fiz.62,87(1985)].

[159] A. Barroso, P. M. Ferreira, I. P. Ivanov, and R. Santos, "Metastability bounds on the two Higgs doublet model," *JHEP*, vol. 06, p. 045, 2013.

[160] P. Bechtle, O. Brein, S. Heinemeyer, G. Weiglein, and K. E. Williams, "HiggsBounds: Confronting Arbitrary Higgs Sectors with Exclusion Bounds from LEP and the Tevatron," *Comput. Phys. Commun.*, vol. 181, pp. 138–167, 2010.

[161] P. Bechtle, O. Brein, S. Heinemeyer, G. Weiglein, and K. E. Williams, "HiggsBounds 2.0.0: Confronting Neutral and Charged Higgs Sector Predictions with Exclusion Bounds from LEP and the Tevatron," *Comput. Phys. Commun.*, vol. 182, pp. 2605–2631, 2011.

[162] P. Bechtle, O. Brein, S. Heinemeyer, O. Stål, T. Stefaniak, G. Weiglein, and K. E. Williams, "HiggsBounds − 4: Improved Tests of Extended Higgs Sectors against Exclusion Bounds from LEP, the Tevatron and the LHC," *Eur. Phys. J.*, vol. C74, no. 3, p. 2693, 2014.

[163] P. Bechtle, S. Heinemeyer, O. Stal, T. Stefaniak, and G. Weiglein, "Applying Exclusion Likelihoods from LHC Searches to Extended Higgs Sectors," *Eur. Phys. J.*, vol. C75, no. 9, p. 421, 2015.

[164] E. Boos and T. Plehn, "Higgs-boson production induced by bottom quarks," *Phys. Rev. D*, vol. 69, p. 094005, May 2004.

[165] J. Alwall, M. Herquet, F. Maltoni, O. Mattelaer, and T. Stelzer, "MadGraph 5 : Going Beyond," *JHEP*, vol. 06, p. 128, 2011.

[166] M. Guchait and A. H. Vijay, "Probing Heavy Charged Higgs Boson at the LHC," *Phys. Rev.*, vol. D98, no. 11, p. 115028, 2018.

Appendix A

THDM: Additional Results for the Heavy Higgs

Heavy Higgs (H) Production near decoupling and in the crescent limit

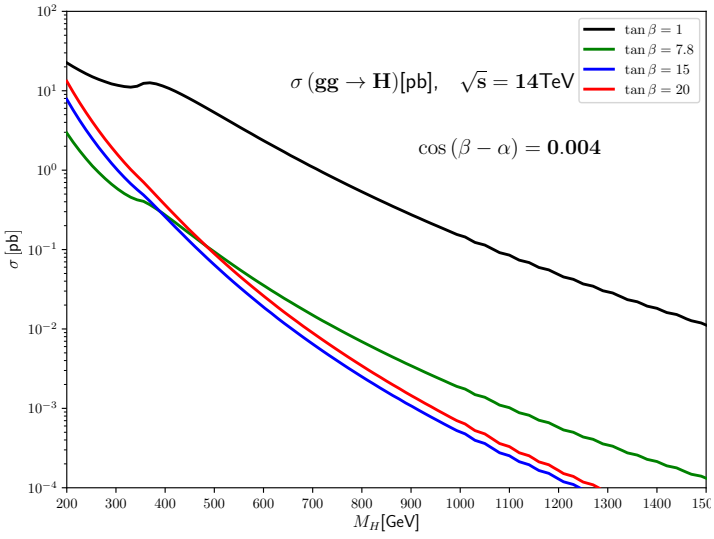

Figure A.1: 2HDM Type II: Gluon fusion production process for heavy Higgs near the decoupling limit at $\tan\beta = 1, 7.8, 15$ and 20

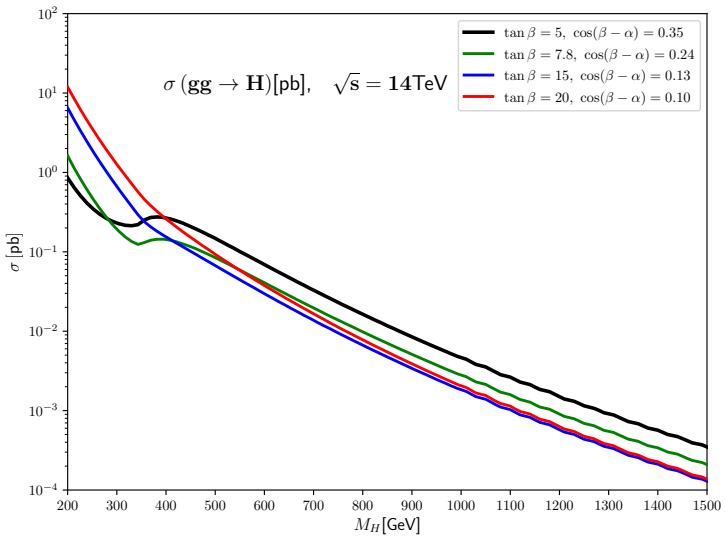

Figure A.2: 2HDM Type II: Gluon fusion production process for heavy Higgs in the crescent limit at $\tan\beta = 5, 7.8, 15$ and 20

BRs for H in the decoupling limit where $\cos(\beta-\alpha)=0$

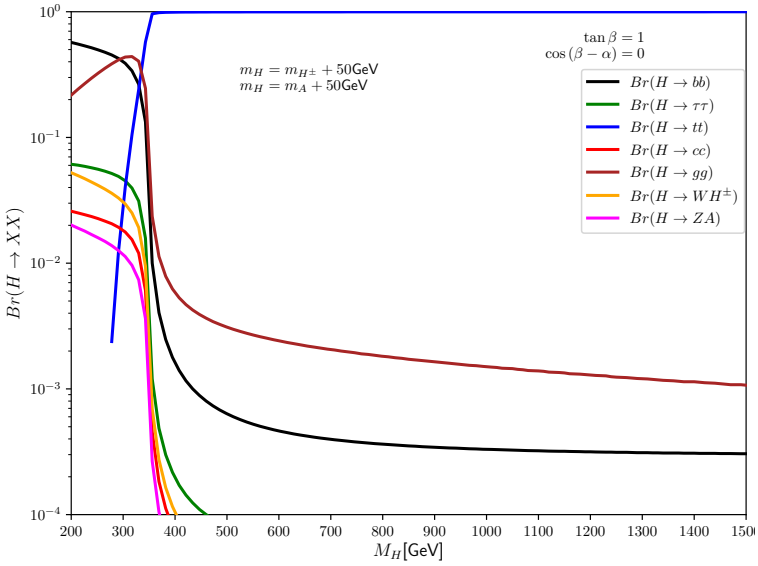

Figure A.3: $Br(H \to XX)$ vrs m_H, for $\tan\beta = 1$ in the decoupling limit.

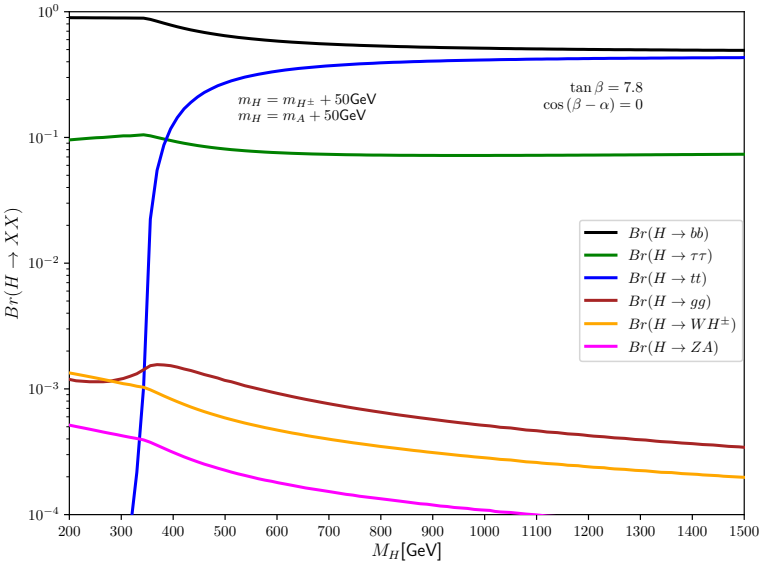

Figure A.4: $Br(H \to XX)$ vrs m_H, for $\tan\beta = 7.8$ in the decoupling limit.

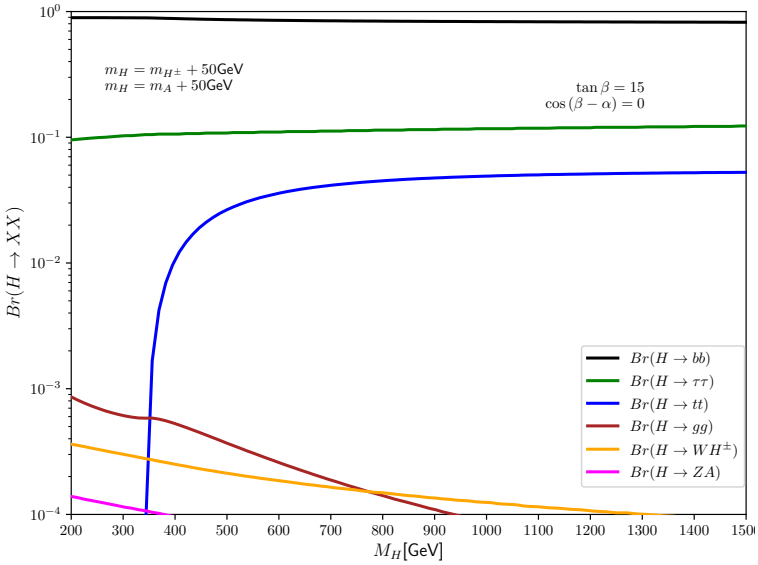

Figure A.5: $Br(H \to XX)$ vrs m_H, for $\tan\beta = 15$ in the decoupling limit.

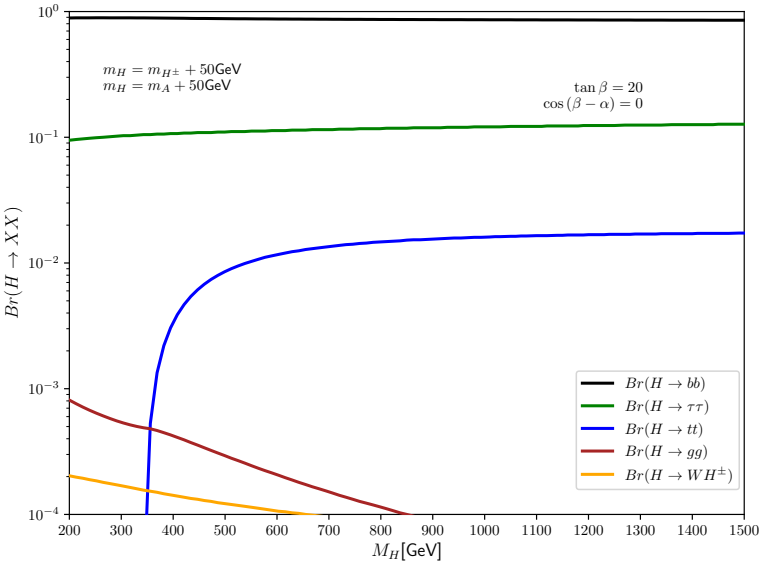

Figure A.6: $Br(H \to XX)$ vrs m_H, for $\tan\beta = 20$ in the decoupling limit.

BRs for H near the decoupling limit where $\cos(\beta-\alpha)=0.004$

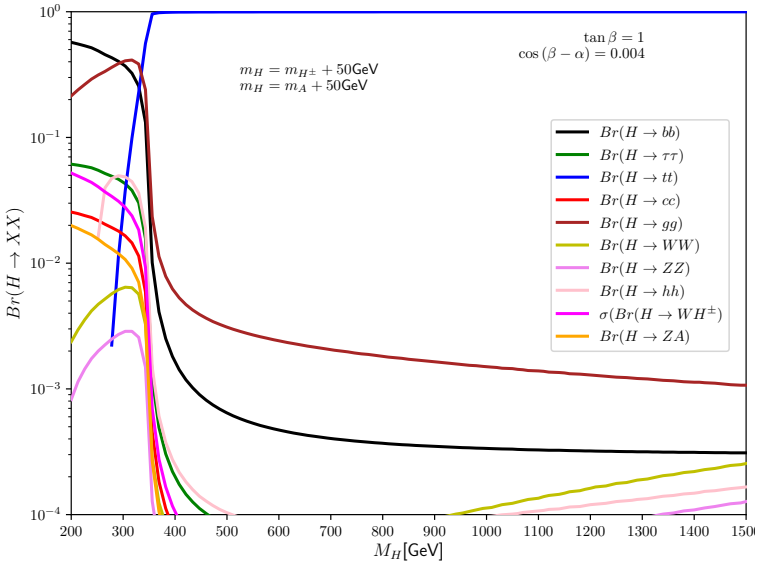

Figure A.7: $Br(H \to XX)$ vrs m_H, for $\tan\beta = 1$ near the decoupling limit.

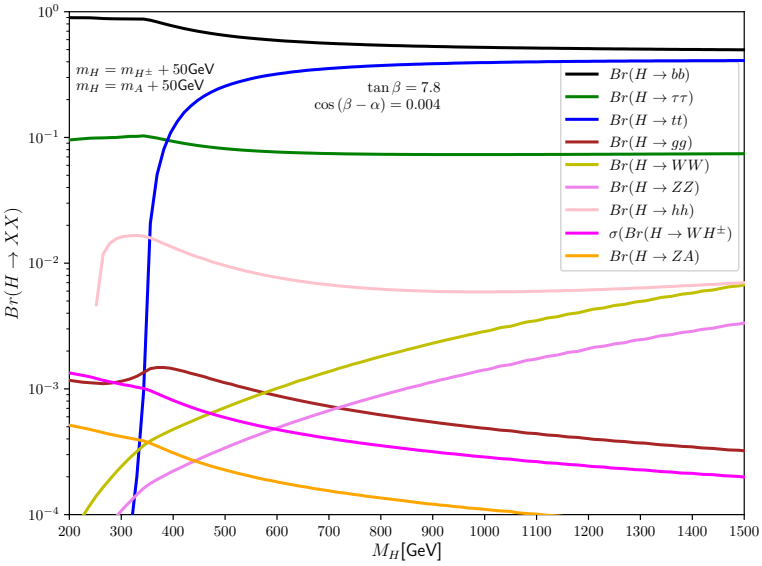

Figure A.8: $Br(H \to XX)$ vrs m_H, for $\tan\beta = 7.8$ near the decoupling limit.

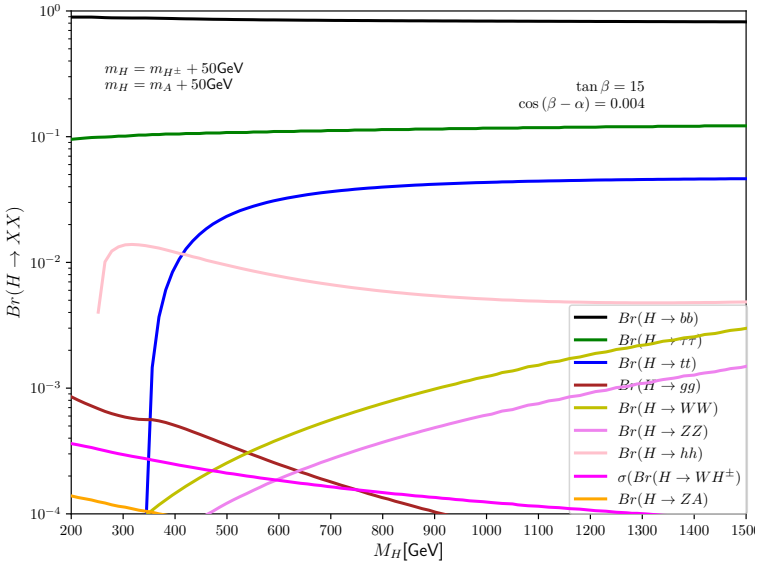

Figure A.9: $Br(H \to XX)$ vrs m_H, for $\tan\beta = 15$ near the decoupling limit.

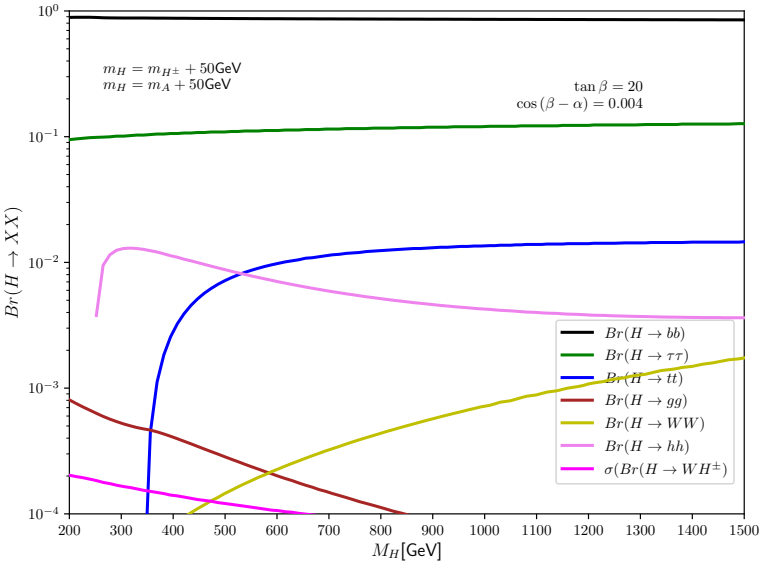

Figure A.10: $Br(H \to XX)$ vrs m_H, for $\tan\beta = 20$ near the decoupling limit.

BRs for H in the crescent limit

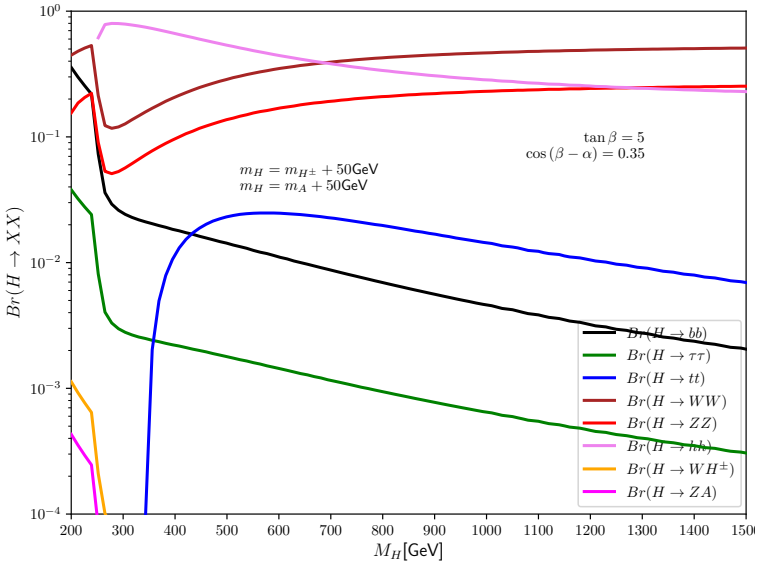

Figure A.11: $Br\,(H \to XX)$vrs m_H, for $\tan\beta = 5$ in the crescent limit

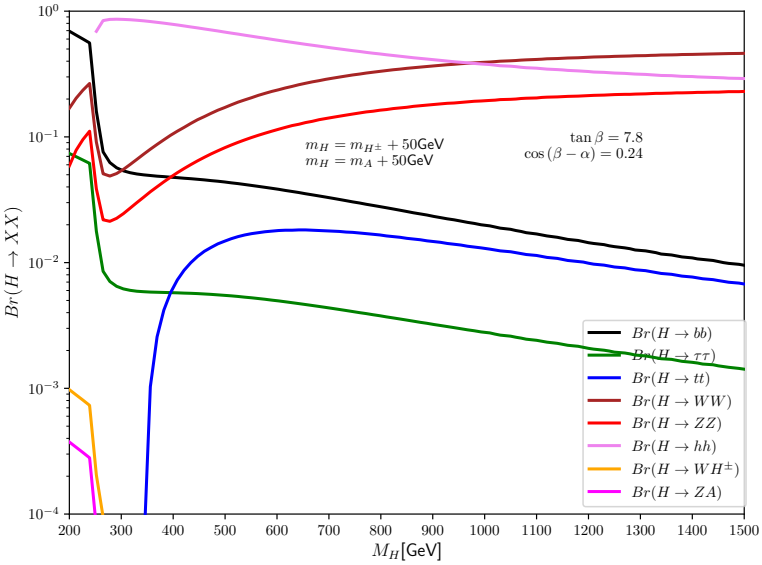

Figure A.12: $Br\,(H \to XX)$ vrs m_H, for $\tan\beta = 7.8$ in the crescent limit

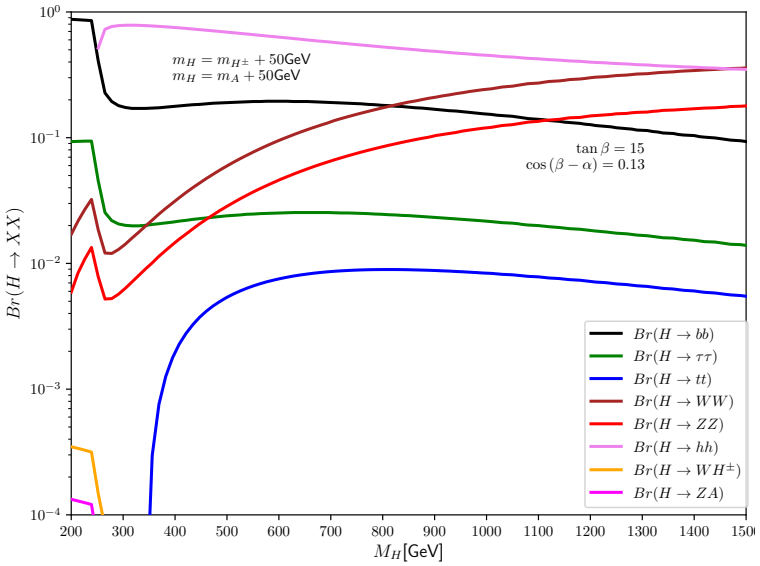

Figure A.13: $Br\,(H \to XX)$ vrs m_H, for $\tan\beta = 15$ in the crescent limit

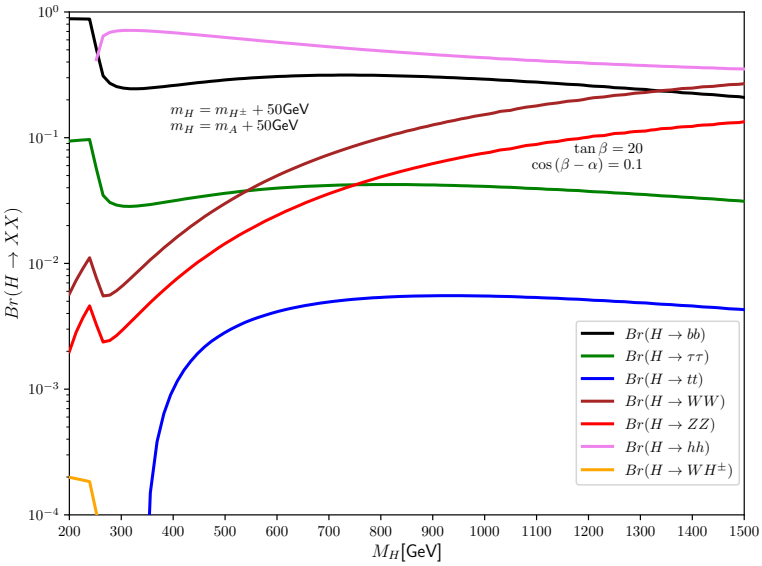

Figure A.14: $Br\,(H \to XX)$ vrs m_H, for $\tan\beta = 20$ in the crescent limit

Constraints on $\cos(\beta-\alpha)$ and $\tan\beta$ in the 2HDM Type II

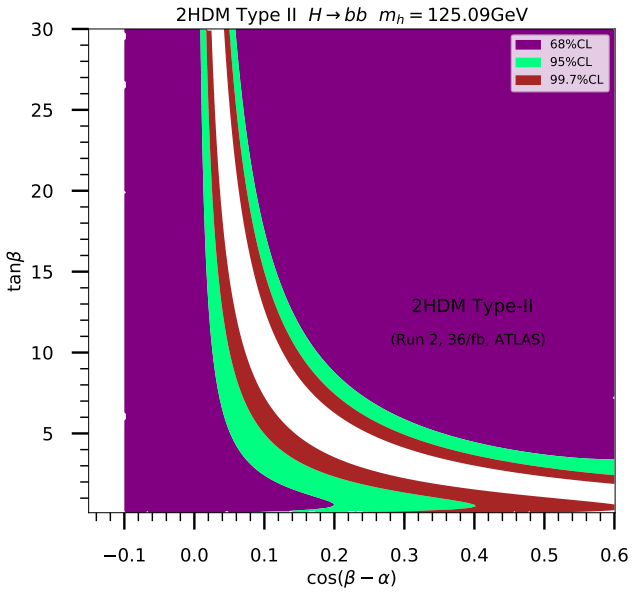

Figure A.15: Constraints on $\cos(\beta-\alpha)$ and $\tan\beta$ from $h\to b\bar{b}$

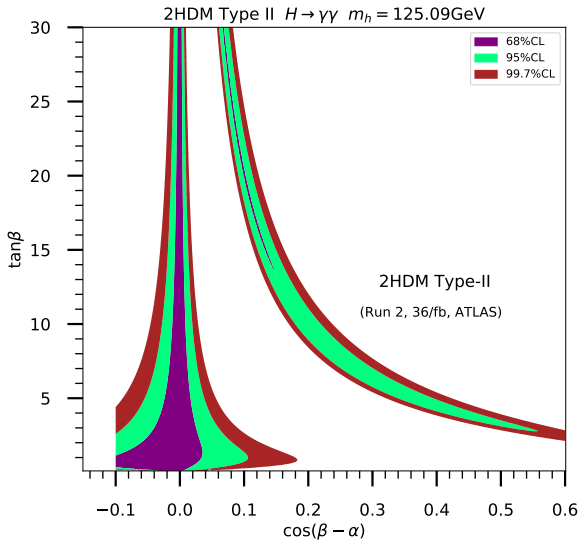

Figure A.16: Constraints on $\cos(\beta-\alpha)$ and $\tan\beta$ from $h\to\gamma\gamma$

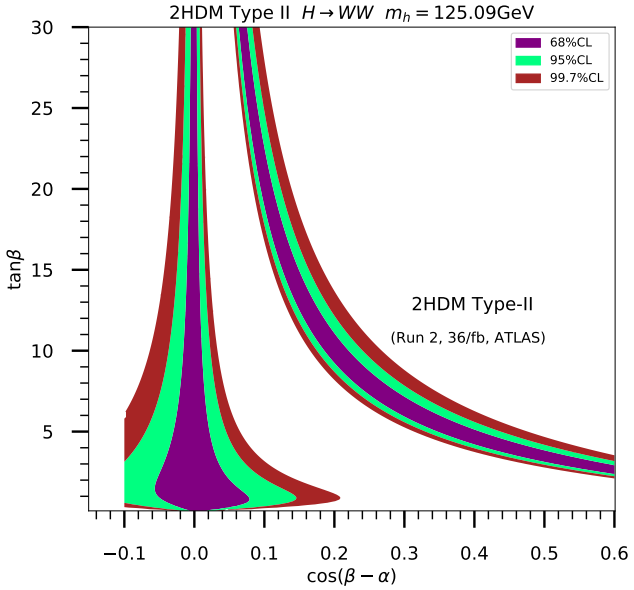

Figure A.17: Constraints on $\cos(\beta-\alpha)$ and $\tan\beta$ from $h\to WW$

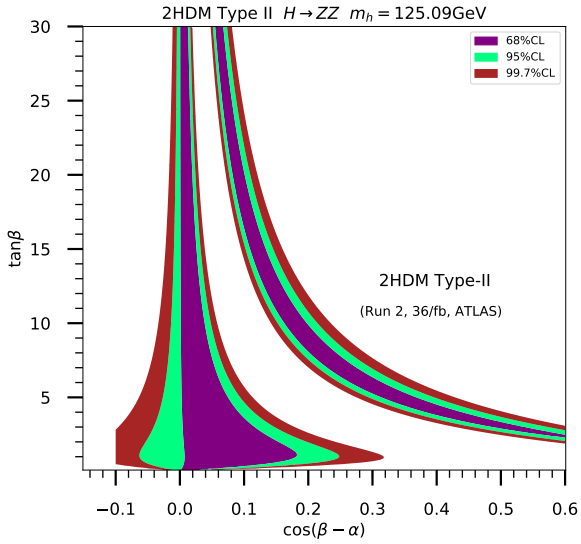

Figure A.18: Constraints on $\cos(\beta-\alpha)$ and $\tan\beta$ from $h\to ZZ$

Appendix B

THDM: Additional Results for the CP Odd Higgs

CP Odd Higgs (A) Production near decoupling and in the crescent limit

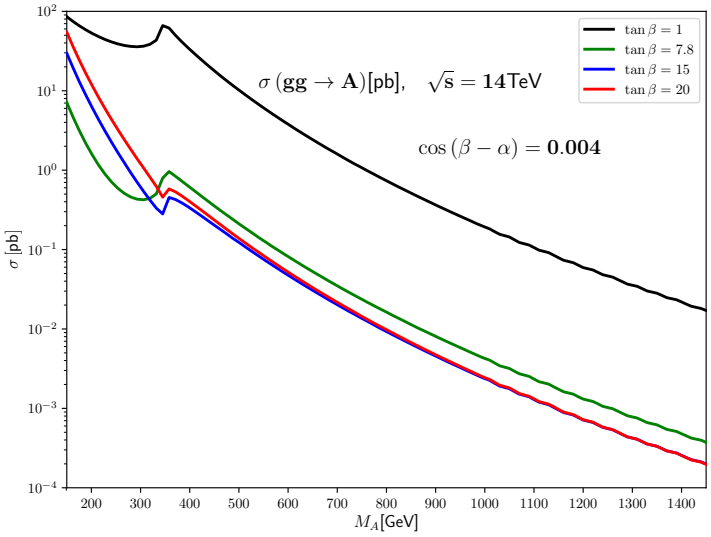

Figure B.1: 2HDM Type II: Gluon fusion production process for CP-odd Higgs (A) near the decoupling limit at $\tan\beta = 1, 7.8, 15$ and 20.

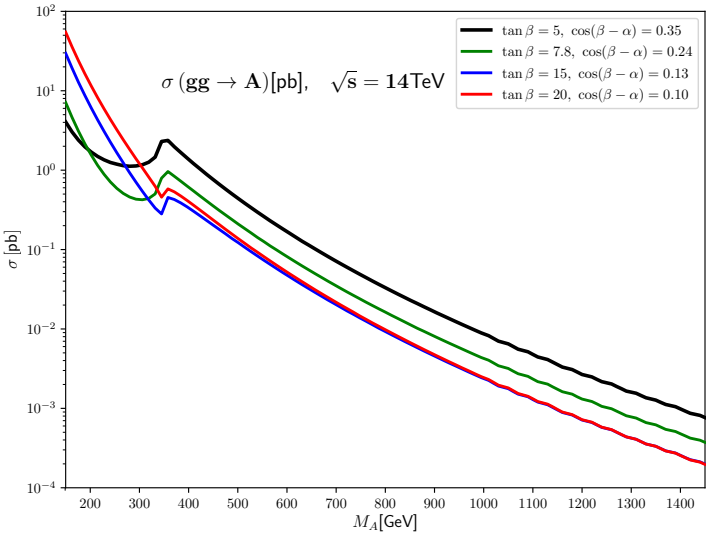

Figure B.2: 2HDM Type II: Gluon fusion production process for CP-odd Higgs (A) in the crescent limit for $\tan\beta = 5, 7.8, 15$ and 20.

BRs for A in the decoupling limit where $\cos(\beta - \alpha) = 0$

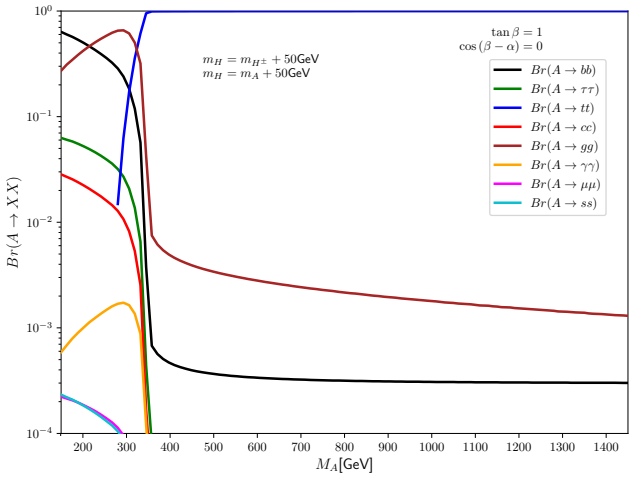

Figure B.3: $Br(A \to XX)$ vrs m_A, for $\tan\beta = 1$ in the decoupling limit

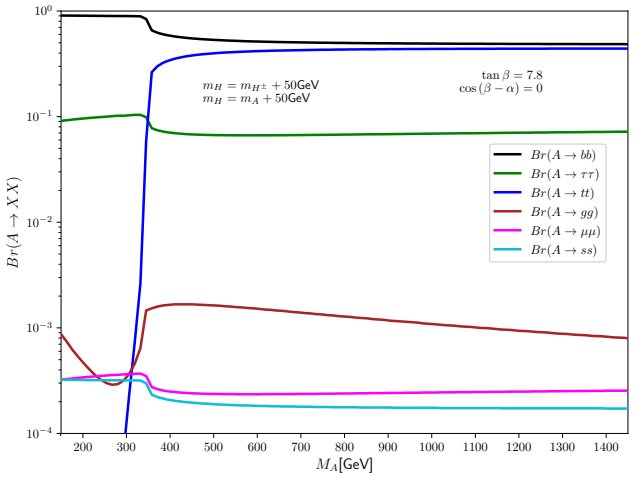

Figure B.4: $Br(A \to XX)$ vrs m_A, for $\tan\beta = 7.8$ in the decoupling limit

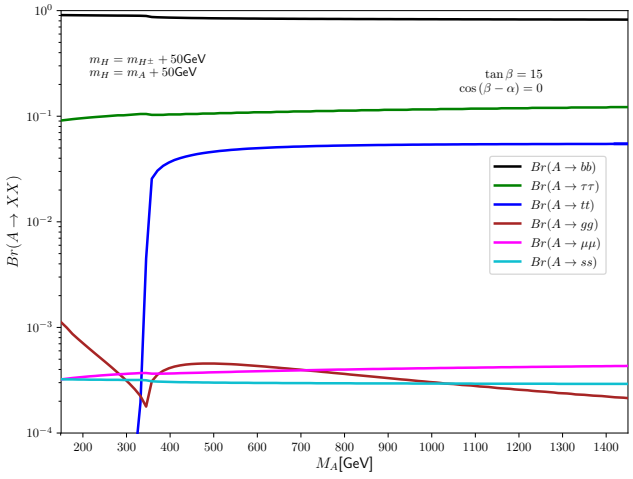

Figure B.5: $Br(A \to XX)$ vrs m_A, for $\tan\beta = 15$ in the decoupling limit

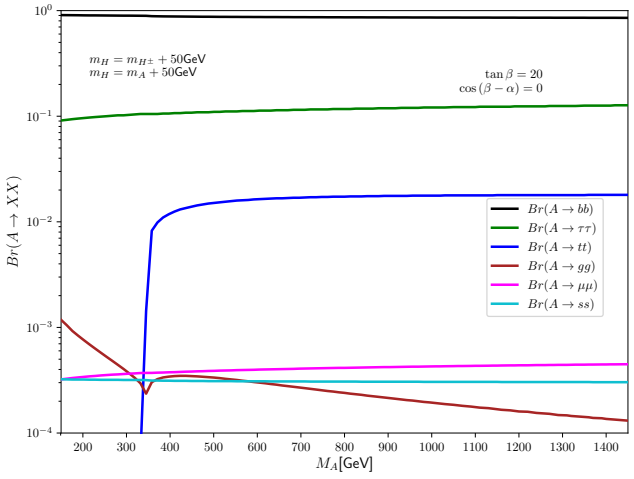

Figure B.6: $Br(A \to XX)$ vrs m_A, for $\tan\beta = 20$ in the decoupling limit

BRs for A near the decoupling limit where $\cos(\beta-\alpha)=0.004$

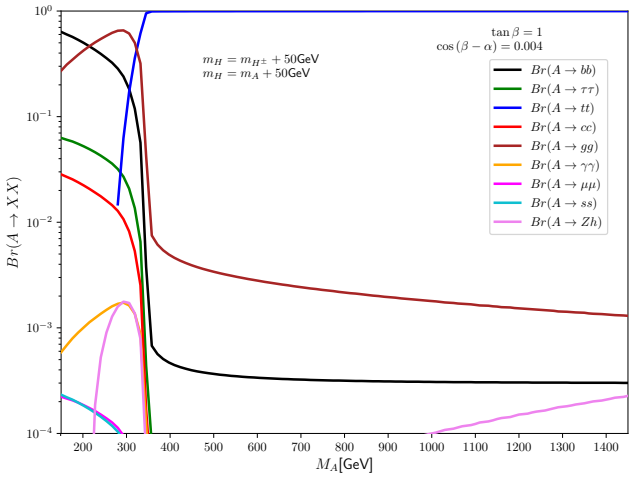

Figure B.7: $Br(A\to XX)$ vrs m_A, for $\tan\beta = 1$ near the decoupling limit

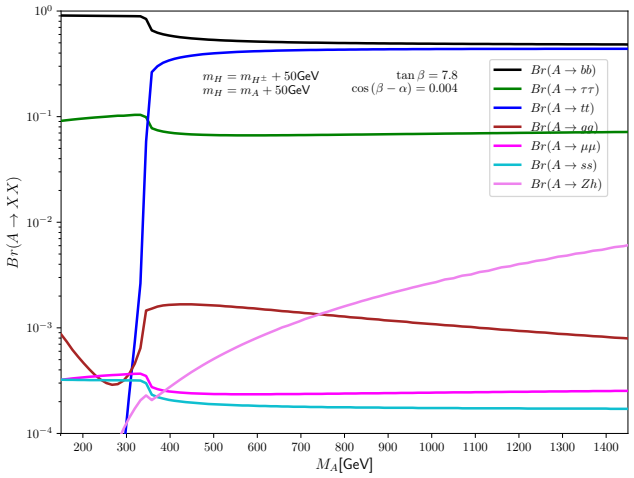

Figure B.8: $Br(A\to XX)$ vrs m_A, for $\tan\beta = 7.8$ near the decoupling limit

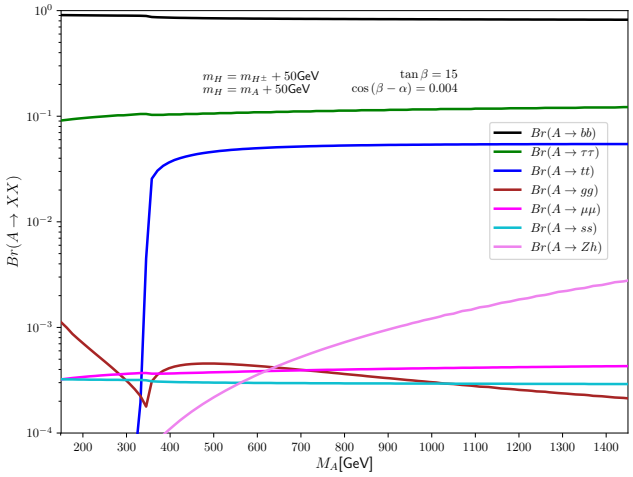

Figure B.9: $Br(A\to XX)$ vrs m_A, for $\tan\beta = 15$ near the decoupling limit

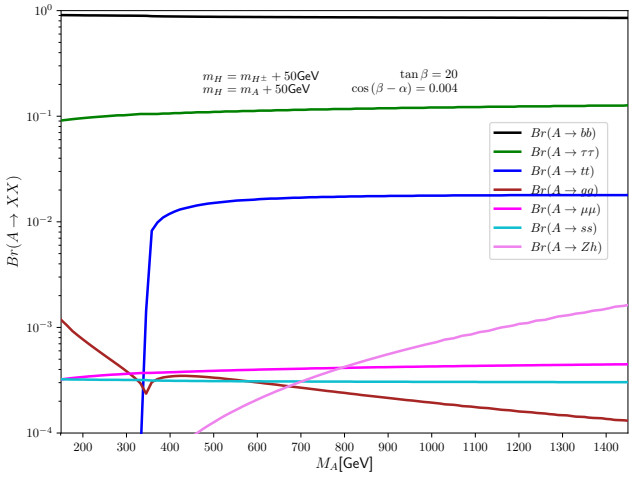

Figure B.10: $Br(A\to XX)$ vrs m_A, for $\tan\beta = 20$ near the decoupling limit

BRs for A in the crescent limit

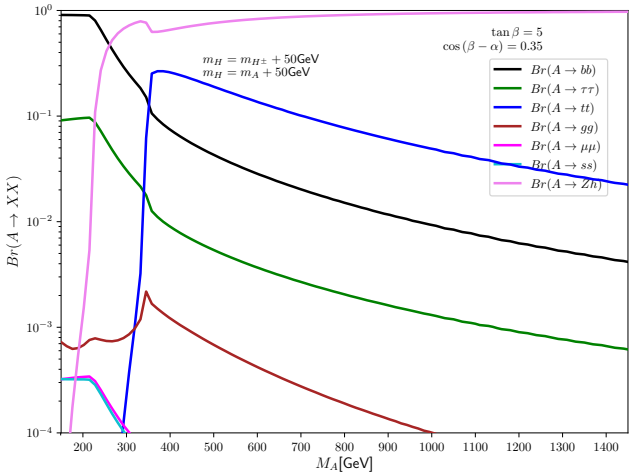

Figure B.11: $Br\,(A \to XX)$ vrs m_A, for $\tan\beta = 5$ in the crescent limit

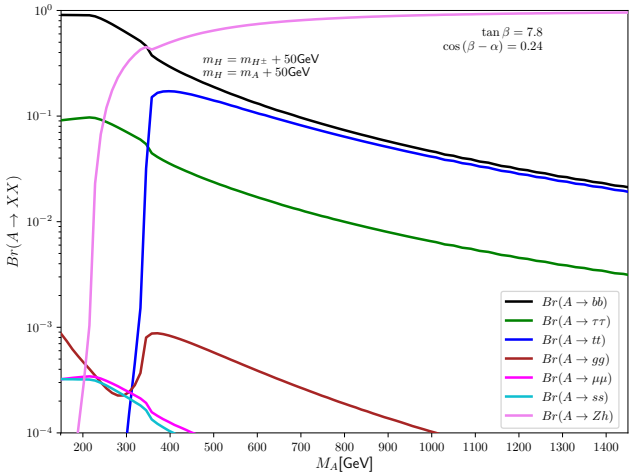

Figure B.12: $Br\,(A \to XX)$ vrs m_A, for $\tan\beta = 7.8$ in the crescent limit

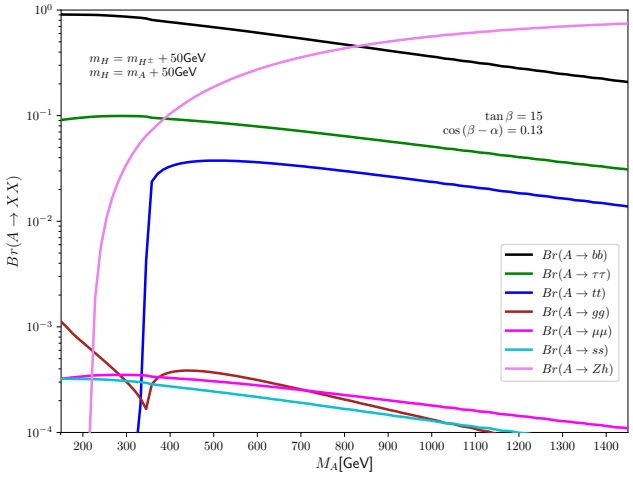

Figure B.13: $Br\,(A \to XX)$ vrs m_A, for $\tan\beta = 15$ in the crescent limit

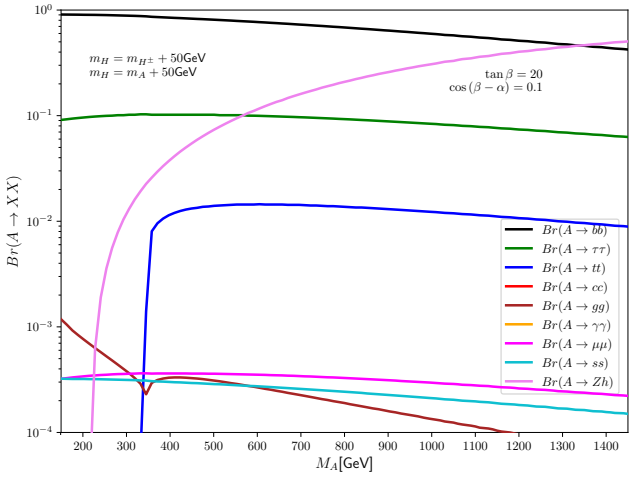

Figure B.14: $Br\,(A \to XX)$ vrs m_A, for $\tan\beta = 20$ in the crescent limit

Appendix C

THDM: Additional Results for the Charged Higgs

Charged Higgs ($H^{\pm}$) Production near decoupling and in the crescent limit

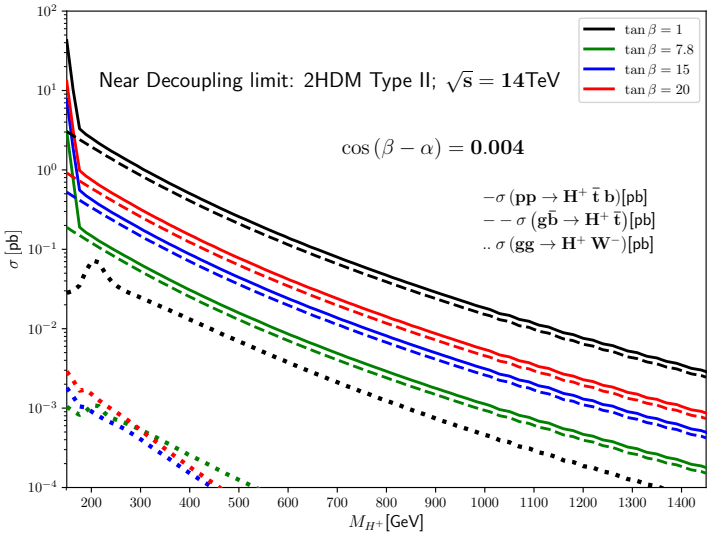

Figure C.1: Cross section rates for charged Higgs near the decoupling limit

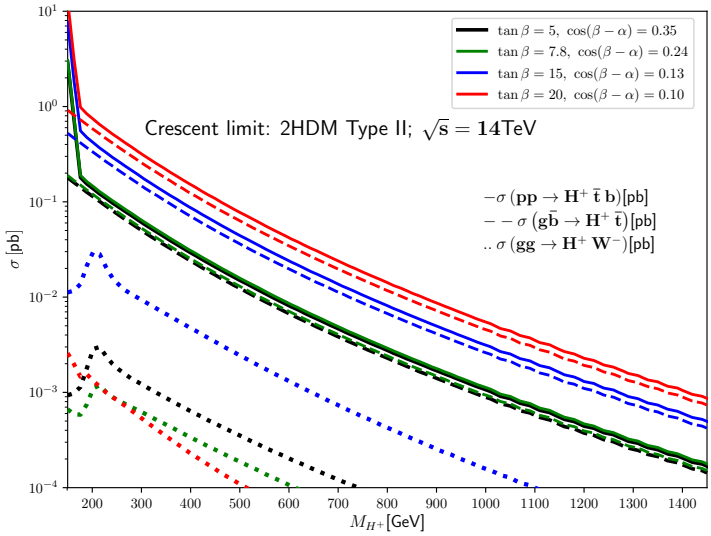

Figure C.2: Cross section rates for charged Higgs in the Crescent limit

BRs for $(H^{\pm})$ in the decoupling limit where $\cos(\beta-\alpha)=0$

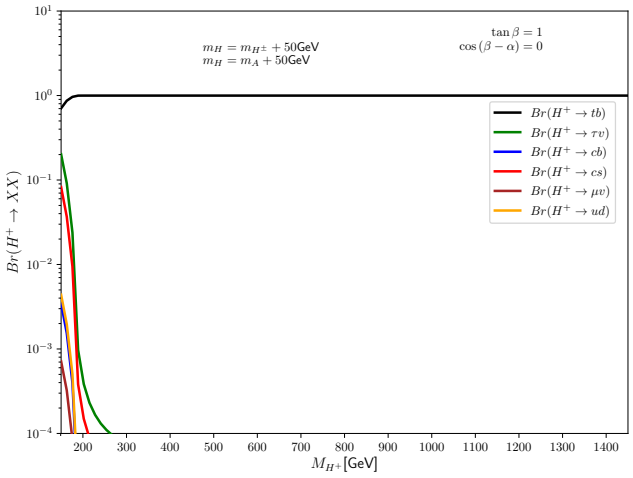

Figure C.3: $Br\,(H^{\pm} \to XX)$ vrs m_{H^+}, for $\tan\beta = 1$ in the decoupling limit

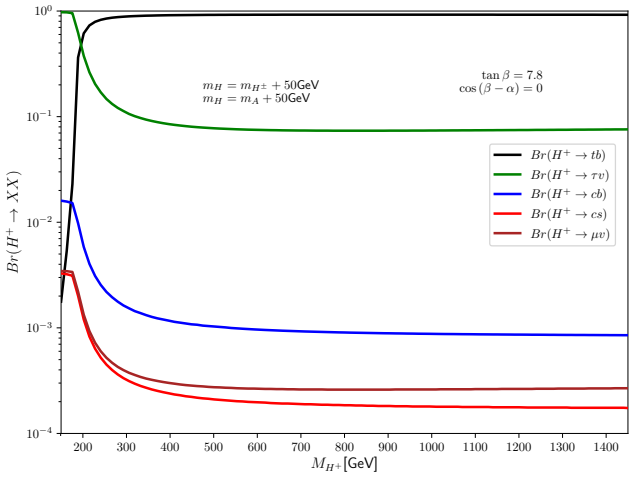

Figure C.4: $Br\,(H^{\pm} \to XX)$ vrs m_{H^+}, for $\tan\beta = 7.8$ in the decoupling limit

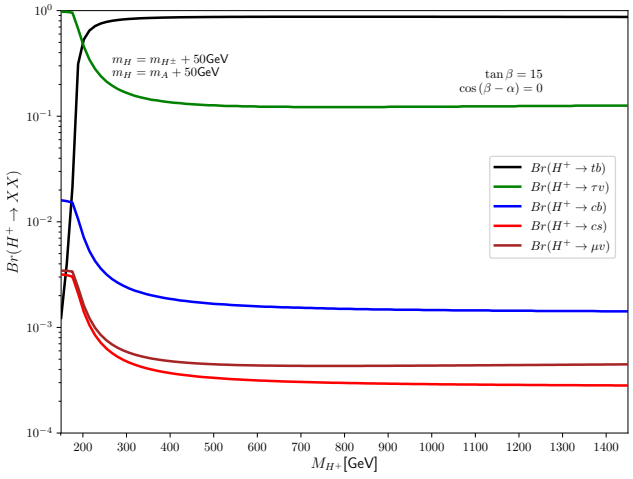

Figure C.5: $Br\,(H^{\pm} \to XX)$ vrs m_{H^+}, for $\tan\beta = 15$ in the decoupling limit

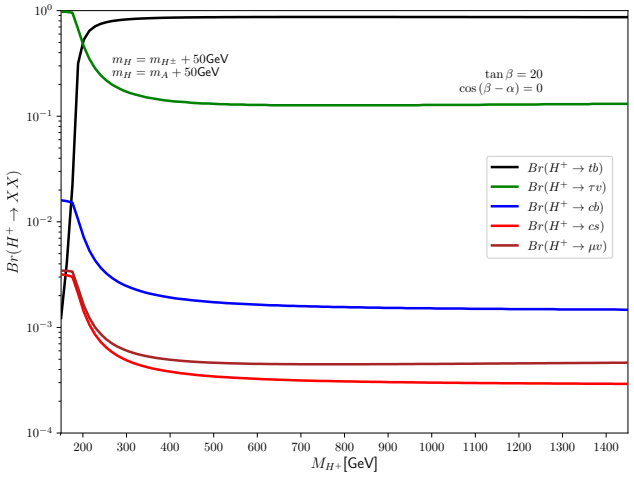

Figure C.6: $Br\,(H^{\pm} \to XX)$ vrs m_{H^+}, for $\tan\beta = 20$ in the decoupling limit

BRs for $(H^{\pm})$ near the decoupling limit where $\cos(\beta-\alpha)=0.004$

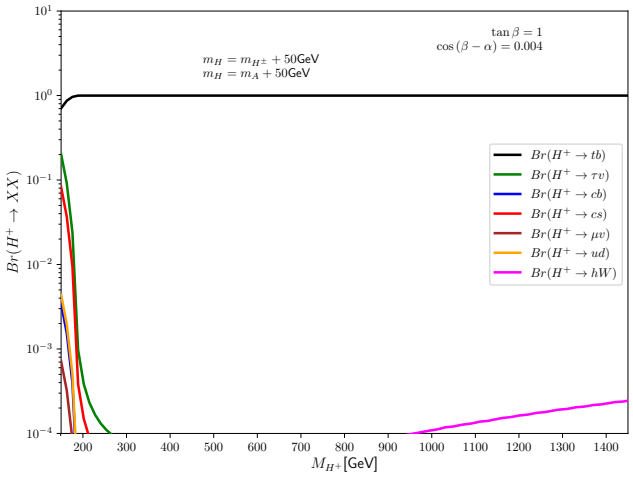

Figure C.7: $Br\,(H^{\pm} \to XX)$ vrs m_{H^+}, for $\tan\beta = 1$ near the decoupling limit

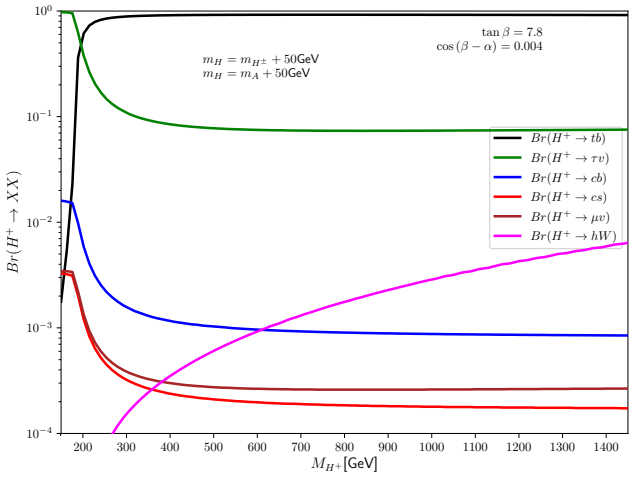

Figure C.8: $Br\,(H^{\pm} \to XX)$ vrs m_{H^+}, for $\tan\beta = 7.8$ near the decoupling limit

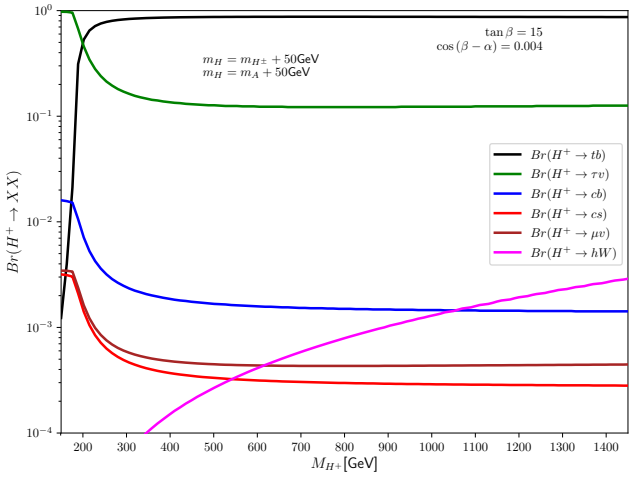

Figure C.9: $Br\,(H^{\pm} \to XX)$ vrs m_{H^+}, for $\tan\beta = 15$ near the decoupling limit

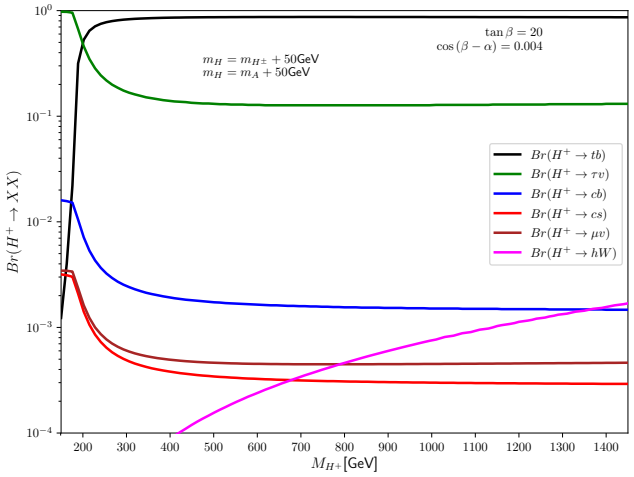

Figure C.10: $Br\,(H^{\pm} \to XX)$ vrs m_{H^+}, for $\tan\beta = 20$ near the decoupling limit

BRs for $(H^{\pm})$ in the crescent limit

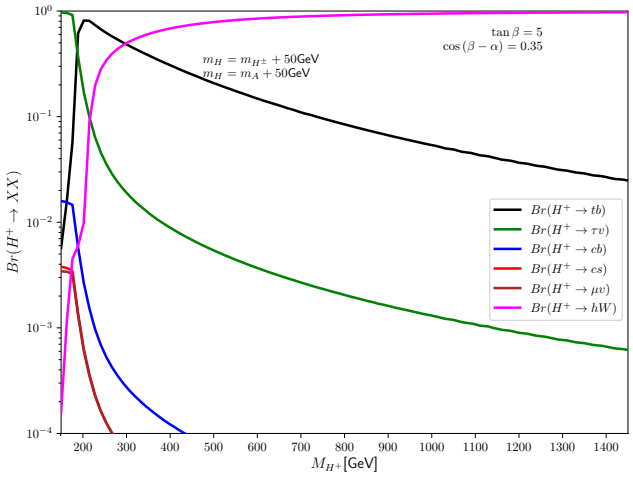

Figure C.11: $Br\,(H^{\pm} \to XX)$ vrs m_{H^+}, for $\tan\beta = 1$ in the crescent limit

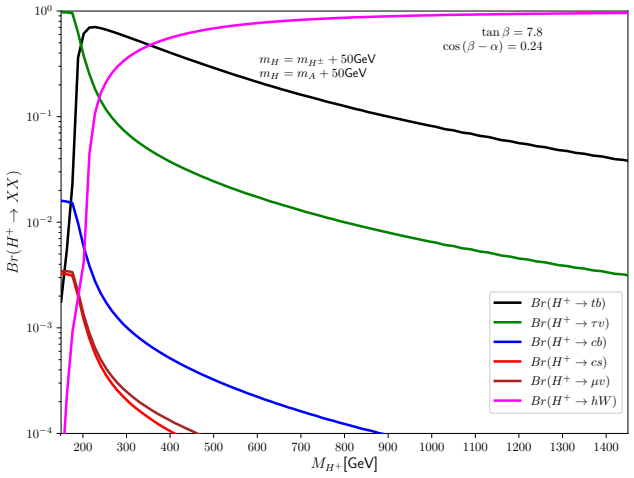

Figure C.12: $Br\,(H^{\pm} \to XX)$ vrs m_{H^+}, for $\tan\beta = 7.8$ in the crescent limit

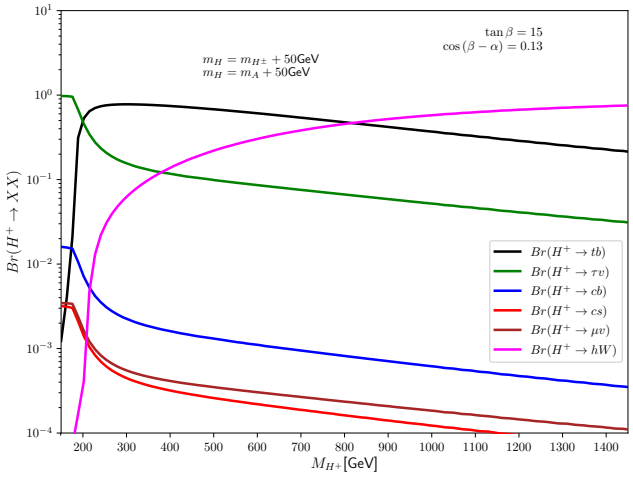

Figure C.13: $Br\,(H^{\pm} \to XX)$ vrs m_{H^+}, for $\tan\beta = 15$ in the crescent limit

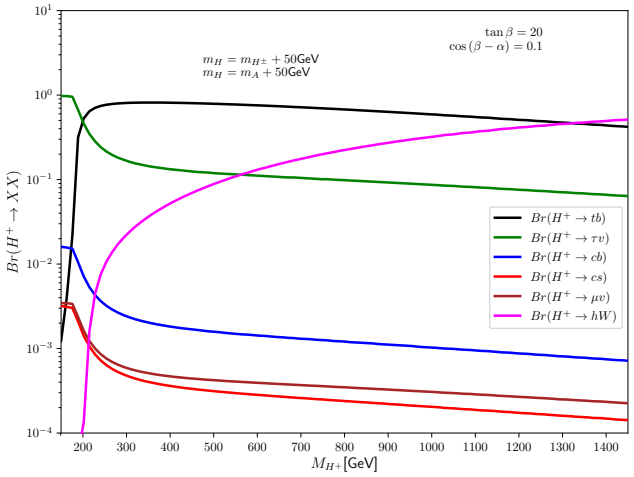

Figure C.14: $Br\,(H^{\pm} \to XX)$ vrs m_{H^+}, for $\tan\beta = 20$ in the crescent limit

Perl Scripts to Compute Branching fractions

```
#!/usr/bin/perl -w
#This is a perl script written by myself to calculate the Branching
fractions of the various Higgs's.
system("cp General_in_file 2HDMC.in");

$pfad="Final_charged_Nserc_banana_tb20"; #define t path
$outdir1 = $pfad;
system("mkdir -p $outdir1"); #make output directory

#Charged Higgs Boson
$count = 0;
$step = 100; #number of steps
$blchna1 = "MASS"; #block name in SLHA style
$blchnr1 = 37; #block number in SLHA style
$min = 150; #minimal value
$max = 1450; #maximal value

#Ratio between the two vevs
$counttb = 0;
$steptb = 100; #number of steps
$blchna1tb = "MINPAR"; #block name in SLHA style
$blchnr1tb = 3; #block number in SLHA style
$mintb = 20; #minimal value
$maxtb = 20; #maximal value

#Light Higgs Boson
$countmh = 0;
$stepmh = 100; #number of steps
```

```
$blchna1mh = "MASS"; #block name in SLHA style
$blchnr1mh = 25; #block number in SLHA style
$minmh = 125.09; #minimal value
$maxmh = 125.09; #maximal value

#Heavy Higgs Boson
$countmH = 0;
$stepmH = 100; #number of steps
$blchna1mH = "MASS"; #block name in SLHA style
$blchnr1mH = 35; #block number in SLHA style
$minmH = 200; #minimal value
$maxmH = 1500; #maximal value

#CP Odd Higgs Boson
$countmA = 0;
$stepmA = 100; #number of steps
$blchna1mA = "MASS"; #block name in SLHA style
$blchnr1mA = 36; #block number in SLHA style
$minmA = 150; #minimal value
$maxmA = 1450; #maximal value

# Mixing angle in terms of alpha and beta
$countsba = 0;
$stepsba = 100; #number of steps
$blchna1sba = "MINPAR"; #block name in SLHA style
$blchnr1sba = 20; #block number in SLHA style
$minsba =  0.99498743710662; #minimal value
$maxsba =  0.99498743710662; #maximal value
```

```
#Z_2 softly breaking parameter
$countm12 = 0;
$stepm12 = 100; #number of steps
$blchna1m12 = "MINPAR"; #block name in SLHA style
$blchnr1m12 = 18; #block number in SLHA style
$minm12 = -32400; #minimal value
$maxm12 = -32400; #maximal value

while ($count <= $step && $counttb <= $steptb && $countmh
 <= $stepmh && $countmH <= $stepmH && $countmA <= $stepmA
 && $countsba <= $stepsba && $countm12 <= $stepm12) {
    $var2 = $min + $count*($max-$min)/$step;
    $count += 1;
    $var2tb = $mintb + $counttb*($maxtb-$mintb)/$steptb;
    $counttb += 1;
    $var2mh = $minmh + $countmh*($maxmh-$minmh)/$stepmh;
    $countmh += 1;
    $var2mH = $minmH + $countmH*($maxmH-$minmH)/$stepmH;
    $countmH += 1;
    $var2mA = $minmA + $countmA*($maxmA-$minmA)/$stepmA;
    $countmA += 1;
    $var2sba = $minsba + $countsba*($maxsba-$minsba)/$stepsba;
    $countsba += 1;
    $var2m12 = $minm12 + $countm12*($maxm12-$minm12)/$stepm12;
    $countm12 += 1;
    #print ("This is run $count of $step.\n");
    changeparam("2HDMC.in",$blchna1,$blchnr1,$var2);
    changeparam("2HDMC.in",$blchna1tb,$blchnr1tb,$var2tb);
    changeparam("2HDMC.in",$blchna1mh,$blchnr1mh,$var2mh);
```

```
    changeparam("2HDMC.in",$blchna1mH,$blchnr1mH,$var2mH);
    changeparam("2HDMC.in",$blchna1mA,$blchnr1mA,$var2mA);
    changeparam("2HDMC.in",$blchna1sba,$blchnr1sba,$var2sba);
    changeparam("2HDMC.in",$blchna1m12,$blchnr1m12,$var2m12);
    system("./Demo 2HDMC.in 2hdmphys.out"); #running the code
    system("mv 2hdmphys.out $outdir1/2hdmphys.$count.txt");
}
sub changeparam {
    my($file,$block,$entry,$val);
    my($failed);
    ($file,$block,$entry,$val) = @_;
    movefile("$file","$file.bak");
    open(FILEIN,"$file.bak") || die;
    open(FILEOUT,">$file") || die "Cannot open file $file.";
    $failed = 1;
  LOOP: while (<FILEIN>) {
      if ((/^Block +$block /i) || (/^Block +$block$/i)) {
  $failed = 0;
  print {FILEOUT} ($_);
  while (<FILEIN>) {
      if (/^[BD]/i) {
  print {FILEOUT} ($_);
  next LOOP;
      }
      if (/^[ \t]+$entry[ \t]+.*\#/) {
  s/^[ \t]+$entry[ \t]+.*\#/ $entry $val \#/;
      }
              if ($block =~ "ALPHA") {print {FILEOUT} (" ".$val." #");}
      print {FILEOUT} ($_);
```

```
  }
      }
else {print {FILEOUT} ($_)}
    }
    if ($failed) {
print("Error in changeparam() when looking for Block $block.\n");
exit 1;
    }
    close(FILEIN);
    close(FILEOUT);
    unlink("$file.bak");
}
sub movefile {
    my($fromfile,$tofile,$targetdir);
    ($fromfile,$tofile) = @_;
    if ($tofile =~ /\//) {
($targetdir = $tofile) =~ s/\/[^\/]*$//;
unless (-d $targetdir) { system("mkdir -p $targetdir") }
    }
    unless (-f $fromfile) {
print("Error in movefile: Cannot find file $fromfile.\n");
exit 1;
    }
    system("/bin/mv -f $fromfile $tofile");
}
```